Temporal Variability in Marine Ecosystems with Implications for Biological Monitoring

Silvana Gonzalez

A dissertation

submitted in partial fulfillment of the

requirements for the degree of

Doctor of Philosophy

University of Washington

2021

Reading Committee:

John K. Horne, Chair

Seth Danielson

Christian E. Torgersen

Timothy E. Essington

Program Authorized to Offer Degree:

School of Aquatic and Fishery Sciences

University of Washington

Abstract

Temporal Variability in Marine Ecosystems with Implications for Biological Monitoring

Silvana Yanet Gonzalez Gonzalez

Chair of the Supervisory Committee:
Dr. John K. Horne
School of Aquatic and Fishery Sciences

Marine environments are changing, and further changes are expected in response to climate change, industry development (e.g. oil and gas explorations and marine renewable energy), pollution, and overfishing. There is an urgent need to understand effects of these stressors on marine ecosystems and to adopt effective management measures that minimize detrimental effects. Accomplishing this goal requires a comprehensive understanding of "natural" temporal patterns of biological components and underlying processes. High-latitude environments and marine renewable energy development sites have been particularly understudied due to sampling challenges (e.g. presence of sea ice, and high currents). This lack of baseline information required to measure biological responses to environmental change has increased the difficulty to document impacts in these areas and to predict effects of further changes in the ecosystems.

Chapter 1 reviews temporal variability in marine ecosystems. Chapters 2 and 3 evaluate high resolution, stationary acoustic data from the Chukchi Ecosystem Observatory (CEO) and concurrent measurements from a large set of environmental sensors to characterize temporal variability in the abundance and behavior of fish and zooplankton in the Chukchi Sea. Chapter 4 quantifies the spatial area that is represented by acoustic point source measurements to define the spatial scope of CEO observations and to inform cost-effective monitoring design at high latitudes. Chapter 5 compares temporal variability in biological characteristics at sites selected for wave and tidal energy industry development to assess the potential for applying standard methods and analytic tools for biological monitoring. Chapter 6 provides a synthesis of results and implications for biological monitoring. This comprehensive characterization of fish and zooplankton dynamics in the Chukchi Sea and at sites selected for marine renewable energy development increases our ability to detect and predict biological responses to environmental change, ensure the collection of representative samples, and assist in the design of standard strategies for biological monitoring at a range of aquatic ecosystems.

TABLE OF CONTENTS

LIST OF FIGURES

LIST OF TABLES

ACKNOWLEDGEMENTS

I would like to thank John Horne, for welcoming me to the lab, treating me like family since the first day, and for pushing me to be a better scientist and scientific writer. Thank you to my committee: Seth Danielson, Tim Essington, Christian Torgersen, and Terrie Klinger for their kindness, their constructive feedback and their encouragement throughout this PhD journey. I want to thank all the funding sources that made my PhD possible: Fulbright-ANII, Oil Spill Research Institute Graduate Student Fellowship, North Pacific Research Board Graduate Student award, JISAO Graduate Student fellowship, SAFS-RASC fellowship, QERM and Friday Harbor Laboratories TA-ships, NOAA Ocean Exploration and Research, and BOEM-DOE. I thank my previous mentors, Fabrizio Scarabino, Leonardo Ortega, Alvar Carranza, Yamandú Marín, Omar Defeo, and Angel Segura for shaping me as a good scientist early on. I thank my future mentor Libby Logerwell and her research group at NOAA for choosing me for an exciting postdoc adventure. I thank all the collaborators of the papers published during my PhD: Eric Ward, Angel Segura, Seth Danielson, Guzman Lopez, and Lilian Lieber and all the people that contributed with their knowledge and expertise and took the time to reply to my emails or sat down with me to answer my questions: Sarah Henkel, Mark Scheuerell, Alex De Robertis, Robert Levine, Franz Mueter, Hisamoto Waga, Dale Jacques, Amy Fox, Mark Centouri, Samantha Scherer. My thanks to all FAR lab members throughout these years: Hannah Linder, Lauren Wiesebron, Kerry Accola, Jackson Swan, Angelee, and specially to Dave McGowan and Beth Phillips who were lighting the

way and have been my source of PhD wisdom and to Ross Hytnen for being a generous and great field trip companion. To the QSCI 381 and Marine Invertebrates students, thank you for making me realize that I truly love teaching and mentoring. To my family in Seattle during most of my stay: Catherine, Jane, and Adrián. Thank you ladies for those weekly swimming + dinner + tea + long chats sessions and for all the amazing hikes! Adrián "Ramita", thank you for supporting me throughout this process, as my partner/housemate/travel buddy for 5 years and now as my long-distance best friend. Thank you to all my housemates and friends in Seattle these years: Kiva Oken, Jenn Purnell, Gwyn, Caz, Omer, Eric Sprecher. I am thankful for the new people and creatures that have brought happiness and love this last year: Samet, Paddy, Johnine, Lore, Charlie, Doris, Richie, Josie, Luna, Wren, and Johnny. Johnny, thank you for your love, kindness, and reassurance. Thank you to Yoga with Adriene, and all the tango, African dance, rowing, and photography lessons, mindfulness groups, the Pacific Northwest mountains, and IMA and West Seattle swimming pools for keeping me sane and entertained. Thank you to my therapist Teresa for being a loving and amazing support all these years. To my friends spread around the world, Chata, Gina, Peti, Flor, and Omer, thank you! To my friends in Uruguay, especially to Inesita, Camila, Analía, and their beautiful fast-growing babies, Rorro, Majo, Guzi, Fabri, Leo, Ana, Florencia, and Amelia: thank you for your long-distance support and for receiving me with delicious meals, adventures, and hugs in each visit.

Sobre todo, quiero agradecer a mi familia en especial a mis papás, que me han apoyado en todo momento y han escondido bastante bien sus miedos y su tristeza de tenerme lejos y han aceptado mi elección de vivir una vida llena de mares y mudanzas intercontinentales. Soy la mejor persona y profesional que puedo ser gracias a ustedes! Los quiero mucho!

DEDICATION

A mis abuelas que ahora son estrellitas o flores.

Chapter 1. TEMPORAL VARIABILITY IN MARINE ECOSYSTEMS WITH IMPLICATIONS FOR BIOLOGICAL MONITORING

1.1 INTRODUCTION

The accelerated pace and extent of environmental change over recent decades has increased the urgency and relevance of detecting and understanding biological responses to changes in natural ecosystems. There is a growing need for effective environmental monitoring strategies to obtain baseline data for ecosystem management, detect effects of anthropogenic perturbations or climate change on biological communities, and to validate model predictions on biological responses to environmental change (Spellerberg 1991). To accomplish these goals in marine environments, understanding natural variability at multiple scales is essential.

Ocean ecosystems are variable across a wide range of spatial and temporal scales. This variability is generated by numerous physical and biological processes acting and/or interacting across an equally-wide range of scales (e.g. Stommel 1963; Haury et al. 1978). Our understanding of these processes is predicated on the scales at which we observe them (Levin 1992). Thus, our ability to detect change and/or predict biological responses to change in marine communities relies on the quantification of natural variability, its dependence on observational scale, and on the understanding of processes driving that variability.

Temporal variability in biological communities has been measured less frequently than spatial variability, especially in aquatic ecosystems. Aquatic biologists typically work with time-series that are short with high resolution or longer with a low sampling frequency due to the discrete nature of biological sampling and constraints of research surveys that include availability of time, resources, and site accessibility. The relative scarcity of high-scope (i.e. long extent, high

resolution) biological time-series may represent a significant gap in our ecological knowledge of patterns and underlying processes, especially in dynamic aquatic environments (Stommel 1963; Haury et al. 1978; Schneider 2001).

Recent innovations in battery life and data storage have facilitated the use of remote sensing technologies, including active acoustics, that enable the collection of high-scope biological data (e.g. Godø et al. 2014). Active acoustic technologies measure fish and macrozooplankton densities using short pulses of sound through the water. Any object with a density different than water will reflect (i.e. backscatter) a portion of the energy to a transceiver (Simmonds and MacLennan 2005). Acoustic backscatter can be scaled to numeric and mass densities and used to characterize biological distributions and dynamics in the water column through time.

The use of active acoustics in instrumented platforms allows simultaneous and continuous collection of biological and physical data, a prerequisite for understanding biological responses to other physical and biological environmental drivers. These autonomous sensors enable high-scope temporal studies at relatively low-cost, which contrasts to data collected from time and resource consuming research vessels. Instrumented platforms may be particularly useful in areas of high environmental dynamics or areas with scarce or no baseline information. High-scope biological and physical datasets can be used to understand temporal variability in communities of marine animals living in the water column (i.e. pelagic communities), design monitoring plans, and increase our capability to detect and predict biological responses to environmental change.

The shift from vessel-based mobile, short range, coarse resolution, discrete samples to ocean observatories with multiple remote sensors collecting high resolution data over long periods brings new challenges. Analytic approaches and tools need to be adapted to include automated processing and to extract relevant information on distribution characteristics of aquatic organisms

from large datasets (Hampton et al. 2013). Also, the spatial equivalence of point-source measurements may limit the interpretation and application of results to larger spatial ranges and the quantification of the spatial scope of these measurements is required to ensure the collection of representative samples (Horne and Jacques 2018).

1.2 OBJECTIVES

This project quantifies temporal patterns in fish and zooplankton densities and behavior, and identifies associated influential environmental processes in dynamic and seasonally variable environments. Specific objectives include:

1a. Quantifying temporal scales of variation in densities and vertical distributions of pelagic fish and zooplankton in a seasonally variable, high latitude marine ecosystem.

1b. Identifying scale-dependent associations of observed temporal variability with dominant environmental processes.

2. Assessing associations between temporal variability in environmental processes and the timing and amplitude of Arctic cod (*Boreogadus saida*) densities in a high latitude marine ecosystem.

3. Analyzing temporal and spatial scales of variation in densities and vertical distributions of pelagic fish and zooplankton to quantify the representative range of point measurements in space.

4. Comparing temporal variability in densities and distributions of pelagic fish and macrozooplankton communities in environments with different dynamics to assess the potential for generic biological monitoring strategies.

Chapter 2. MULTI-SCALE TEMPORAL VARIABILITY IN BIOLOGICAL-PHYSICAL ASSOCIATIONS IN THE NE CHUKCHI SEA[1]

2.1 INTRODUCTION

Biological and physical processes that shape marine communities typically operate over multiple scales (Stommel 1963; Haury et al. 1978; Levin 1992; Schneider 1994). Consequently, efforts to attribute/associate observed variability with potential causes must also be conducted over a range of spatial and or temporal scales (McIntire and Fajardo 2009). This approach increases our ability to detect and predict biological responses to environmental change (Horne and Schneider 1994), and identify relevant scales for effective impact assessments and resource management (Hewitt et al. 2007; Godø et al. 2014).

The dependence of observed patterns on observational scale coupled with potential trends over time increases the effort needed to understand temporal variability in biological variables. A complete characterization of time-dependent patterns requires high resolution and long-term (i.e. high scope) data. High scope data can be difficult to obtain due to available resources or constrained accessibility. These challenges are amplified in high latitude marine environments where the presence of sea ice during most of the year limits vessel-based sampling (e.g. Mueter et al. 2017; Spear et al. 2019). In these areas, data acquisition is typically limited in extent and/or resolution, fragmenting our understanding of important biological and physical processes over the annual cycle. In particular, long term studies in the Pacific Arctic have focused on descriptions of biological variability from samples mainly collected during summer months either through

[1] Published as: Gonzalez S, Horne JK, Danielson SL (2021) Multi-scale temporal variability in biological-physical associations in the NE Chukchi Sea. Polar Biol 44:837–855. https://doi.org/10.1007/s00300-021-02844-1

systematic (e.g. Bluhm et al. 2010; Hopcroft and Day 2013; Moore and Stabeno 2015) or opportunistic (e.g. Ershova et al. 2015; Randall et al. 2019) surveys and data compilations. Studies examining high frequency temporal patterns (e.g. diel vertical migrations) over limited temporal extents (i.e. days to a few months) prevent an assessment of the consistency in observed patterns over longer periods (Fortier et al. 2001; Berge et al. 2009; Darnis et al. 2017; Geoffroy et al. 2017). A few studies have collected year-long biological data (e.g. Geoffroy et al. 2016; Kitamura et al. 2017), but to our knowledge, none have assessed biological patterns over a range of temporal scales through multiple years.

The seasonally ice-covered Chukchi Sea receives a nearly continual input of heat, nutrients, organic carbon, and organisms from Pacific-origin water flowing northward in response to an oceanic pressure head that results from an elevation difference between the Pacific and Arctic Oceans (Stigebrandt 1984). This input from the Bering Sea, combined with shallow depths enhances biological productivity in the Chukchi Sea (Grebmeier et al. 2015). A large phytoplankton bloom that occurs in late spring and summer (Questel et al. 2013) supports the largest soft bottom benthic faunal biomass in the world ocean (Grebmeier et al. 2006a, 2015), and corresponding populations of zooplankton (Ershova et al. 2015), seabirds (Kuletz et al. 2015), and marine mammals (Hannay et al. 2013). The Chukchi shelf is also home of Arctic cod (*Boreogadus saida*), a fish species that plays a key role in the transfer of energy from lower to higher trophic levels in high latitudes (Lowry and Frost 1981; Whitehouse et al. 2014). Located over the Northeast Chukchi shelf on the southern flank of Hanna Shoal (Figure 2.1), the Chukchi Ecosystem Observatory (CEO), is a set of instrumented moorings that has been collecting high-resolution, continuous biological, biogeochemical, and physical measurements since 2014

(Danielson et al. 2017b; Hauri et al. 2018; Lalande et al. 2020). The CEO provides a unique opportunity to quantify biological and physical patterns over a continuum of temporal scales.

Continuous datasets from remote sensing technologies fill existent data gaps and provide data to characterize these highly dynamic and rapidly changing ecosystems. In this study, I conducted a time-scale decomposition of biological metrics derived from acoustic backscatter and environmental variables to (a) quantify temporal scales of variation in densities and vertical distributions of fish and zooplankton, and (b) identify scale and time-dependent biological-physical associations using the CEO as a study case. Results from this study will contribute to improve our mechanistic understanding of the ecosystem dynamics and constitute first steps towards an effective prediction and detection of biological responses to a rapidly changing environment.

2.2 METHODS

2.2.1 *Study site*

The CEO is located in the NE Chukchi Sea shelf between Hanna Shoal and Barrow Canyon (71° 35.976' N, 161° 31.621' W) at 46 m depth (Figure 2.1). The CEO seascape varies seasonally: a late fall and winter homogeneous water column with thickening sea ice and light-limited primary production (Weingartner et al. 2005), a spring with diatoms and sea ice algae blooms triggered by the return of light (Gradinger 2009; Arrigo et al. 2014), and a stratified, warmer, nutrient-rich water column after May when sea ice starts to melt, triggering massive phytoplankton blooms under the ice (Arrigo et al. 2012a) and through the summer (Hill et al. 2018a). In the fall, the intensification of winds and diminishing solar input allows the water column to re-homogenize and surface waters are replenished with nutrients that supports fall phytoplankton blooms until sunlight fades.

Most universities have strict rules on the style of chapter titles and heading titles. The safest way is to follow this template and to consult with the appropriate parties who certify the formatting of a thesis or dissertation.

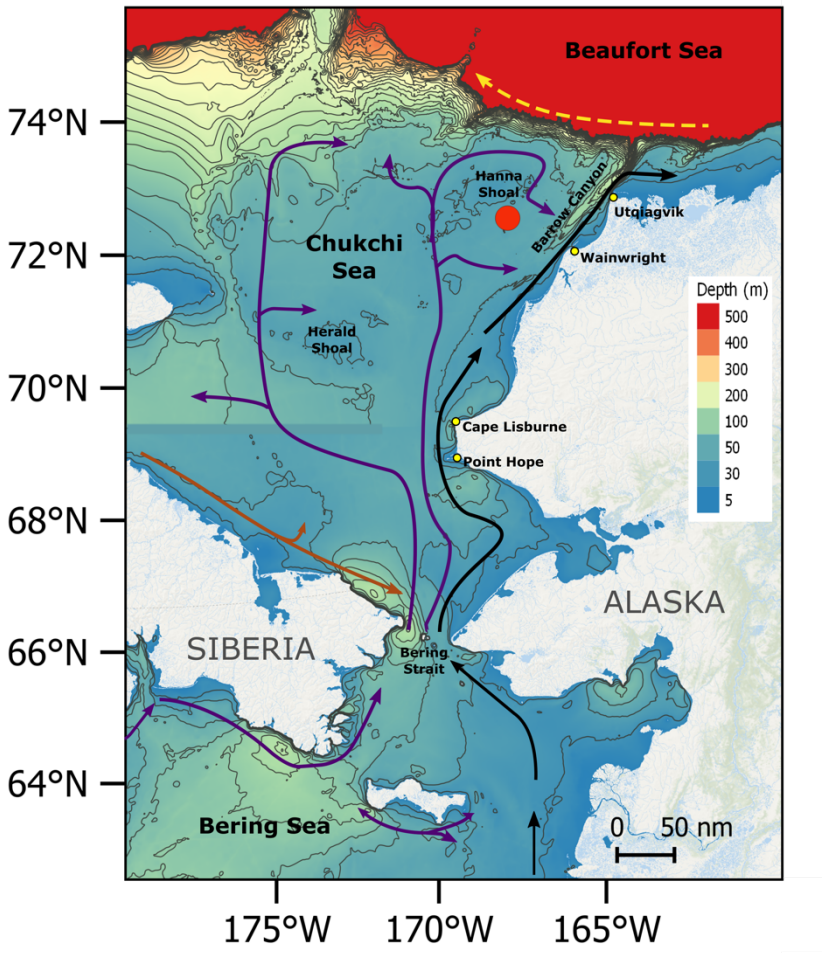

Figure 2.1. Study region map with bathymetric depths, and main flow pathways. The yellow arrow represents the Beaufort Gyre, black arrows represent the Alaskan Coastal Current, the brown arrow represents the Siberian Coastal Current, and purple arrows represent pathways of Bering Shelf, Anadyr, and Chukchi shelf waters. The red circle indicates the location of the Chukchi Ecosystem Observatory.

2.2.2 *Environmental data*

To examine biological-physical associations that vary over time and among temporal scales, I supplemented physical data collected at the CEO with data from other sources. Near-bottom and midwater salinity and temperature measurements were collected hourly at the CEO during the five deployment years using a Sea-Bird SBE-37 MicroCat located at a depth of 43 m (seafloor depth of 46 m) and a Sea-Bird Scientific SBE-16 SeaCat deployed at 28¬–33 m depth. Daily averages of satellite-based sea ice concentration (%) data were downloaded from the National Snow and Ice Data Center (NSIDC) archive (http://nsidc.org/data/seaice/pm.html#pm_seaice_conc) (Maslanik and Stroeve 1999). Hourly sun altitudes relative to the horizon at the CEO were calculated using the 'sunAngle' function of the R package *oce* (v. 1.1–1, Kelley & Richards 2019). Daily sunrise and sunset times were calculated using the 'sunriset' function of the R package *maptools* (v. 0.9-9, Bivand & Lewin-Koh 2019). Also, daily maximum and minimum air temperatures recorded at the nearby coastal city of Utqiaġvik were obtained from the U.S. climate data website (https://www.usclimatedata.com/climate/barrow/alaska/united-states/usak0025). Hourly wind speed and direction data for the CEO location were obtained from the Copernicus Climate Change Service (Hersbach et al. 2018).

2.2.3 *Acoustic data acquisition*

Active acoustic data were used to characterize temporal patterns in fish and zooplankton densities and behavior in the Chukchi Sea. Acoustic backscatter (i.e. ensemble reflected energy) data were collected using an ASL, Acoustic Zooplankton Fish Profiler (http://www.aslenv.com/AZFP.html), deployed at 28–35 m depth (depending on year), looking upwards (Figure 2.1). The instrument operated at 38 (12°), 125 (8°), 200 (8°), and 455 (7°) kHz (nominal beam width, measured between half power points in parenthesis) since September 9, 2014. The AZFP collected data every 15

seconds (0.067 Hz) at a vertical resolution of 4 cm. Every summer, a new mooring with a manufacturer-calibrated AZFP was deployed followed by the recovery of the previous mooring to ensure continuity of data collection.

2.2.4 *Acoustic data processing and classification*

Acoustic data from the CEO was processed using Echoview software (v. 9.0). Background noise was subtracted and a minimum signal-to-noise ratio filter of 6 dB re 1 m-1 (hereafter dB) was applied. Echoes within 3 m from the face of the transducer were excluded from the analyses to avoid the integration of echoes in the acoustic nearfield. Sea water surface and sea ice edges were delimited using Echoview's linear offset operator algorithm followed by visual inspection and manual correction. A surface exclusion line was set 0.5 m below the corrected surface and echoes above the line were excluded to ensure that backscatter from surface turbulence or sea ice were not included in analyses.

I classified acoustic backscatter into fish and zooplankton categories using differences in mean volume backscattering strength (MVBS) (Madureira et al. 1993; Kang et al. 2002; Korneliussen and Ona 2003) between 125 and 38 kHz data ($\Delta MVBS_{125\text{-}38\ kHz}$). Backscatter measurements were averaged in 4 pings (1 min) horizontal by 1 m vertical cells for each frequency. Cells with $\Delta MVBS_{125\text{-}38\ kHz}$ values in the range of -16 to 8 dB were classified as fish and $\Delta MVBS_{125\text{-}38\ kHz}$ values in the range of 8 to 30 dB were classified as zooplankton (cf. De Robertis et al. 2010). A minimum volume backscattering strength (Sv) integration threshold of -70 dB was applied to the 38 kHz ("fish") data (c.f. De Robertis et al. 2017) and a -80 dB Sv integration threshold was applied to the 125 kHz ("zooplankton") data (cf. Ressler et al. 2012).

Although no direct fish and zooplankton sampling was conducted in association with acoustic measurements, we can rely on catch data from surveys carried out in the NE Chukchi Sea

to attribute most of the observed fish backscatter to Arctic cod (*Boreogadus saida*). Arctic cod accounted for 81–90% of total fish biomass and abundance from bottom (Barber et al. 1997; Goddard et al. 2014; Sigler et al. 2017; Logerwell et al. 2018) and pelagic (Lowry and Frost 1981; De Robertis et al. 2017) trawl surveys conducted in spring-fall ice-free seasons. From four midwater trawls conducted on Hanna Shoal in close proximity to the CEO in summer of 2017, De Robertis (*pers. comm*) observed that Arctic cod constituted 66–99% of the fish biomass and 93–99% of the fish abundance. Other species occasionally caught included capelin (*Mallotus villosus*), *Lumpenus* spp, staghorn sculpin *Gymnocanthus tricuspis*, and Liparidae snailfish. As further support of this backscatter categorization, age-0 Arctic cod was the dominant contributor to 38 kHz backscatter in the northern region of the Chukchi Sea in acoustic-trawl surveys conducted in 2012 and 2013 as part of the Arctic Ecosystem integrated survey (De Robertis et al. 2017).

Zooplankton communities in the Hanna Shoal area are dominated numerically by small copepods such as *Oithona similis* and *Pseudocalanus* spp. and in biomass by the larger *Calanus glacialis*/*marshallae* (Lane et al. 2008; Elliott et al. 2017; Lalande et al. 2020). The arctic copepod *Calanus hyperboreus* has also been observed in this area (Lane et al. 2008; Hopcroft and Day 2013; Lalande et al. 2020). Other non-copepod groups that contribute to the Chukchi zooplankton community biomass, especially during summer, are the appendicularians *Fritillaria borealis* and *Oikopleura vanhoeffeni*, the chaetognath *Parasagitta elegans*, and some meroplankton species, particularly bivalve, polychaete and echinoderm larvae (Hopcroft et al. 2010; Ashjian et al. 2017; Lalande et al. 2020).

Electric interference was visible in the 125 kHz data throughout most of the first deployment year (September 2014–August 2015) and as a result, the first year of data was excluded

from further analyses. Fish and zooplankton Sv were integrated into hourly averages from September 1, 2015 to August 18, 2019 and used in all analyses.

2.2.5 *Data analysis*

The analytic approach consists of (1) characterizing temporal scales of variability in density and vertical distributions metrics for fish and zooplankton using wavelet analysis, (2) describing scale- and time-dependent associations of these metrics with physical environmental variables using wavelet coherence, and (3) assessing synchronicity and lags in biological-physical associations using phase angle differences between pairs of variables.

2.2.5.1 Characterization of biological vertical distributions

A suite of metrics derived from acoustic data, collectively referred as to Echometrics (Burgos and Horne 2008; Urmy et al. 2012), were used to describe variations in density and vertical distributions of fish and macrozooplankton in the water column at the CEO. Echometrics can be used to efficiently summarize temporal variability in abundance and behavior in large datasets and to detect and quantify variability across a broad range of temporal scales (e.g. transient events, diel vertical migrations, and interannual changes). The Echometrics suite includes: (1) mean Sv (units: dB re m^{-1}), an index of organism mean density (MacLennan et al. 2002); (2) center of mass (units: m), the mean weighted location of backscatter in the water column relative to the bottom; (3) inertia (units: m2), a measure of organism dispersion (i.e. variance) from the center of mass; and (4) an aggregation index (units: m-1), which measures vertical patchiness of backscatter through the water column. The aggregation index is calculated over a scale from 0 to 1, with 0 being evenly distributed throughout the water column and 1 being aggregated.

2.2.5.2 Scales of variation in biological characteristics

To identify the dominant scales of temporal variability in fish and zooplankton metrics and to examine the consistency in dominant scales of variability through time I used wavelet analysis (Torrence and Compo 1998). A wavelet transform decomposes a time series across time and frequency domains through the convolution of a waveform—the wavelet—that is stretched or compressed (i.e. scaled) and slid through the time series (i.e. translation). The result is a 2-dimensional heat-map, called a scalogram, that represents the wavelet power (i.e. variance) contributed by each temporal period (or scale) at each time step. Therefore, a wavelet transform allows not only the detection of constituent periods or frequencies (analogous to a Fourier Transform), but also the temporal location of frequency components within the record (Torrence and Compo 1998; Cazelles et al. 2008).

A continuous Morlet mother wavelet function (Torrence and Compo 1998) was applied to each time series. Continuous wavelets enable the localization of transient patterns in variance and have been previously used for the analysis of temporally-indexed acoustic data (e.g. Urmy 2012, Viehman & Zydlewski 2017, Gonzalez et al. 2019). Temporal scales analyzed ranged from two hours (twice the hourly aggregated data resolution) to 11,585 hours (one third of the time series length). Wavelet power was calculated using the R package *WaveletComp* (v. 1.1, Roesch & Schimidbauer 2018). Statistical significance in localized wavelet power was evaluated through comparison to a white noise (constant value, equal to the time series variance) null hypothesis at a 95% confidence level (Torrence and Compo 1998) using 100 simulations. Edge effects were minimized by adding zeroes at the beginning and end of each data series to increase the total length of the series to the next power of two (Torrence and Compo 1998).

Horizontal integration of wavelet power at each scale over the entire deployment—the global wavelet spectrum—allows the measurement of variance contributed by each scale across

the entire series. The global wavelet spectrum was calculated using the R package *WaveletComp* (v. 1.1, Roesch & Schimidbauer 2018). Significance of this time-averaged variance was tested against white noise at a 95% confidence level (Torrence and Compo 1998).

2.2.5.3 Time- and scale-dependent biological and physical associations

To assess time and scale-dependent correlations between biological metrics and the marine environment I used wavelet coherency. Wavelet coherency measures the correlation (taking values from 0 to 1) and phase (values from $-\pi$ to π) of two variables at each time step and scale of the decomposed series enabling the description of localized (in scale and time) and lead-lag relationships between two time series (Torrence and Compo 1998). Daily averages of all variables were used to compute wavelet coherences between the four biological metrics and physical variables. Daily values correspond to the highest common temporal resolution for all biological and physical variables. The R package *WaveletComp* (v. 1.1, Roesch & Schimidbauer 2018) was used to calculate wavelet coherence and phase. Statistical significance of localized wavelet coherency between each pair of variables was also tested against white noise using 100 simulations at a 95% confidence level. Global wavelet (i.e. time averaged) coherence was calculated and its significance was tested against white noise at a 95% confidence level (Torrence and Compo 1998). To look at potential predator-prey interactions between fish and zooplankton communities I calculated wavelet coherence between hourly series of fish and zooplankton densities (i.e. mean Sv).

2.3 RESULTS

2.3.1 *Echometrics and environmental conditions*

Densities and vertical distributions of fish and zooplankton displayed intra-annual temporal variability (Figure 2.2). Seasonal patterns were observed in all metrics for both backscatter groups. Backscatter corresponding to fish and zooplankton was observed throughout the year with greater densities (i.e. mean Sv) in summer than in winter. Peak densities of fish were observed in July–September and highest densities of zooplankton were recorded in August–November (Figure 2.2a). In general, fish were located deeper in the water column than zooplankton. Both backscatter groups were located deeper in the water column during winter and started ascending around February, reaching depths closest to the surface by the end of the summer (i.e. late August–September) and then descended to deeper waters (Figure 2.2b). Fish dispersion (i.e. inertia) was relatively low throughout the year with highest values observed in autumn. Zooplankton dispersion was higher in autumn and winter months (Figure 2.2c). Fish and zooplankton were more strongly aggregated in winter and spring months while weaker aggregations were observed in autumn each year (Figure 2.2d). Short-period (24 hours or less) variability was also present in the data, with high hourly variability observed in all metrics (not shown).

Inter-annual variability was observed in the timing and amplitude of seasonal changes. For example, the peak in fish and zooplankton production was much higher and more extended during late summer¬–early fall of 2017 (Figure 2.2a). This high production was coincident with the highest water temperatures recorded in 2017 (Figure 2.2e). The timing of the peaks in fish and zooplankton density occurred earlier each year, shifting from September in 2016 to August in 2018 for fish and from November in 2016 to August in 2018 for zooplankton (Figure 2.2a).

I observed seasonal and inter-annual variations in sea ice concentration, midwater temperature, and salinity (Figure 2.2e and f). Sea ice started to concentrate in November each year reaching 50% concentrations at midwater temperatures near 0 °C. Sea ice melting started in June in 2016 and earlier in following years (Figure 2.2e). Summer of 2017 was the warmest in the series with midwater temperatures reaching 4 °C by mid-September. This year, sea ice melting started in April and the onset of sea ice formation was delayed until December (Figure 2.2e). Midwater salinity values were lowest (ca. 31) in November-December each year (Figure 2.2f) with the exception of 2017 when salinity remained near 32.

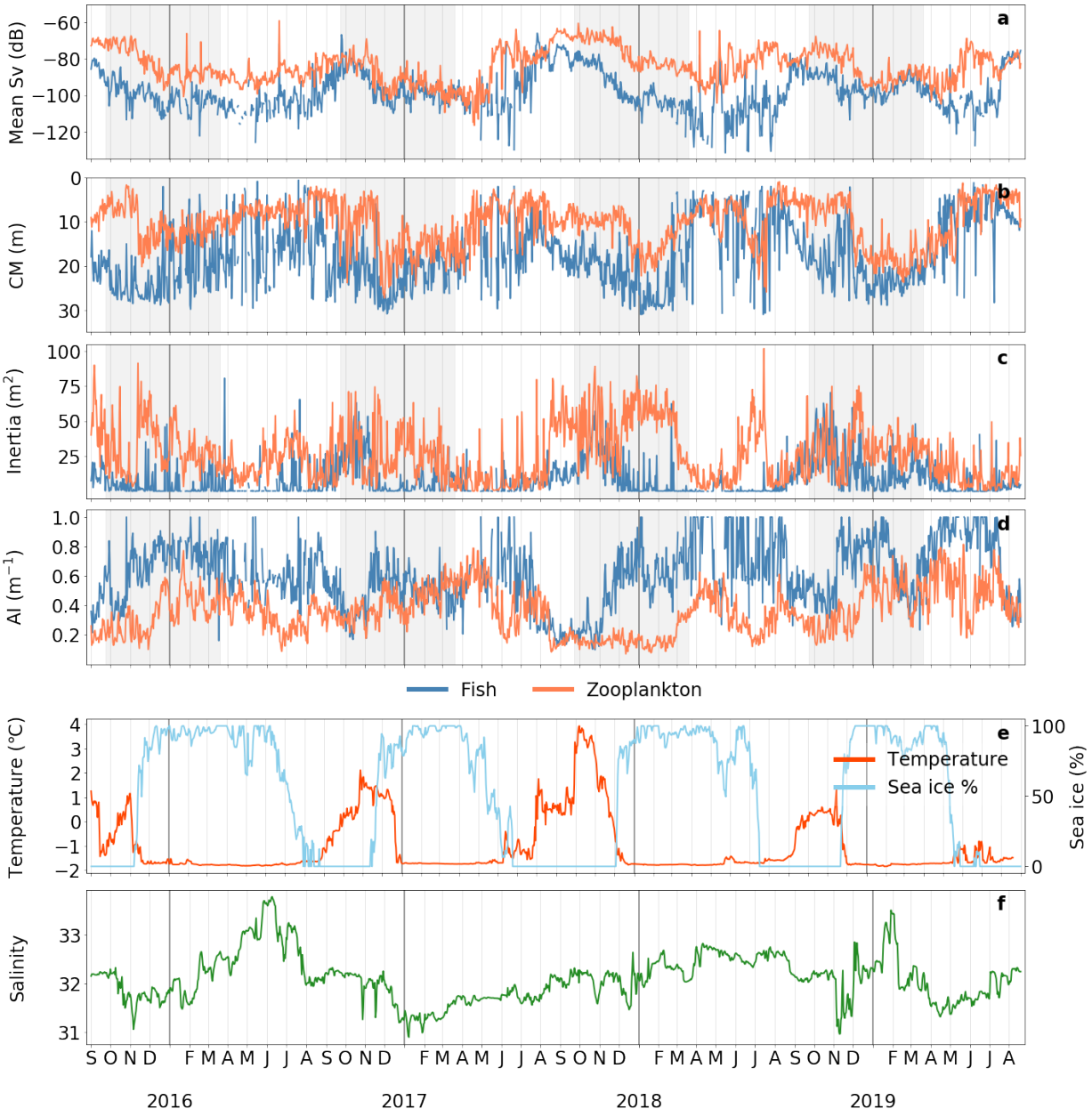

Figure 2.2. Daily averages of fish and zooplankton density and vertical distributions derived from acoustic backscatter data (a–d), and physical variables (e–f) at the Chukchi Ecosystem Observatory from September 1, 2015 to August 18, 2019. CM: center of mass, AI: aggregation index. Shaded areas highlight months between Fall and Spring equinoxes. Temperature and salinity values correspond to midwater measurements.

2.3.2 *Dominant scales of temporal variability in biological metrics and their consistency through time*

Variability in biological characteristics at the CEO was observed at multiple temporal scales (i.e. periods) with varying degrees of consistency through time (Figure 2.3 and Figure 2.4). Variability in fish metrics (Figure 2.3) was concentrated at the ~ 1-year period (~ 8679 hours), indicating a strong signal of intra-annual variations in fish densities and vertical distributions. A consistent band of high wavelet power was observed around a 4096-hour period (ca. 5.5–6 months) and was represented as a peak in the global wavelet plots. This peak in wavelet power at the ~ 6-month period was present in all metrics, but this signal was much weaker for the aggregation index (Figure 2.3d). Variability at this scale, although present throughout the year, was more pronounced in summer months (Figure 2.3). A third peak in average wavelet power was observed at a ~ 24-hour period representing diel changes in fish metrics. The occurrence of the 24-hour period signal was less consistent through time than annual and ~ 6-month periods but the strength of the signal (i.e. wavelet power) was high when present (Figure 2.3a). For aggregation index, the ~ 24-hour period wavelet power was particularly accentuated in 2019, compared to previous years (Figure 2.3d). High wavelet power values localized at specific times within the series were observed in the scalograms and as smaller peaks in global wavelet spectra at 2435-hour (~ 3 months), 683-hour (~ 28 days), and 341-hour (~ 14 days) periods for mean Sv, center of mass, and inertia (Figure 2.3a–c). Variability at these time scales was stronger from late fall to early spring each year (Figure 2.3a–c). For inertia, wavelet power was noticeably high around the ~ 3-month period from July to March with some variations in temporal extent among years (Figure 2.3c).

Variability in zooplankton metrics was also concentrated in three main scales with peaks at the ~ 1-year and ~ 24-hour periods, matching observations for fish, and at the 2896-hour (~ 4 months) period (Figure 2.4) with a few exceptions. For the aggregation index, the local peak

observed at the 1-year period for all other metrics was not present but a peak in the average wavelet power spectra occurs at a 9-month period (Figure 2.4d). For zooplankton center of mass, a peak occurs at the ~ 5.5-month period instead of the ~ 4-month period that was observed for all other metrics and an additional peak was observed at the 1933-hour (~ 3 months) period (Figure 2.4b). Variability at the 574-hour (~ 28 days) and 341-hour (~ 14 days) periods was observed for all metrics during November-June and were represented as small peaks in the average wavelet power spectra (Figure 2.4). These two scales of temporal variability suggest monthly and fortnightly influences of moon cycles on zooplankton density and vertical distribution through the modulation of tides and light in winter months. Variability at an 80-hour (~ 3 days) period was also observed during September-November for center of mass and inertia in both fish and zooplankton groups each year (Figure 2.3b-c and Figure 2.4b-c). This peak is attributed to the occurrence of storms that are typically accentuated in fall.

In summary, variability in biological metrics occurred over a range of time scales with peaks observed at the annual, seasonal (3–6 months), and diel (24-hour) periods. Smaller peaks resulting from a less consistent occurrence throughout the series occurred at intermediate time scales of 3–28 days. Variations in observed peaks emphasize the importance of a multi-scale approach for a thorough characterization and better understanding of biological and physical patterns in Arctic marine ecosystems.

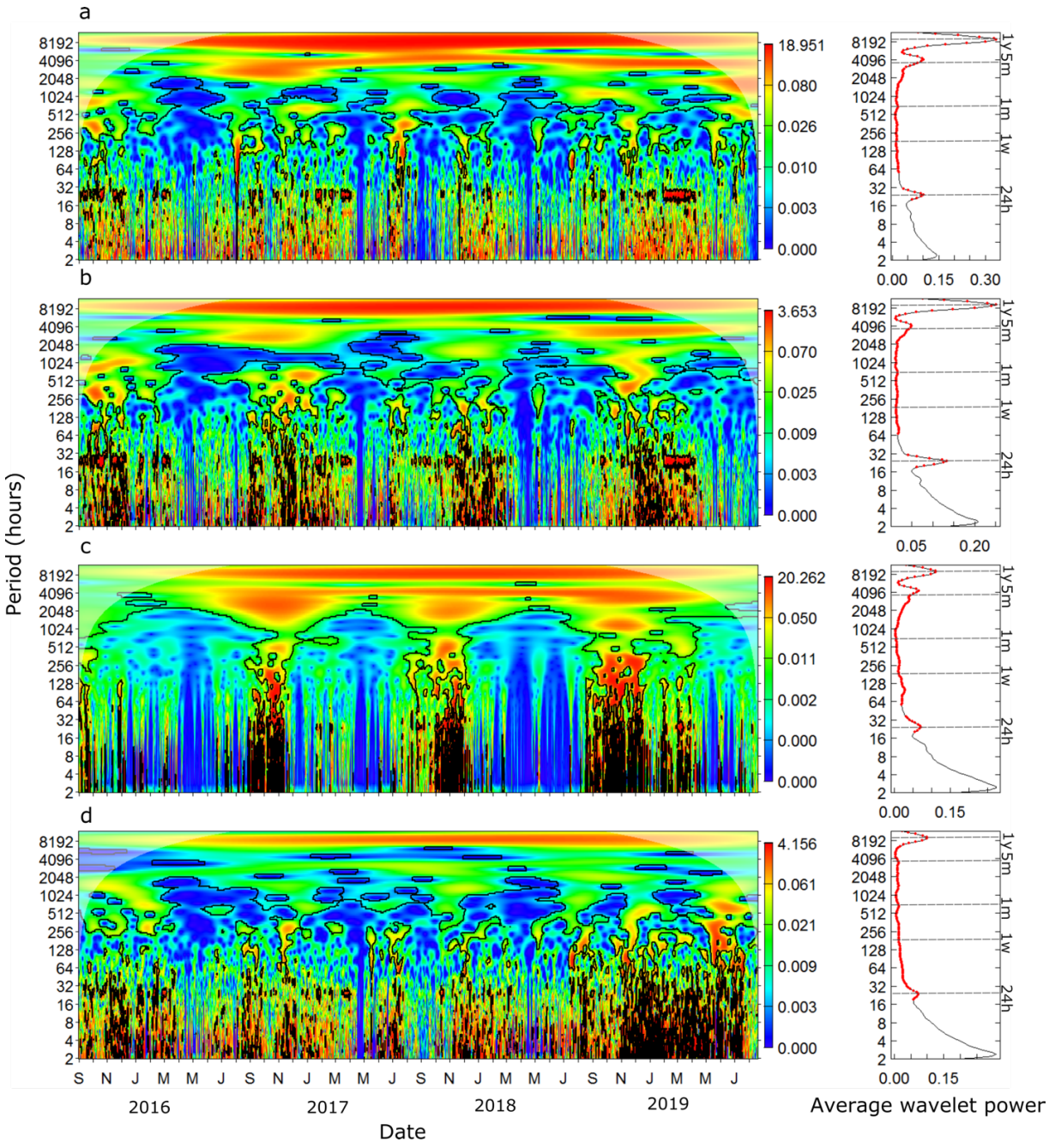

Figure 2.3. Time-scale decomposition of hourly values of fish density and vertical distribution metrics derived from acoustic backscatter at the CEO.Mean Sv, (b) center of mass, (c) inertia, (d) aggregation index. The color bar represents the wavelet power (σ^2). The shaded area represents the cone of influence (edge effects) and the black contour lines indicate areas of significance (95% confidence against white noise). Time averaged wavelet power (global wavelet spectrum) is shown on the right for each metric. Significant periods (95% confidence against white noise) are shown in red. Dashed lines indicate 1-year, 5-month, 1-month, 1-week, 24-hour periods.

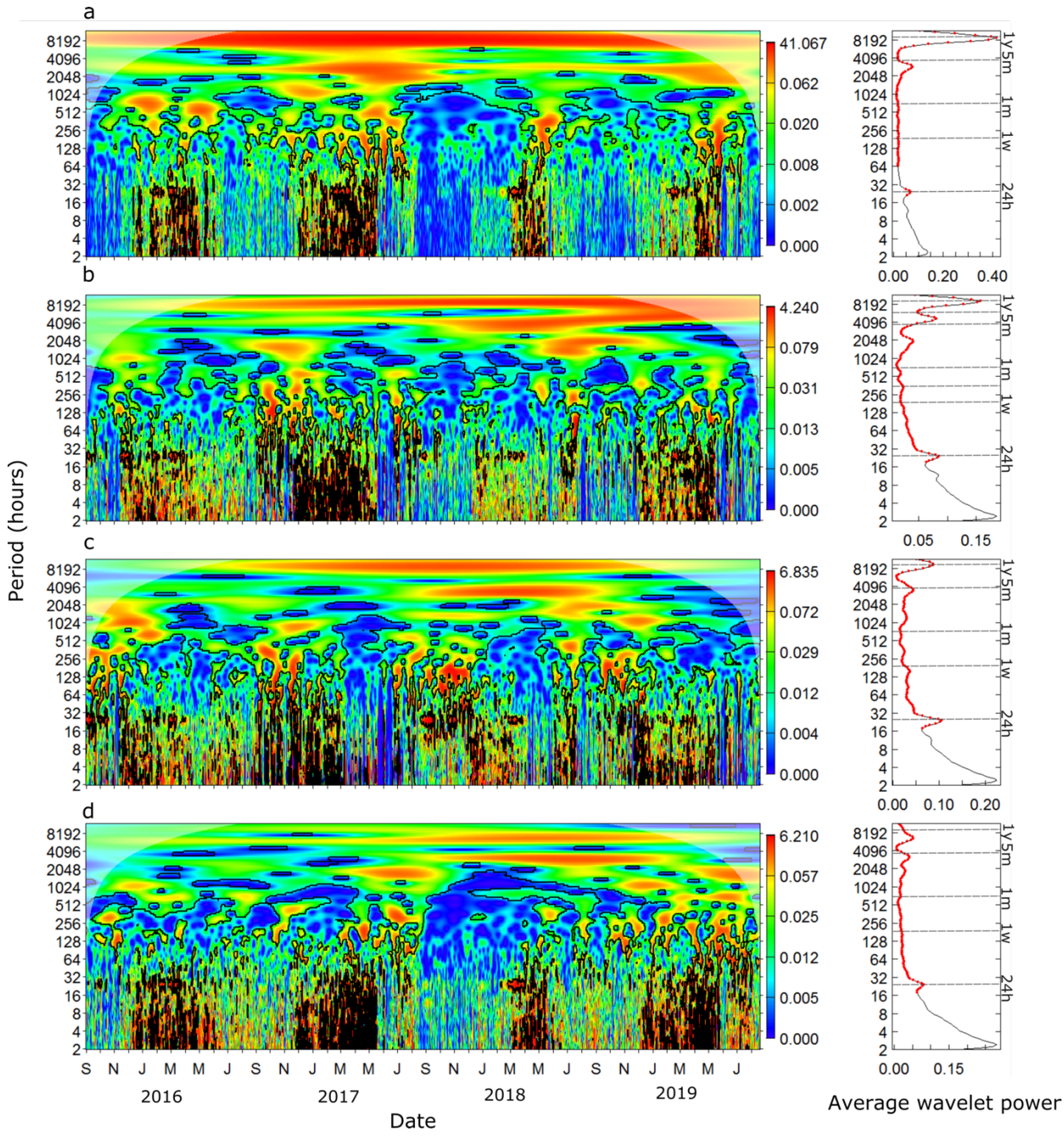

Figure 2.4. Time-scale decomposition of hourly values of zooplankton density and vertical distribution metrics derived from acoustic backscatter at the CEO. (a) Mean Sv, (b) center of mass, (c) inertia, (d) aggregation index. The color bar represents the wavelet power (σ^2). The shaded area represents the cone of influence (edge effects) and the black contour lines indicate areas of significance (95% confidence against white noise). Time averaged wavelet power (global wavelet spectrum) is shown on the right for each metric. Significant periods (95% confidence against white noise) are shown in red. Dashed lines indicate 1-year, 5-month, 1-month, 1-week, 24-hour periods.

2.3.3 *Biological-physical associations*

Scale- and time-dependent associations between biological metrics and environmental variables were observed for fish and zooplankton with variations in strength and phase (i.e. coherence).

2.3.3.1 Predator-prey associations

Coherence between fish and zooplankton densities was observed at multiple temporal scales with variations in lagging group at each scale (Figure 2.5). A significant peak in average wavelet coherence between both backscatter groups was observed at a 1-year period. At this period, a significant positive association was observed throughout the entire deployment led by zooplankton (Figure 2.5) with phase differences (i.e. fish phase – zooplankton phase, hereafter phase) of -0.2 rad (~ -11 days) to -0.4 rad (~ -23 days). Significant positive associations at 2.5-month, 1-month, and 11-day periods were observed in winter and spring months each year with fish (mean phase: +1.6 rad or +19 days), zooplankton (mean phase: -0.6 rad or -3 days), and fish (mean phase: +0.3 rad or +12 hours) as the leading variables (Figure 2.5), respectively. Significant coherence between both groups was also observed at the diel scale (Figure 2.5).

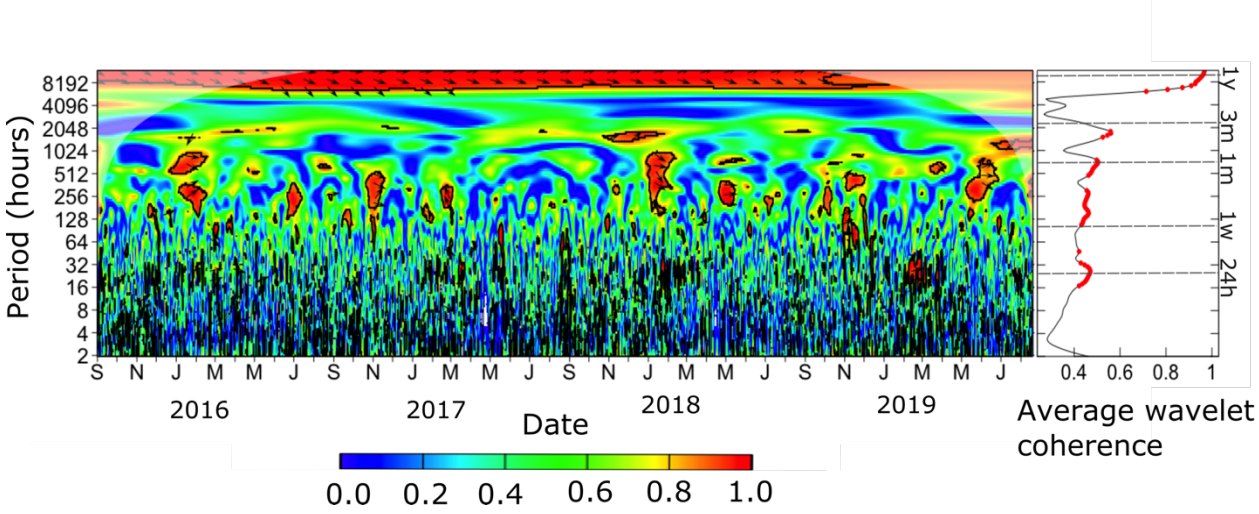

Figure 2.5. Wavelet coherence between hourly values of fish and zooplankton density (mean volume backscattering strength). The color bar represents the wavelet coherence. The shaded area

represents the cone of influence (edge effects) and the areas of significance are traced with a black line (95% confidence against white noise). Arrows indicate the phase difference between the two variables of the wavelet spectra (right arrows indicate series are in phase, left arrows indicate series are completely out of phase (180°), and an arrow pointing vertically upward means the second series lags the first by 90°. Time averaged wavelet coherence is shown on the right with significant periods (95% confidence against white noise) shown in red. Dashed lines indicate 1-year, 3-month, 1-month, 1-week, 24-hour periods.

2.3.3.2 Scale- and time-dependent coherence among biological metrics and physical environment

Strength of bio-physical associations varied between backscatter groups, among biological metrics, and among temporal scales of variation (Figure 2.6 and Figure 2.7). Significant biological-physical associations presented in this section result from consistently significant coherence throughout the entire time series and can therefore be considered as robust associations. Only biological-physical associations occurring at time scales identified as dominant scales of temporal variability in biological metrics in section 3.2 (i.e. peaks in metrics global wavelet spectra) are described here and further discussed in section 4.

2.3.3.2.1 Diel variability

The strength of the 24-hour period signal in fish and zooplankton location and dispersion (i.e. center of mass and inertia) in the water column, indicative of diel vertical migrations (DVM), varied throughout the year (Figure 2.6). In general, highest peaks in the strength of the diel signal in both metrics occurred at intermediate daylengths (i.e. autumn and spring) for both fish and zooplankton. In particular, diel cycles in center of mass for both backscatter groups were stronger during autumn and spring months each year but did persist with lower values throughout winter

months. From March to September this signal was non-significant for fish and was low or non-significant for zooplankton (Figure 2.6a).

The diel signal in fish dispersion was only present during late summer and autumn months, with highest wavelet power values observed in November when there exists < 5 hours of daylight at the CEO site (Figure 2.6b). Significant values of diel dispersion outside autumn months were only observed in February–April of 2019 with a peak in wavelet power in March (10 hours of daylight) that had an amplitude similar to observations in fall. Diel cycles in zooplankton dispersion were more persistent throughout the year, with lower but still statistically significant values during both midnight sun (i.e. 24 hours of daylight) and polar night (i.e. 0 hours of daylight) months. Annually, the highest values in wavelet power of the 24-hour period for zooplankton dispersion were observed in September for 2015–2017, while in 2018 the highest values were observed in November (Figure 2.6b). The observed association between vertical distribution metrics and light radiation patterns at the DVM period was supported by high significant coherence between hourly values of fish and zooplankton metrics, and sun altitude around the 24-hour period (Appendix A).

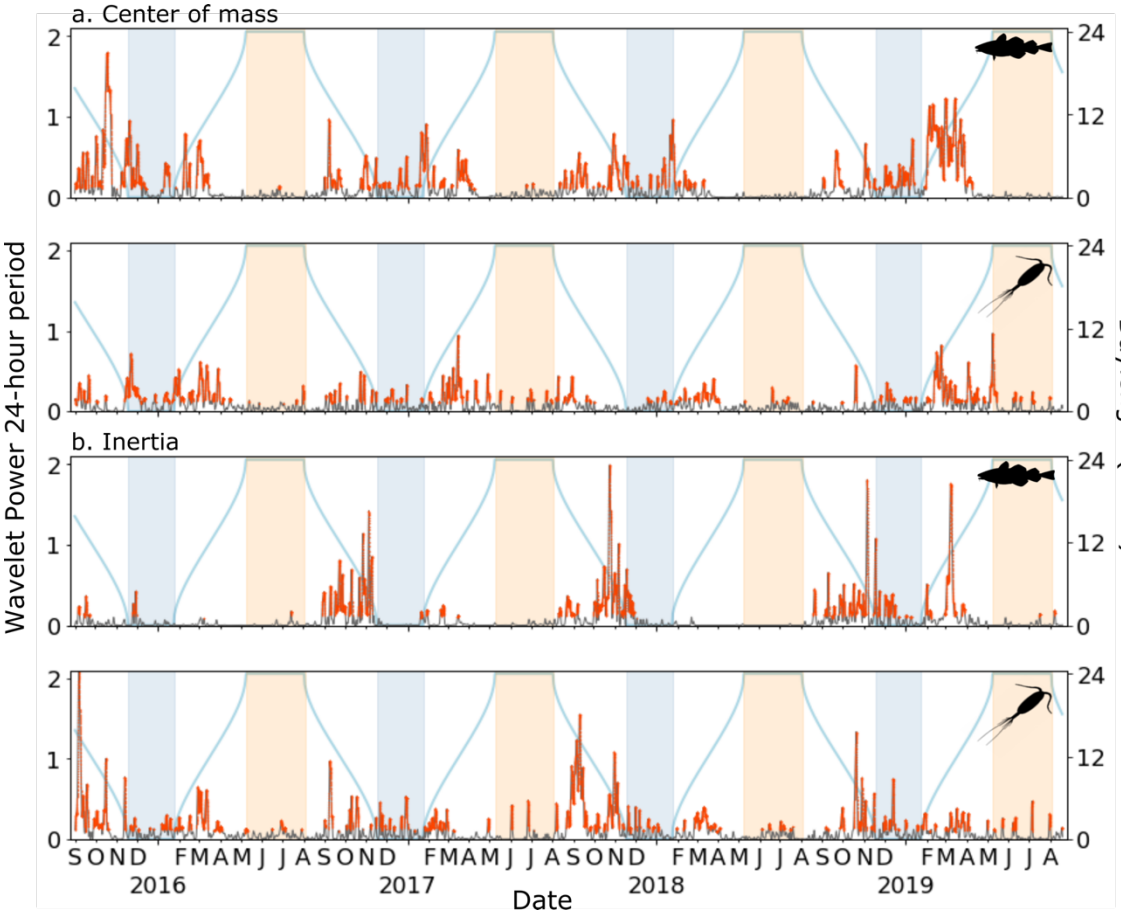

Figure 2.6. Temporal variation in the strength of the 24h-period signal in center of mass (a) and inertia (b) for fish (top) and zooplankton (bottom) in association with daylength at the Chukchi Sea Observatory. Significant peaks in wavelet power are shown in red. Shaded areas in orange and blue indicate periods of midnight sun and polar night, respectively.

2.3.3.2.2 Multi-day to monthly variability

At the ~ 1-month scale, I found significant associations between echometrics and light, salinity, and wind. In particular, fish mean Sv and center of mass were associated with wind direction, while fish aggregation index was associated with light patterns (Figure 2.7 left panel). For zooplankton, patterns in mean Sv and center of mass were associated with wind and light patterns. (Figure 2.7 right panel). At this scale, water salinity was associated with fish center of mass and density and patchiness of zooplankton (Figure 2.7). Biological associations with wind patterns were tighter in autumn when storms are stronger and more frequent. Associations with salinity

were stronger in autumn and spring months, typically October-November and April-May (see Appendix B) potentially associated with periods of sea-ice formation and melting.

Patterns in zooplankton mean Sv and aggregation index observed at the 14-day period were associated with wind speed (Figure 2.7d) and minimum air temperature, respectively (Figure 2.7a and d right panel), whereas no significant associations were observed for fish metrics at this scale (Figure 2.7 left panel). At the 6-day period midwater salinity and wind direction were associated with the fish aggregation index and zooplankton inertia (Figure 2.7d left panel and Figure 2.7c right panel). Peaks in variance observed between 1–3-day periods in fish and zooplankton location and dispersion in the water column (i.e. center of mass and inertia) could not be associated with any environmental variables (Figure 2.7).

2.3.3.2.3 Seasonal and annual variability

Variability in biological metrics at scales ranging from 3 to ~ 6 months was associated with distinct environmental covariates and potentially reflects differences in seasonality among physical drivers (see Appendices B and C). Covariates associated with biological metrics at each of these periods varied between fish and zooplankton (Figure 2.7). For fish, significant coherence at the ~ 3-month period was observed between mean Sv and bottom salinity, and between inertia and sun altitude. No significant associations were found for center of mass (Figure 2.7 left panels). For zooplankton, significant coherence at a 3-month period was present between mean Sv, center of mass, inertia, and sea ice concentration (Figure 2.7 right panels).

High variance at the ~ 5.5-month time scale observed in fish metrics (mainly mean Sv, center of mass, and inertia, Figure 2.3a-c) was associated with multiple temperature metrics (Figure 2.7a-c left panels). In particular, water temperature (both midwater and bottom) was associated with fish mean Sv, inertia, and aggregation index. Center of mass was associated with

midwater ocean temperature and daily maximum air temperature (Figure 2.7 left panels). Water temperature values that remain at the freezing point half of the year (October–April) undergo warming-cooling cycles over a ~ 5-month period. Water temperature starts to increase in June-July, reaches maximum values in August–September, and returns to minimum values by October-November (Figure 2.2e). Biological variability shifted from a time scale of ~ 5.5 months in 2015, 2016, and 2018 to ~ 6 months in 2017 (Figure 2.3) coinciding with temperatures remaining relatively high for an extended period of time in summer of 2017 (Figure 2.2e). In particular, I observed that coherence between fish mean Sv and water temperature was highest from October to February each year and was particularly strong in 2017. Significant, in-phase associations between water temperature and fish dispersion were present through April 2016–February 2017 and September 2017–February 2019 whereas significant, out-of-phase associations with the aggregation index were present only during 2018 (see Appendix B). Significant associations were also observed with wind speed during fall and winter months each year (November 2016–January 2017 and October 2018–April 2019) when stronger winds enhance mixing of the water column. For zooplankton, variance in the center of mass at this scale (Figure 2.4b) was not associated with temperature but with fluctuations in sea ice concentration and wind speed (Figure 2.7b, right panel). This association between center of mass and sea ice concentration was present throughout the time series except for January–October 2017 and January–August 2019 when significant, out-of-phase coherence with light irradiance was observed (Table 2.1, Appendix B).

Variability observed at the ~ 4-month time scale in zooplankton mean Sv (Figure 2.4a) was associated with air temperature and light irradiance (Figure 2.7a, right panel) whereas 4-month cycles in inertia (Figure 2.4c) were associated with temporal patterns in sea ice concentration (Figure 2.7c, right panel). These associations were present throughout the year although stronger

in October 2016-September 2017 and again from October of 2018 until the end of the time series. For fish, significant coherence at a ~ 4-month period between mean Sv and bottom salinity were only observed during summer months with both variables out of phase (Table 2.1, Appendix B).

At the largest time scale (i.e. 1-year period), all biological metrics of both backscatter groups were associated with all physical variables except for salinity (Figure 2.7). This observation is consistent with weak annual cycles observed in the salinity time series (Figure 2.2f). At the 1-year period, significant associations were consistent through time, except for wind speed where coherence with fish and zooplankton metrics decreased to non-significant values in January 2018 (Appendix B). Sea ice concentration was out of phase with mean Sv and inertia and in phase with center of mass for both backscatter groups at the annual scale. Minimum densities and dispersion of organisms located deeper in the water column were associated with highest sea ice concentrations in winter months (Figure 2.2e and Appendix B). Water temperature was in phase with mean Sv and inertia (Figure 2.7). Highest densities of highly dispersed organisms were recorded around October each year associated with warmest waters (Figure 2.2e). Light irradiance and wind direction led fish and zooplankton densities by ~ 90°, whereas the two variables were out of phase with center of mass (Table 2.1). The largest scale of variation in the zooplankton aggregation index, observed at a 9-month period (Figure 2.4d), was associated with patterns in air temperature, sea ice concentration, light irradiance, and wind direction (Figure 2.7d right panel).

In summary, despite the shallow depths of the CEO and the lack of changes in light intensity during polar night and midnight sun, fish and zooplankton displayed DVM throughout most of the year. Water temperature, sea ice concentration, and light radiation patterns tended to be the most important environmental factors associated with biological metrics at the longest time scales. Salinity and wind patterns were important at seasonal-related (time scales ranging from 3 to ~6

months), and intermediate (3–28 days) scales. Sea ice concentration was strongly associated with zooplankton metrics at time scales from 28 days to one year, while its association with fish metrics was only significant at the annual scale. Wind speed and direction were sporadically associated with biological metrics over a broad range (6 days–1 year) of time scales.

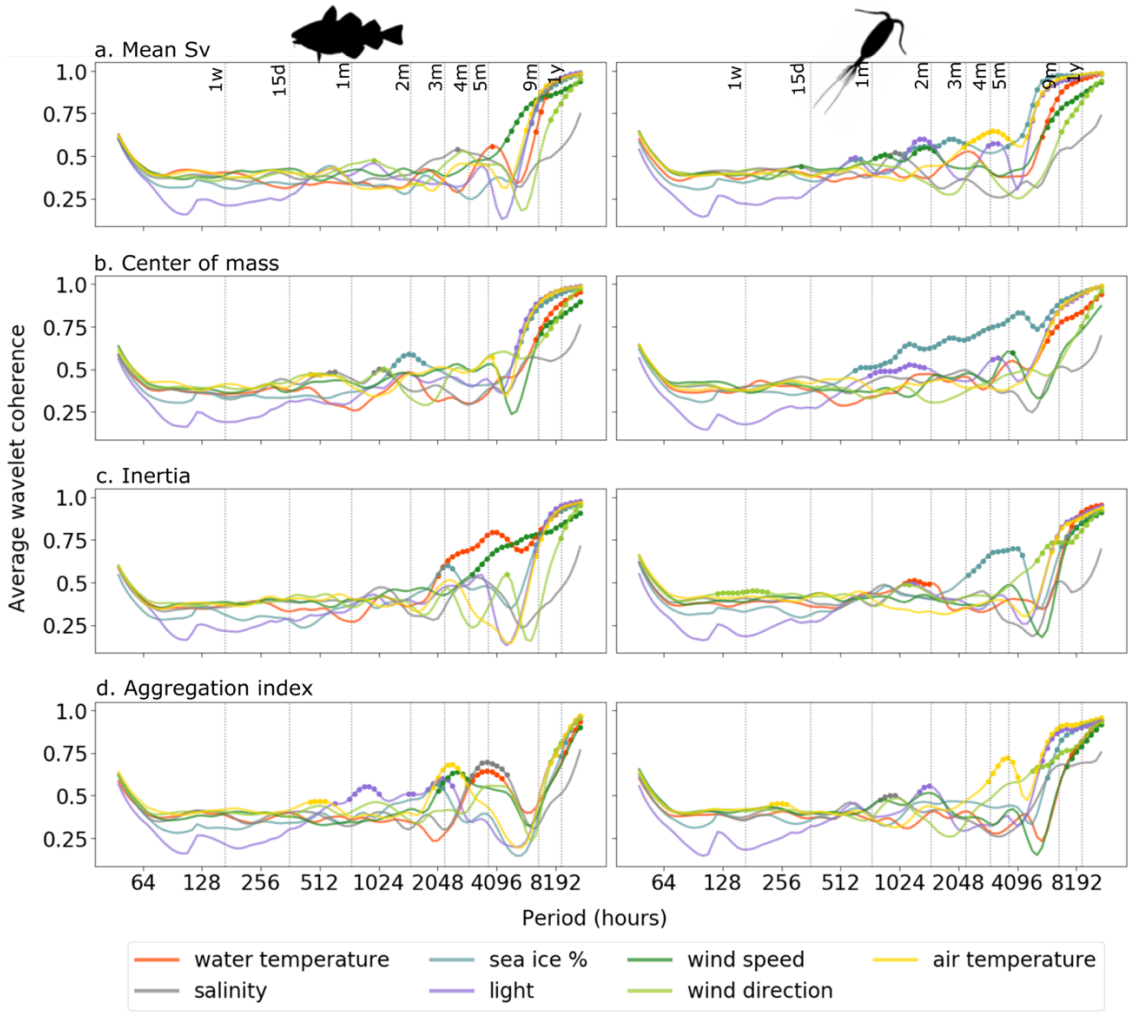

Figure 2.7. Average wavelet coherence between daily values of fish (left panel) and zooplankton (right panel) density and vertical distribution metrics derived from acoustic backscatter and physical environmental variables at the CEO. (a) Mean Sv, (b) center of mass, (c) inertia, (d) aggregation index. Circles represent significant values at the 95% confidence. Water temperature corresponds to midwater temperature and bottom salinity is shown for fish and midwater salinity is shown for zooplankton. Dotted lines indicate periods of 1 week, 15 days, 1–5 months, 9 months, and 1 year.

Table 2.1. Summary table indicating presence (colored cells) of each of the scales of variability (identified as dominant in section 3.2) in metrics for fish (blue) and zooplankton (orange). When present, significant associations between metrics and environmental variables at each scale are represented using + or – depending if the variables are in phase or out of phase, respectively. Sv: mean Sv; Cm: center of mass; In: inertia; Ai: aggregation index; MW temp.: midwater temperature; Air temp.: air temperature; Sea ice %: sea ice concentration; Sun alt.: sun altitude; Ws.: wind speed; Wdir.: wind direction; B sal.: bottom salinity; MW sal.: midwater salinity.

	Fish				**Zooplankton**			
	Sv	Cm	In	Ai	Sv	Cm	In	Ai
1 year								
MW temp.	+	+	+	-	+	+	+	-
Air temp.	+	-	+	-	+	-	-	-
Sea ice %	-	-		+	-	+	-	+
Sun alt.	-	-	-	-	-	-	-	+
Ws.	+	+	+	-	+		+	-
Wdir.	-	-	-	+	-	-	-	+
9 months								
Air temp.								-
Sea ice %								+
Sun alt.								+
Wdir.								+
5 months								
MW temp.	+		+					
Air temp.		-						
Sea ice %						+		
Ws.						+		
Wdir.			-					
4 months								
Air temp.					+			
Sea ice %							+	
Sun alt.					-			
3 months								
Sea ice %						+		
Sun alt.			+					
B sal.	-							
2 months								
28 days								
Sea ice %						+		
Sun alt.				+	-	-	-	
Ws.					+			
Wdir.	+	+					+	
MW sal.					+			+
B sal.		+						
14 days								
Air temp.								-
Ws.					+			
6 days								
3 days								
24 hours								

2.4 DISCUSSION AND CONCLUSIONS

In this study, focused on a high latitude marine ecosystem, I used multi-year abundance and behavior metrics of pelagic fish and macrozooplankton, and environmental covariates to identify scales of temporal variability. I observed that (1) variability in biological characteristics occurs at multiple temporal scales, (2) the relative importance of scale-dependent patterns in biological metrics varies through time, (3) coherence between environmental factors and biological metrics is scale-dependent, and (4) the strength of those biological-physical associations varies through time.

2.4.1 *Diel variability and predator-prey associations*

A strong diel signal (i.e. variability at a 24-h period) was observed in all metrics and backscatter groups. Diel variations in the vertical distribution of fish and zooplankton densities have been well described in many aquatic systems (Hays 2003; Cohen and Forward 2009). DVM is thought to be an evolved response to limited food at depth and avoidance of visual predators in shallow waters (Hays 2003). These vertical movements typically involve the upward migration of organisms to feed in surface waters at night and movements to depth to seek refuge from visual predators during the day, all cued by changes in light irradiance (Cohen and Forward 2009). In high latitudes, DVM have been observed during fall and spring, when pronounced day-night cycles are present (Falk-Petersen et al. 2008; Gjelland et al. 2009; Darnis et al. 2017). Despite the shallow depth at the CEO site, I observed fish and zooplankton DVM throughout most of the year, with the diel signal strongest during fall and spring.

A growing body of studies have shown that organisms respond to subtle changes in background light in the dark winter (Berge et al. 2009; Cohen et al. 2015; Hobbs et al. 2018). At the CEO, DVM by both fish and zooplankton persisted through the polar night (November–

January), with the signal more pronounced in fish. Age-0 Arctic cod is by far the most abundant species in the NE Chukchi Sea during summer (De Robertis et al. 2017) and can also be reasonably expected to be dominant under the sea ice in winter. Benoit et al. (2010) reported that young Arctic cod undergo DVM from December to May (beginning of midnight sun) possibly to avoid feeding interference with adult Arctic cod that remain at depth in the Beaufort Sea. For zooplankton, weakening of the DVM signal during winter could be a result of decreases in zooplankton abundances combined with the presence of both migrant and non-migrant zooplankton species in the CEO's winter assemblage. In winter, high abundances of *O. similis* copepods and lower abundances of stage five copepodites of *C. glacialis* were observed in sediment trap samples obtained at the CEO (Lalande et al. 2020). *O. similis* has been reported to perform small scale DVM in the Arctic (Ashjian et al. 2003; Daase and Falk-Petersen 2016) whereas stage five copepodites of *C. glacialis* enter diapause to overwinter at depth (Falk-Petersen et al. 2009; Elliott et al. 2017) and would not contribute to an acoustically-detected DVM signal in winter.

Occurrence of zooplankton DVM during midnight sun has been variable among study sites (Fortier et al. 2001; Blachowiak-Samolyk et al. 2006; Cottier et al. 2006; Wallace et al. 2010) suggesting that local characteristics (e.g. species composition, presence/absence of sea ice, and prey distribution) influence the occurrence and strength of DVM. Coarse temporal and vertical depth resolution of previous studies could be failing to detect DVM that occurred over a shorter duration and vertical distance in summer (Daase and Falk-Petersen 2016). At the CEO during midnight sun (May–August), the diel signal was absent for fish but present with minimal but significant strength for zooplankton. Benoit et al. (2010) reported a lack of synchronized movements of Arctic cod during midnight sun but the authors suggest that short individual (unsynchronized) migrations were possible. In this period of continuous light irradiance, Arctic

cod and other planktivorous fish use shoaling in surface layers as an alternative or complementary strategy for predation avoidance (Gjelland et al. 2009; Matley et al. 2012). DVM persistence for zooplankton in May-June could be attributed to the presence of sea ice and phytoplankton aggregations at the CEO. Sea ice and dense phytoplankton layers that often occur near the subsurface pycnocline could attenuate light in the water column and provide these smaller (and less visible) organisms refuge from visual predators for a longer period of time (Lorenzen 1972; Wallace et al. 2010). Fortier et al. (2001) observed that herbivorous copepods *C. hyperboreus*, *C. glacialis*, and *Pseudocalanus acuspes* displayed normal DVM under ice despite the midnight sun in Barrow Strait. Once sea ice melts, the lack of light attenuation and increased phytoplankton availability as food throughout the water column could make zooplankton DVM unnecessary (Blachowiak-Samolyk et al. 2006), limited to a part of the population (Dale and Kaartvedt 2000), or become unsynchronized (Cottier et al. 2006).

At the diel scale, I observed co-variations in fish and zooplankton densities, which were accentuated around March. We cannot determine if this co-variation is a result of fish chasing their zooplankton prey or an avoidance response to their own visual predators. Supporting the latter, DVM patterns displayed by Arctic cod under ice in the Beaufort Sea were associated with the presence of ringed seals (Benoit et al. 2010), a known predator of Arctic cod (Born et al. 2004). Synchronicity between zooplankton and fish was also observed at an annual scale. Fluctuations in organisms' densities occur throughout the year, with densities increasing from late spring to early autumn due to increased local production and arrival of organisms from the Bering Sea (Kitamura et al. 2017). At the annual scale zooplankton was leading in phase, indicating a faster response to changes in the environment than fish throughout the year. Densities of fish and their zooplanktonic prey were synchronized at several other intermediate temporal scales, mainly during winter

months. This high coherence of fish and zooplankton abundance in winter could be attributed to the overall reduction of organisms in the region during this season rather than to an interaction between predators and their prey. Even though feasible interpretations for strong covariations in fish and zooplankton densities are provided, there are caveats that need to be considered. First, fish and zooplankton density estimates are not independent, and we could expect some bias caused by a misclassification of fish and/or zooplankton acoustic backscatter. Second, acoustic backscatter classified as zooplankton represents a species assemblage. Fish, predominantly age-0 Arctic cod, could be preying on a subset of zooplankton species or on smaller zooplankton that were excluded in this study. Third, covariations between predator and prey could be generated by a common response of fish and zooplankton to a single or a combination of environmental drivers operating at a similar scale, rather than by a true interaction between predators and prey.

2.4.2 *Multi-day to monthly variability*

Cyclic extrinsic (e.g. moon phase) or intrinsic (e.g. hunger-satiation) cues can shape patterns in fish and zooplankton biomass distributions at temporal scales ranging from days to several weeks (e.g. Campbell et al. 2008; Berge et al. 2015; Last et al. 2016). Variability in fish and zooplankton vertical distributions observed at a ~ 28-day and ~ 14-day periods from late fall to early spring could be associated with lunar and semi lunar cycles. During polar night, the moon is the dominant source of ambient light and may facilitate visual predation during winter (Berge et al. 2015). Last et al. (2016) observed that zooplankton sink to deeper waters every 29.5 days in winter coincident with periods of the full moon in the lunar cycle. Marine species can synchronize their distribution and behavior to the semi-lunar cycle, which is coincident with full or new moon phases (Berge et al. 2015).

Periodicities of 4–12 days in fish center of mass observed during winter at the CEO could be a result of hibernation cycles interrupted by short feeding excursions by small arctic cod. During winter in the Southern ocean, Campbell et al. (2008) observed that Antarctic cod (*Notothenia coriiceps*) enter a state of dormancy interrupted by awakenings of a few hours every 4–12 days. Benoit et al. (2010) suggested that Arctic cod could also be undergoing dormant-wake cycles in the Beaufort Sea during winter.

Temporal patterns in salinity and wind were also associated with fish and zooplankton density and vertical distribution metrics at scales of 6–28 days. Wind direction and strength affect properties of Chukchi shelf waters through changes in circulation or stratification/mixing of the water column in summer and fall (Weingartner et al. 2013; Danielson et al. 2017a). In autumn, enhanced mixing by strong wind events can re-nourish depleted surface waters with nutrients from below the stratified layer, triggering a phytoplankton bloom (Lin 2012; Zhao et al. 2015) with cascading effects to higher trophic levels (Fujiwara et al. 2018). Changes in salinity, that are associated with changes in water masses and sea ice cycles, have also been reported to influence species' distributions in the Pacific Arctic (e.g. Norcross et al. 2010; Ershova et al. 2015). Bottom salinity is one of the main environmental factors affecting demersal fish assemblages in the Chukchi Sea (Norcross et al. 2010) whereas surface salinity has been reported as an important factor influencing zooplankton distributions (Ershova et al. 2015). In this study, fish and zooplankton distribution patterns were associated with salinity. The occurrence of these associations coincided with sea ice formation and melt as well as with autumn strengthening of local winds at the CEO.

2.4.3 *Seasonal and annual variability*

There was no single scale of seasonal variability in fish and zooplankton metrics values, nor could seasonal time scales be attributed to a single environmental factor. Scales of seasonal variability and scale-dependent associations with environmental factors were also different for fish and zooplankton.

A seasonality of 3 months in zooplankton metrics corresponded to temporal patterns in sea ice concentration, whereas 3-month cycles in fish metrics appeared related to variability in water salinity. Temporal patterns in sea ice formation and melt modulate light irradiance and stratification of the water column, directly affecting temporal patterns of ice algae, phytoplankton (Palmer et al. 2014), and in turn, zooplankton production (Matsuno et al. 2011; Questel et al. 2013; Amano et al. 2019). Ice algae initiate primary production underneath the ice during late winter–early spring (typically in March) at very low light intensities and constitute an early food source for zooplankton (Søreide et al. 2010). In spring, increased insolation, stratification from ice melt, and availability of nutrients accumulated during the winter, trigger the onset of a phytoplankton bloom that sustains annual zooplankton production (Søreide et al. 2010; Leu et al. 2011; Arrigo et al. 2012a; Leu et al. 2015). In particular, *Calanus glacialis* has synchronized its seasonal vertical migrations, reproduction, and growth to these two bloom events. The ice algae bloom is thought to fuel early maturation and reproduction of zooplankton whereas the subsequent phytoplankton bloom provides high-quality food to the resulting zooplankton offspring (Søreide et al. 2010; Leu et al. 2011; Barber et al. 2015). This tight control exerted by seasonal sea ice on densities and vertical distributions of zooplankton is consistent with patterns observed in this study.

Temperature is known to structure habitats of Arctic fish species and to affect their distribution (Benoit et al. 2014; Sigler et al. 2017), growth (Bouchard and Fortier 2011; Laurel et

al. 2016), and abundance (Mueter et al. 2016). Chukchi shelf water masses that start cooling approximately in October and remain close to the freezing point through April warm in summer when northward transport of warmer waters from the Bering Sea is highest (Danielson et al. 2017a; Lu et al. 2020). In the NE Chukchi Sea, the arrival of warmer waters from the Bering Sea generally increases the abundance of organisms in summer through the addition of imported boreal organisms and enhancement of local growth (Questel et al. 2013; Ashjian et al. 2017). As water temperature cools in autumn, densities of organisms decrease. This has been attributed to unsuccessful overwintering of boreal species (Kitamura et al. 2017) or horizontal migrations of local species to overwinter in adjacent deeper waters (Kosobokova 1999; Benoit et al. 2008, 2010; Geoffroy et al. 2011). I observed water temperature-associated variability in fish metrics at the ~ 5-month period mainly from late spring to early fall, which corresponds to transitional periods from cold to warm and return to cold "seasons". Similar patterns in fish location and dispersion at the ~ 5-month scale might also be indicative of seasonal vertical migrations associated with species life cycles (i.e. ontogenetic migrations; Geoffroy et al. 2016; LeBlanc et al. 2019) and behavioral changes (e.g. summer shoaling, Gjelland et al. 2009; Benoit et al. 2010) that typically occur from late spring to fall. However, variability in the vertical distributions of zooplankton species during these transitional periods seemed to respond to seasonal transitions from ice covered to open waters (and the reverse), and changes in wind speed. These two factors affect stratification of the water column, that in turn, modulate the timing and amplitude of primary production blooms. Some zooplankton species (e.g. *C. glacialis*) perform ontogenetic seasonal vertical migrations that are tightly synchronized with blooms events (Søreide et al. 2010; Darnis and Fortier 2014).

Similarly, ~ 4-month cycles in zooplankton densities associated with air temperature and light irradiance at the CEO might be indicative of transitional periods between seasons. During these

periods high variations in zooplankton densities are expected in response to changes in sun radiation and air temperature that control the onset of primary production (Søreide et al. 2010). Shorter seasonal cycles in zooplankton, compared to fish, could be associated with a faster response to changes in the environment and synchronicity of their life cycles to temporal patterns in food availability that are triggered mainly by changes in irradiance (Mundy et al. 2014). Longer seasonal cycles in fish are possibly explained by slower changes in water temperature throughout the year.

Variations in water temperature, sea ice concentration, light irradiance, and wind throughout a year shape the conspicuous annual cycles in fish and zooplankton metrics at the CEO. As described above, these factors play a key role in pelagic organisms' growth, reproduction, and distribution. Temperature regulates the growth rate of fish and zooplankton, while light irradiance, sea ice concentration and winds modulate primary and secondary production, either directly or through the modulation of light and nutrient availability. Biological interactions might also play a role shaping fish and zooplankton temporal patterns in addition to the physical environment. In particular, predation pressure and light irradiance could be responsible of the 9-month cycles observed in zooplankton patchiness instead of the annual cycle observed for all other metrics. Persistence of dense patches of zooplankton individuals throughout periods of continuous daylight in summer have been described as a strategy to reduce predation risk (Majaneva et al. 2013).

2.4.4 *Importance and applications*

The need to address scale-dependency of biological patterns is well recognized in ecological literature (Stommel 1963; Haury et al. 1978; Levin 1992; Schneider 1994). Understanding temporal variability across a broad range of scales is essential to derive general conclusions about species abundance and behavior dynamics. As demonstrated in this study, fish and zooplankton

metrics not only undergo variability at a range of temporal scales but also the relative importance of these scales may vary through time. As a result, an extrapolation of observed patterns from a short temporal extent may not be representative of patterns occurring at other times of the year. This emphasizes the importance of continuous year-round studies to obtain a complete description of biological patterns in high latitude marine ecosystems. Scale- and time-dependent characterization of marine ecosystems requires continuous, high-resolution, long-term datasets that are not possible to obtain using traditional vessel-based sampling methods, especially in high latitudes. The use of active acoustics integrated with other sensors in ocean observing platforms provides simultaneous measurements of multiple ecosystem components at high temporal resolution over long periods. Time-frequency decomposition of biological and physical series using wavelets and wavelet coherence enabled identification of dominant scales of variability, located the occurrence of those periodicities in time, and helped identify potential environmental processes associated with observed biological patterns. Studies of temporal variability typically look at variations in the amplitude of a variable in the time domain (e.g. Gaston and McArdle 1994). Even though variability is rarely used as a response variable to assess the influence of environmental disturbances, it is an extremely sensitive metric that can provide ecological information about underlying causal processes (Fraterrigo and Rusak 2008).

A characterization of scale-dependent biological patterns and associations with environmental factors is a first step towards a mechanistic understanding of ecosystem dynamics. This understanding is necessary to predict biological responses to environmental change. Rapid changes in the Chukchi physical environment have been reported and further changes are expected (Wood et al. 2015; Woodgate 2018). Some of these changes include reduced seasonal sea ice extent and duration, increased ocean temperatures, and increased freshwater content (Stroeve et al. 2007;

Polyakov et al. 2010; Steele et al. 2010; Lu et al. 2020). Changes in the physical environment are expected to alter amplitude, periodicity, and timing of biological production (Grebmeier 2012). Predicting the potential direction and magnitude of these changes will help design or improve mitigation strategies and management of arctic marine species. Arctic cod has been identified as a species of potential commercial importance in the Arctic Fishery Management Plan (NPFMC 2009). In the context of potential harvest, a characterization of variability scales in Arctic cod abundance can be used to inform stock assessments that provide accurate biomass estimates and detect trends in population variability. A characterization of scale-dependent temporal patterns can also be used to inform the design of monitoring programs to ensure detection of change in an already highly variable environment. Both sampling resolution and extent can be defined using natural scales of biological variation rather than arbitrary or convenience scales (e.g. annual surveys during open water season), allowing the distinction between "natural" variability from differences in the timing or resolution of sampling. A continuous, long term characterization of biological patterns can be used to identify a baseline, and subsequent deviations can be quantified to characterize and determine change.

Chapter 3. MACROSCOPIC TEMPORAL PATTERNS AND ENVIRONMENTAL DRIVERS OF ARCTIC COD ("*BOREOGADUS SAIDA*") DENSITIES IN THE NE CHUKCHI SEA

3.1 INTRODUCTION

Changes in the Arctic environment are indisputable. Increases in water temperature over the last century that have intensified since 1995 (Steele et al. 2008) are coupled with drastic reductions in the duration of the sea-ice covered season (Serreze et al. 2016), summer minimum and winter maximum sea-ice spatial extents (Comiso and Parkinson 2004), and sea-ice and snow cover thickness (Kwok 2018). Changes in sea-ice affect the entire underwater climate as sea-ice modulates underwater light irradiance, sea surface temperature, stratification/mixing of the water column and subsequent nutrient replenishment (Mundy et al. 2005; Hill et al. 2018b). Impacts of climate warming on biological communities have been documented for arctic marine ecosystems including an increase in primary production (e.g. Arrigo and van Dijken 2015; Lewis et al. 2020), a shift towards smaller phytoplankton and zooplankton species (e.g. Hop et al. 2006; Li et al. 2009; Møller and Nielsen 2020), changes in species phenology (e.g. Søreide et al. 2010; Ji et al. 2013; Ardyna and Arrigo 2020), and northward expansion of boreal fish and zooplankton species distributions (e.g. Fossheim et al. 2015; Polyakov et al. 2020)

Biological responses to large and rapid changes in the physical environment at high latitudes remain poorly understood (Grebmeier 2012; Post et al. 2013; Assmy et al. 2017; Drinkwater et al. 2018). This lack of understanding is attributed to the uncertainty of the overall effects of changes in combined factors (e.g. increase in light availability due to thinner ice and

snow cover or the decrease in light availability due to increased cloud cover) and limited, long term synchronous measurements of biological and physical environmental components. A better understanding of biological responses to further changes in the Arctic ecosystem requires identification of primary environmental factors associated with current biological patterns, and the characterization (i.e. strength and shape) of those associations using long term physical and biological time series.

Sea ice and water temperature have been proposed as the main environmental factors influencing fish and zooplankton biomass and behavior patterns. Sea ice constitutes a habitat for sea ice algae and regulates the light available for primary production (Søreide et al. 2010; Janout et al. 2016). Changes in sea ice thickness and break-up timing potentially affects timing and amplitude of sea ice algae and phytoplankton blooms, that in turn, affect zooplankton and fish production (Arrigo et al. 2012b, 2014; Arrigo and van Dijken 2015). Fish and zooplankton production are also affected by water temperature that is crucial for their optimal reproduction and development (Leu et al. 2011).

Arctic cod (*Boreogadus saida*) is the most abundant fish species in Arctic waters and has been identified as a species of potential commercial importance in the Arctic Fishery Management Plan (NPFMC 2009). This dominant species constitutes a key link between lower and higher trophic levels within the Arctic ecosystem (Welch et al. 1992; Whitehouse et al. 2014) being an important prey for birds, seals and whales (Bluhm and Gradinger 2008; Harter et al. 2013). Arctic cod lives in association with sea ice, where it feeds and spawns (Graham and Hop 1995; Bouchard and Fortier 2011). Therefore, changes in sea ice concentrations and timing will have direct and indirect effects on temporal patterns of Arctic cod densities that will affect the flow of energy in

marine Arctic food webs and the services they provide to northern communities (Darnis et al. 2012).

Four years of continuous, high-resolution biological and physical data streams from the Chukchi Ecosystem Observatory (CEO) will be used to (1) characterize macroscopic patterns in Arctic cod densities and (2) identify and quantify relationships between Arctic cod densities and environmental factors in years with different environmental conditions. Understanding bio-physical patterns in years with different sea ice conditions can help elucidate potential biological responses to further changes in the Arctic Ocean.

3.2 METHODS

3.2.1 *Study area*

The CEO is located on the NE Chukchi Sea shelf between Hanna Shoal and Barrow Canyon (71° 35.976' N, 161° 31.621' W) at 46 m depth (Figure 2.1). Located in the midst of a hotspot of benthic biomass (Grebmeier et al. 2015), the CEO area attracts populations of upper trophic level consumers (Jay et al. 2012; Hannay et al. 2013). The CEO seascape varies seasonally with a late fall and winter homogeneous water column with thickening sea ice and light-limited primary production (Weingartner et al. 2005), and a spring with diatoms and sea ice algae blooms triggered by the return of light (Gradinger 2009; Arrigo et al. 2014). When sea ice starts to melt after May, a stratified, warmer, nutrient-rich water column triggers massive phytoplankton blooms under the ice (Arrigo et al. 2012a) that continue through the summer (Hill et al. 2018a). In the fall, the intensification of winds and diminishing solar input allows the water column to re-homogenize and surface waters are replenished with nutrients that supports fall phytoplankton blooms until sunlight fades.

The Chukchi Sea continental shelf waters are highly influenced by northward-flowing waters from the North Pacific carrying heat, freshwater, and nutrients through the Bering Strait (Figure 2.1). This transport is driven by a seasonally fluctuating Pacific–Arctic pressure head (Stigebrandt 1984; Aagaard et al. 2006) that transmits 1.0–1.2 Sv during summer and 0.5–0.6 Sv during winter months (Woodgate et al. 2005a). Water flowing through Bering Strait is routed across the Chukchi shelf along three main pathways: Herald Canyon in the west, Barrow Canyon in the east and the Central Channel across the mid-shelf, although wind driven and other fluctuations episodically modify or even reverse these flows (Weingartner et al. 2005; Woodgate et al. 2005b).

3.2.2 *Environmental data*

A set of environmental data collected at the CEO during the study period (2016–2019) was supplemented with data from other sources for this study. Midwater measurements of salinity, temperature, photosynthetically active radiation (PAR), fluorescence, and nitrate concentration were collected hourly at the CEO using a Sea-Bird Scientific SBE-16 SeaCat and a Satlantic SUNA sensor deployed at 28–33 m depth. Bottom temperature and salinity measurements were collected hourly using a Sea-Bird SBE-37 MicroCat located at a depth of 43 m (seafloor depth of 46 m).

In situ fluorescence concentration measurements (a proxy for chlorophyll a concentration) were not available for the August 15th 2017–August 5th 2018 period and were predicted using the auto-sklearn machine learning tool kit (Feurer et al. 2015). The automatic machine learning framework takes a Bayesian optimization algorithm as the core method to conduct the automation of feature engineering, classifier selection, and hyper-parameter adjustment (Feurer et al. 2015). This method involved fitting a statistical model to observed *in situ* fluorescence based on daily

averages of all the variables described, and then using model-based predictions when observations were absent. Daily measurements of chlorophyll a from the MODIS sensor on the NASA Aqua satellite (https://polarwatch.noaa.gov/) were also included as a predictor in the models. A 10-fold cross validation data resampling method was used to split the dataset into train and test samples. The coefficient of determination (R^2) between observed and predicted fluorescence values was used as the optimization metric during training. The accuracy of predictions was evaluated using R^2, mean absolute percentage error, and root mean squared error (RMSE).

Daily averages of satellite-based sea ice concentration (%) data were downloaded from the National Snow and Ice Data Center (NSIDC) archive (http://nsidc.org/data/seaice/pm.html#pm_seaice_conc) (Maslanik and Stroeve 1999). Sea ice retreat and advance days were identified for each year, defined as the first day with sea ice concentration less than 30% and exceeding 30% each year, respectively (Serreze et al. 2016). Daily sunrise and sunset times at the CEO obtained using the 'sunriset' function of the R package *maptools* (v. 0.9-9, Bivand & Lewin-Koh 2019) were used to calculate daylength, a proxy of light irradiance throughout the year. Daily air temperatures recorded at the nearby coastal city of Utqiaġvik were obtained from the U.S. climate data website (https://www.usclimatedata.com/climate/barrow/alaska/united-states/usak0025). Hourly wind speed data for the CEO location were obtained from the Copernicus Climate Change Service (Hersbach et al. 2018).

3.2.3 *Acoustic data acquisition*

Four years (2016–2019) of active acoustic data were used to characterize temporal patterns in Arctic cod densities in the Chukchi Sea (Figure 2.1**Error! Reference source not found.**). Acoustic backscatter data, a proxy for fish density, were collected using an ASL, Acoustic

Zooplankton Fish Profiler (http://www.aslenv.com/AZFP.html), deployed at 28–35 m depth (depending on year), looking upwards. The instrument operated at 38 (12°), 125 (8°), 200 (8°), and 455 (7°) kHz (nominal beam width, measured between half power points given in parenthesis). The AZFP collected data every 15 seconds (0.067 Hz) at a vertical resolution of 4 cm. Every summer, a new mooring with a manufacturer-calibrated AZFP was deployed followed by the recovery of the previous mooring to ensure continuity of data collection.

3.2.4 *Acoustic data processing and classification*

Acoustic data from the CEO was processed using Echoview software (v. 11.0). Background noise of -135.45 dB re 1 m-1 (hereafter dB) was subtracted and a minimum signal-to-noise ratio filter of 6 dB was applied to each analytic cell. Backscattered energy within 3 m from the face of the transducer were excluded from the analyses to avoid the integration of echoes in the acoustic near-field. Sea water surface and sea ice edges were delimited using Echoview's linear offset operator algorithm followed by visual inspection and manual correction. A surface exclusion line was set 0.5 m below the corrected surface and echoes above the line were excluded to ensure that backscatter from surface turbulence or sea ice were not included in analyses.

Acoustic backscatter corresponding to fish was discriminated from other sources of backscatter using differences in mean volume backscattering strength (MVBS) (Madureira et al. 1993; Kang et al. 2002; Korneliussen and Ona 2003) between 125 and 38 kHz data (ΔMVBS125-38 kHz). Backscatter measurements were averaged in 4 pings (1 min) horizontal by 1 m vertical cells for each frequency. Cells with ΔMVBS125-38 kHz values in the range of -16 to 8 dB were classified as fish (cf. De Robertis et al. 2010). A minimum volume backscattering strength (Sv) integration threshold of -70 dB was applied to the 38 kHz ("fish") data (c.f. De Robertis et al.

2017b). Fish Sv values were integrated into hourly averages from January 1, 2016 to December 31, 2019.

Although no direct fish sampling was conducted in association with acoustic measurements, we can rely on catch data from fisheries surveys carried out in the NE Chukchi Sea to attribute most of the observed fish backscatter to Arctic cod (*Boreogadus saida*). Arctic cod accounted for 81–90% of total fish biomass and abundance from bottom (Barber et al. 1997; Goddard et al. 2014; Sigler et al. 2017; Logerwell et al. 2018) and pelagic (Lowry and Frost 1981; De Robertis et al. 2017) trawl surveys conducted from spring through autumn, ice-free seasons. From four midwater trawls conducted on Hanna Shoal in close proximity to the CEO in summer of 2017, Levine and De Robertis (pers. comm) observed that Arctic cod constituted the majority of fish biomass (63–99%) and abundance (93–99%). Other species caught near Hanna Shoal included capelin (*Mallotus villosus*), *Lumpenus* spp, staghorn sculpin (*Gymnocanthus tricuspis*), and Liparidae snailfish. As further support of this backscatter categorization, age-0 (i.e born within the past year) Arctic cod was the dominant contributor to 38 kHz backscatter in the northern region of the Chukchi Sea in acoustic-trawl surveys conducted in 2012 and 2013 as part of the Arctic Ecosystem integrated survey (De Robertis et al. 2017) and constituted > 85% of the catch per unit effort in a 2019 survey in the Chukchi Sea (Levine et al. 2021).

3.2.5 *Data analysis*

3.2.5.1 Macroscopic characterization of temporal patterns in Arctic cod backscatter

Ecosystems have complex dynamics that result from the combined effects of population dynamics, environmental variability, and species interactions. Macroscopic patterns (e.g. power laws and fluctuations distributions) are useful to provide general descriptions of a system without including

detailed information on interacting agents (Maurer 1999; Cohen et al. 2012; Segura et al. 2021). These macroscopic patterns allow to characterize dynamical and static patterns and compare among populations, ecosystems, or environmental conditions.

3.2.5.1.1 Taylor's power law

One effective way to summarize temporal patterns of a species is using Taylor's power law (TPL). TPL states that the spatial or temporal variance (V) in population abundance (N) is related to the mean (M) population abundance via: $V[N]=aM[N]^b$; b ~ 2) (Taylor 1961), with the coefficient a and the scaling exponent b. Conceptually, the scaling component b captures the level of aggregation between individuals in a population, while the coefficient a is considered an artefact of sampling methodology (Taylor 1961). When mean–variance pairs are estimated from abundances measured through time at the same location, the temporal aggregation in the populations is described. This is referred to as temporal TPL, where the scaling exponent, b, can be considered a measure of the magnitude of fluctuations in population abundance through time. The scaling exponent has been used as an ecological metric to compare fish populations between regions of contrasting environmental characteristics (e.g. Cobain et al., 2019; Mellin et al., 2010), at varying levels of fishing pressure (e.g. Cohen et al., 2012; Fujiwara & Cohen, 2015; Kuo et al., 2016; Segura et al., 2021), and between fish species with different life histories (e.g. Kuo et al., 2016).

Daily mean and variance in backscattering strength from Arctic cod were calculated from hourly values of the volume backscatter coefficient (sv: units: m-1; linear form of Sv [dB]). Days with less than 5 backscatter observations were excluded from the analysis to avoid bias in variance estimates. The TPL exponent and coefficient were estimated from the linear relationship of the base 10 logarithms of the sample's sV variance and mean described by:

$$log_{10}(V[s_V]) = log_{10}(a) + b\ log_{10}(M[s_V]) + \varepsilon \quad (3.1)$$

where ε is the residual error. TPL exponents and coefficients estimated using ordinary least squares linear relationships were compared among years. The null expectation for Taylor's power law for temporal variation is that the slope of the log variance versus log mean plot equals 2. Confidence intervals (95% level) were used to contrast estimated scaling exponents against the null hypothesis and to compare the exponents among years.

3.2.5.1.2 Backscatter fluctuation distributions

To characterize and compare Arctic cod population dynamics among years with different environmental conditions, I analyzed the distribution of fluctuations in Arctic cod mean Sv. Daily fluctuations in backscatter values (r) were calculated as the first difference between daily values of Sv for each year:

$$\mathrm{r} = N_{t+1} - N_t \quad (3.2)$$

where N are Sv values in a 10*log10 scale (dB). To identify what type of distribution better describes backscatter fluctuations at the CEO, a suit of candidate distributions including Gaussian distribution, t-distribution, skewed t-distribution and mix of Gaussians were fitted to Sv daily fluctuations each year. These distributions have been previously used to describe population fluctuations (e.g. Halley and Inchausti 2002; Anderson et al. 2017). The distributions were fitted using the R packages *MASS* (Venables and Ripley 2002), *fGarch* (Wuertz et al. 2020), and *mixtools* (Benaglia et al. 2009). For each year, a model (i.e. adjusted distribution) was selected using the Akaike Information Criterion (AIC).

3.2.5.2 Environmental drivers of Arctic cod densities

To identify associations between Arctic cod densities and environmental variables at the CEO I used Generalized Additive Models (GAMs). GAMs are nonlinear regression models in which the relationships between the response variable and the predictor variables are modeled using nonparametric smooth functions (Hastie and Tibshirani 1990; Wood 2004, 2017). GAMs represent an effective modeling approach for assessing the responses of fish communities to environmental factors (e.g. Sigler et al. 2015; Logerwell et al. 2018; Forster et al. 2020). The advantage of this method is that it is not necessary to specify the type of relationship between the variables a priori because these can be determined from the data. Specifically, given a response variable y and a set of m predictor variables x (covariates), the relationship between the two is established by:

$$y_i = \alpha + \sum_{j=1}^{m} s_j(x_{ji}) + e_i \quad (3.3)$$

The error term, e_i is generally assumed to be independent and identically distributed with zero mean and common variance. The g_j are smooth nonparametric functions estimated using thin plate regression splines (Wood 2017). Smoothing parameters were selected using restricted maximum likelihood (REML) which penalizes overfitting more than other methods (Wood 2011). Daily averages of mean volume backscattering strength attributed to Arctic cod were used as a response variable. Days with no backscatter (7% of measurements) were excluded so fitted GAMs describe the densities of Arctic cod when present. Daily averages of midwater and bottom temperature and salinity, sea ice concentration, number of days after sea ice retreat, air temperature, chlorophyll a concentration, PAR, nitrate concentration, wind speed, and daylength were included as covariates in candidate models. Year was included as a factor in all models. Time series of environmental covariates included in candidate GAMs are shown in Appendix D.

Collinearity among covariates was identified from the variance inflation factor (VIF) using a value of less than 5 as a cutoff for inclusion of covariates in the same candidate model (Zuur et al. 2009).

GAMs were fitted using the *mgcv* (version 1.8–38; Wood, 2017) package in R using a Gaussian distribution and identity link function. To account for autocorrelation in the time series, an AR(1) (i.e. autocorrelation of order one) term was included in all candidate models. The model with the lowest AIC was selected. Residuals from each model were visually compared to the normal distribution using quantile-quantile plots. Autocorrelation functions (ACF), and partial autocorrelation functions (PACF) were calculated to check for any remaining autocorrelation within the residuals.

3.3 RESULTS

3.3.1 *Macroscopic temporal patterns in environmental variables and Arctic cod backscatter*

Sea ice retreat occurred earlier in 2017 (June 3rd) and 2019 (May 12th) compared to 2016 (July 13th) and 2018 (July 14th) (Figure 3.1a). Sea ice advance occurred later in 2017 (December 5th) and 2019 (December 7th) compared to 2016 (November 21st) and 2018 (November 23rd) (Figure 3.1a). This resulted in longer open water periods (i.e. period between retreat and advance dates) in 2017 (185 days) and 2019 (209 days) than in 2016 (131 days) and 2018 (132 days). Retreat and advance dates in 2016–2019 were up to two months earlier than the historic mean retreat date (July 27th) and about one month later than the historic advance date (October 31st) resulting in open water seasons longer than the historic average of 96 days. Annual average sea ice concentrations were lower in 2017 (43%) and 2019 (40%) than in 2016 (58%) and 2018 (57%). Annual average sea ice concentrations for all years were below the historic (1975–2015) annual average of 67%.

Maximum midwater temperatures recorded at the CEO were greater in 2017 (3.87 °C) and 2019 (3.83 °C) than in 2016 (2.11 °C) and 2018 (1.31 °C) (Figure 3.1b). Midwater temperature peaks occurred on October 28th in 2016, October 6th in 2017, November 15th in 2018, and on November 1st in 2019 (Figure 3.1b). Average midwater temperatures were -1.04 °C in 2016, -0.53 °C in 2017, -1.31 °C in 2018, and -1.02 °C in 2019. Midwater temperatures in 2017 and 2019 were higher than in 2016 and 2018 during late spring–early summer (June–mid July) and during Autumn (late October–mid November) (Figure 3.1b).

Years 2016 and 2018 (hereafter "cold" years) were characterized by later sea ice retreat, earlier advance, greater sea ice concentration, and lower water temperatures than 2017 and 2019 (hereafter "warm" years).

Peaks in fish backscatter attributed to Arctic cod had higher amplitude and occurred earlier in the summer in "warm" than in "cold" years (Figure 3.1c). Peak Sv values of -80.97 dB (9/29/2016), -70.60 (7/31/2017), -82.81 dB (9/2/2018), and -77.80 dB (8/19/2019) were observed in the 7-day smoothed series (Figure 3.1c). In "warm" years, peak values were ~3–12 dB greater than in "cold" years corresponding to ~2–16 times more fish in years with earlier sea ice retreat and higher water temperatures. Peaks in Sv values occurred 14–60 days earlier in "warm" than "cold" years. Peaks in Sv occurred 78 days after sea ice retreat in 2016, 58 days in 2017, 50 days in 2018, and 99 days in 2019.

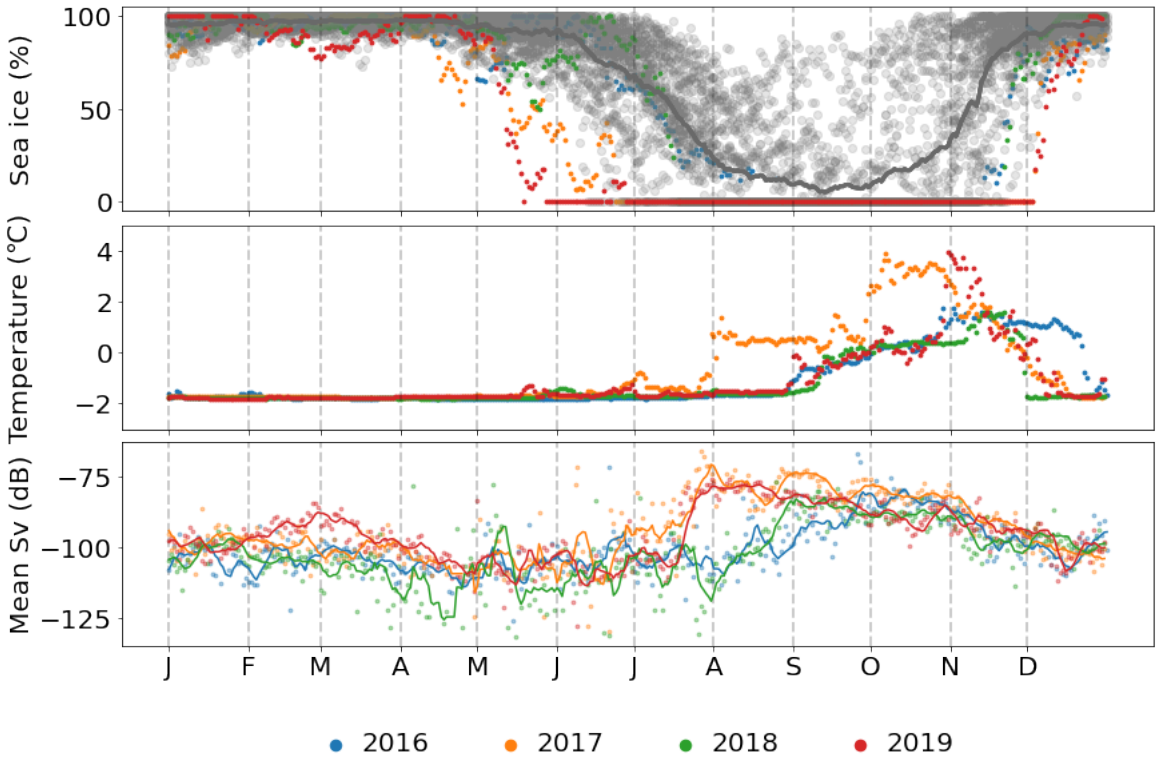

Figure 3.1. Biological and physical patterns at the Chukchi Ecosystem Observatory. (a) Daily sea ice concentration from satellite data. Grey circles represent values from 1978–2015 and the grey line represents the average sea ice concentration for that period. (b) Daily averages of *in situ* measurements of midwater temperature. (c) Daily mean backscattering strength (mean Sv) values corresponding to Arctic cod. Lines represent weekly moving averages and horizontal lines indicate days from sea ice retreat date to the peak in Arctic cod backscatter each year.

The medians of the non-zero backscatter values were greater (Kruskal-Wallis $p < 0.05$) in "warm" years (-95.10 dB in 2017 and -95.31 dB in 2019) than in "cold" years (-101.47 dB in 2016 and -101.10 dB in 2018 (Figure 3.2). Most frequent backscatter values were ~ -100 dB all years but a second mode at relatively high backscatter values (greater than ~ -85 dB) was observed during "warm" years (Figure 3.2). During "cold" years the percentages of hours with no backscatter were greater (69% in 2016 and 63% in 2018) than in "warm" years (51% in 2017 and 43% in 2019).

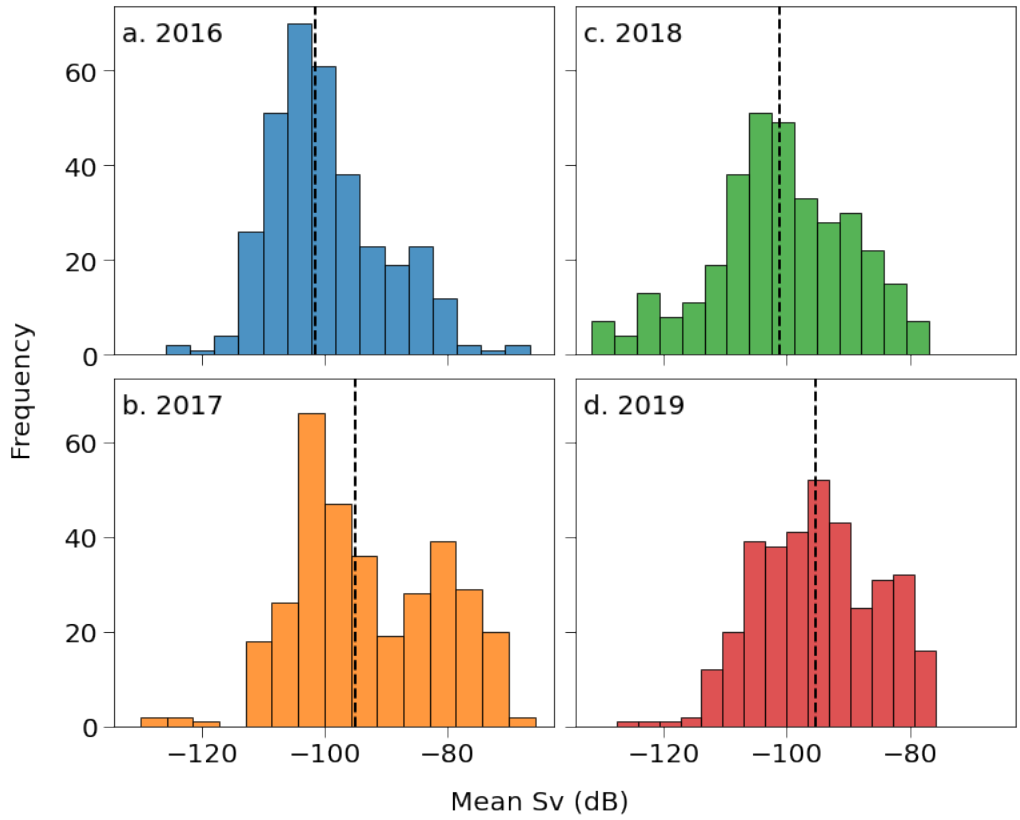

Figure 3.2. Distribution of daily averages of hourly mean backscattering strength (mean Sv) values corresponding to Arctic cod (*Boreogadus saida*) for 2016–2019. The dashed line indicates the median.

Peaks in variance occurred 27–56 days earlier in "warm" years than in "cold" years (Figure 3.3). Highest variances were observed during autumn months in 2016 (October 7th) and 2018 (September 11th) and in the summer in 2017 (August 12th) and 2019 (August 14th). Overall, variability was highest in 2017 (-153.40 dB) followed by 2016 (-157.16 dB), 2019 (-167.03 dB), and 2018 (-172.64 dB). In "warm" years variance was higher than "cold" years during July–September and mid-January–April.

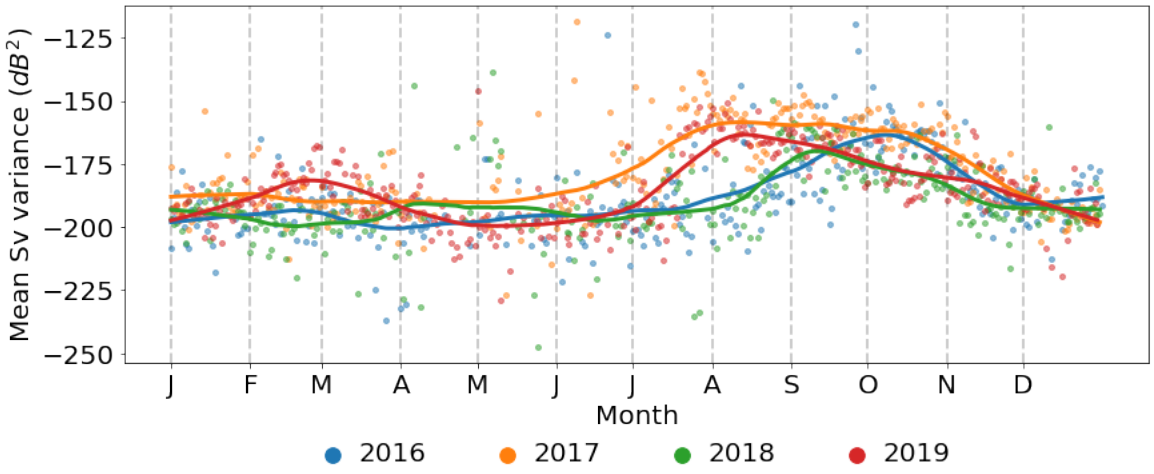

Figure 3.3. Variance calculated over a 1-day period from hourly mean backscattering strength (mean Sv) values corresponding to Arctic cod (*Boreogadus saida*). Lines represent lowess smoothing with window size =0.2 for each year.

3.3.1.1 Backscatter mean and variance: Taylor's power law

Significant log–log relationships between variance and mean s_V were observed all years at the p=0.05 level with coefficients of determination (R^2) greater than 0.94 (Figure 3.4). Variance increased faster (i.e. slope *b* significantly greater) in 2016 (*b*=2.36) and 2018 (*b*=2.16) than in 2017 (*b*=1.79) and 2019 (*b*=1.93). The scaling exponent *b* was significantly greater than the theoretical value of 2 in "cold" years, and significantly below 2 in "warm" years (Figure 3.4). These observations suggest that overall, Arctic cod at the CEO experiences greater temporal fluctuations (i.e. shorter persistence time) in density during "cold" years than in "warm" years. Regression lines intersect each other at $\log_{10}M(s_v) \sim$ -9 dB (mean Sv = -90 dB) with "warm" years exhibiting higher variability at low fish densities and lower variability at relatively high densities than "cold" years.

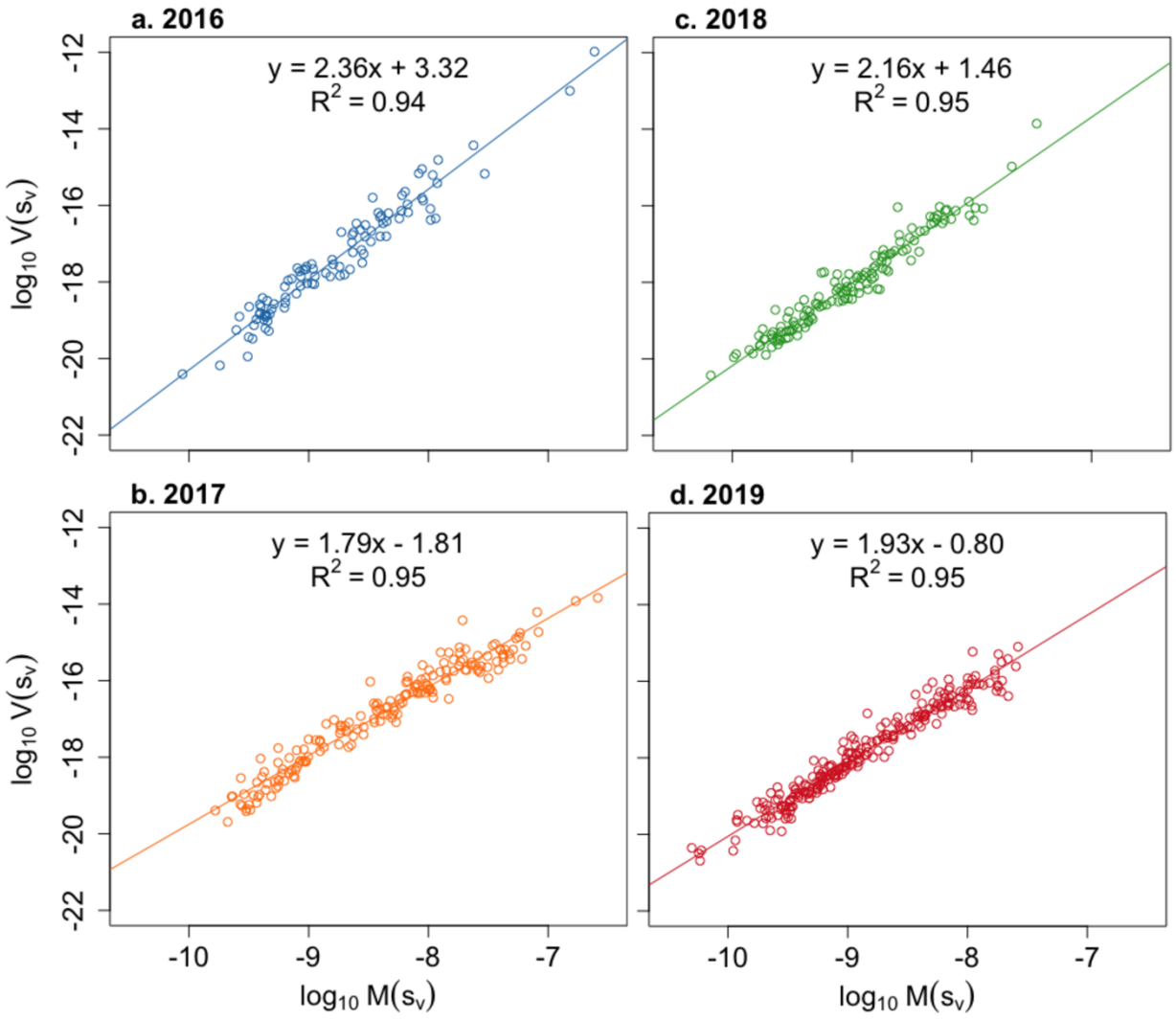

Figure 3.4. Relationship between daily averages and variance calculated from hourly backscattering values corresponding to Arctic cod (*Boreogadus saida*) at the Chukchi Ecosystem Observatory. The quantity sv is the volume backscatter coefficient (linear form of volume integrated energy Sv [dB]), units: m-1.

3.3.1.2 Backscatter fluctuations distributions

Daily fluctuations in Arctic cod backscatter values did not follow a Gaussian distribution (Shapiro-Francia test $p < 0.05$) but were adequately described by a t-distribution (Table 3.1) in all years. In 2018, the AIC was lowest for the mix of Gaussian distributions but very close to the AIC for the

t-distribution (ΔAIC = 4.461) so the latter was selected to enable parameter comparison among years. The standard deviation of the fitted t-distributions were significantly lower in 2019 and significantly greater in 2018 than the rest of the years but no significant differences were observed for the mean and degrees of freedom among years (Figure 3.5). The mean was close to 0 in all years indicating an absence of any trend in density fluctuations each year.

Table 3.1. Akaike information criterion (AIC), AIC differences (ΔAIC), and log likelihood for candidate theoretical distribution models fitted to empirical backscatter fluctuations distributions for each year of deployment (2016–2019) at the Chukchi Ecosystem Observatory.

Year	Model	AIC	ΔAIC	log likelihood
2016	t	2031.492	1.89	-1012.746
	t skewed	2033.382	6.446	-1012.691
	mix Gaussians	2037.938	48.62	-1013.969
	Gaussian	2080.112	1.89	-1038.056
2017	t	2013.348	0	-1003.674
	mix Gaussians	2014.203	0.855	-1002.101
	t skewed	2015.137	1.789	-1003.569
	Gaussian	2101.549	88.201	-1048.774
2018	mix Gaussians	2106.711	0	-1048.355
	t	2111.172	4.461	-1052.586
	t skewed	2113.051	6.34	-1052.526
	Gaussian	2177.938	71.227	-1086.969
2019	t	1939.535	0	-966.767
	t skewed	1940.955	1.42	-966.478
	mix Gaussians	1949.08	9.545	-969.5398
	Gaussian	2020.189	80.654	-1008.095

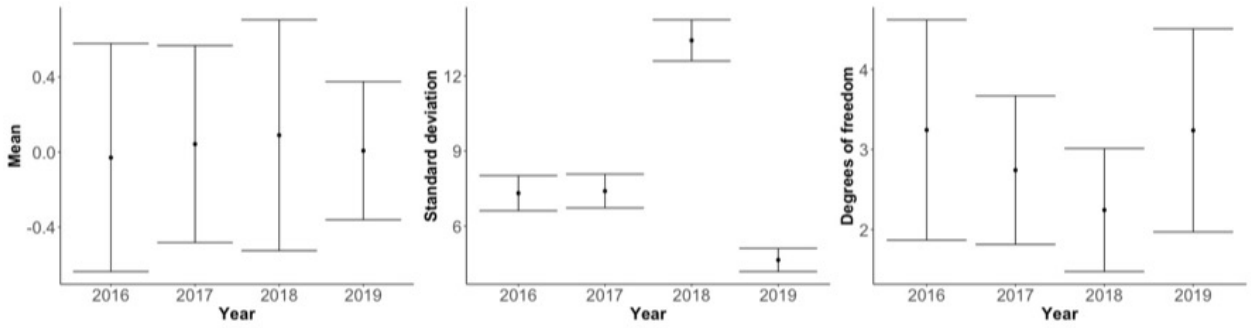

Figure 3.5. Estimated mean, standard deviation, and degrees of freedom from fitted t-distributions for each year (2016–2019).

3.3.2 *Environmental drivers of Arctic cod densities*

Arctic cod backscatter was predominantly associated with bottom temperature, days after sea ice retreat, midwater salinity, PAR, daylength, and the cube of wind speed (Figure 3.6 and Table 3.2). The resulting GAM had an R^2 of 0.626 and the autocorrelation of the residuals was reduced significantly by the inclusion of an autoregressive lag 1 process in the model. The relationship between Arctic cod densities and bottom temperature was linear and slightly positive (Figure 3.6). The association between Arctic cod and sea ice was positive from ~ 30 days before and until ~ 100 days after sea ice retreat when fish densities started to decrease. Highest backscatter values were observed at salinities above 32, cubed wind speed of less than 1000 (m^3/s^{-3}), PAR values of 5–7 μmol photons m^{-2} sec^{-1}, and daylengths of 10–20 hours (Figure 3.6). Parametric coefficients (i.e. intercepts) significantly differed between "cold" (2016 and 2018) and "warm" years (2017 and 2019) (Figure 3.7).

Table 3.2. Results of Generalized Additive Models for Arctic cod (*Boreogadus saida*) backscatter at the Chukchi Ecosystem Observatory.Mw. temp.: midwater temperature, mw. salinity: midwater salinity, ice retreat: days after sea ice retreat, ws: wind speed, PAR: photosynthetically active radiation, chl-a: chlorophyll a concentration, sea ice %: sea ice concentration, NO_3: nitrate concentration, b. temp: bottom temperature, b. salinity: bottom salinity.

Model	AIC	ΔAIC
Mw. temp. + ice retreat + mw. salinity + ws^3 + PAR + daylength	8791.14	0
B. temp. + ice retreat + mw. salinity + chl-a + ws^3 +PAR + daylength	8794.258	3.118
B. temp. + ice retreat + mw. salinity + chl-a + ws^3 + PAR + daylength + NO_3	8796.438	5.298
B. temp. + ice retreat + mw. salinity + chl-a + ws^3 + PAR	8809.9	18.76
Air temp. + mw. salinity + sea ice % + NO_3 + daylength + PAR + ws	8862.274	71.134
Mw. salinity + sea ice % + NO_3 + daylength + PAR + ws	8862.94	71.8
Mw. temp. + mw. salinity + sea ice % + NO_3 + daylength + PAR + ws	8863.786	72.646
Mw.temp. + mw. salinity + sea ice % + NO_3 + daylength + PAR + chl-a + ws	8866.059	74.919
B. temp. + mw. salinity + sea ice % + NO_3 + daylength + PAR + chl-a + ws	8866.621	75.481
B. temp. + mw. salinity + sea ice % + NO_3 + daylength + PAR + chl-a	8869.056	77.916
B. temp. + sea ice % + mw. salinity + chl-a + ws^3 + PAR	8891.294	100.154
B. temp. + sea ice % + mw. salinity + chl-a + ws^3	8896.673	105.533
B. temp. + sea ice % + mw. salinity + chl-a	8898.18	107.04
B. temp. + sea ice %	8910.002	118.862
B. temp. + sea ice % + b. salinity	8912.937	121.797

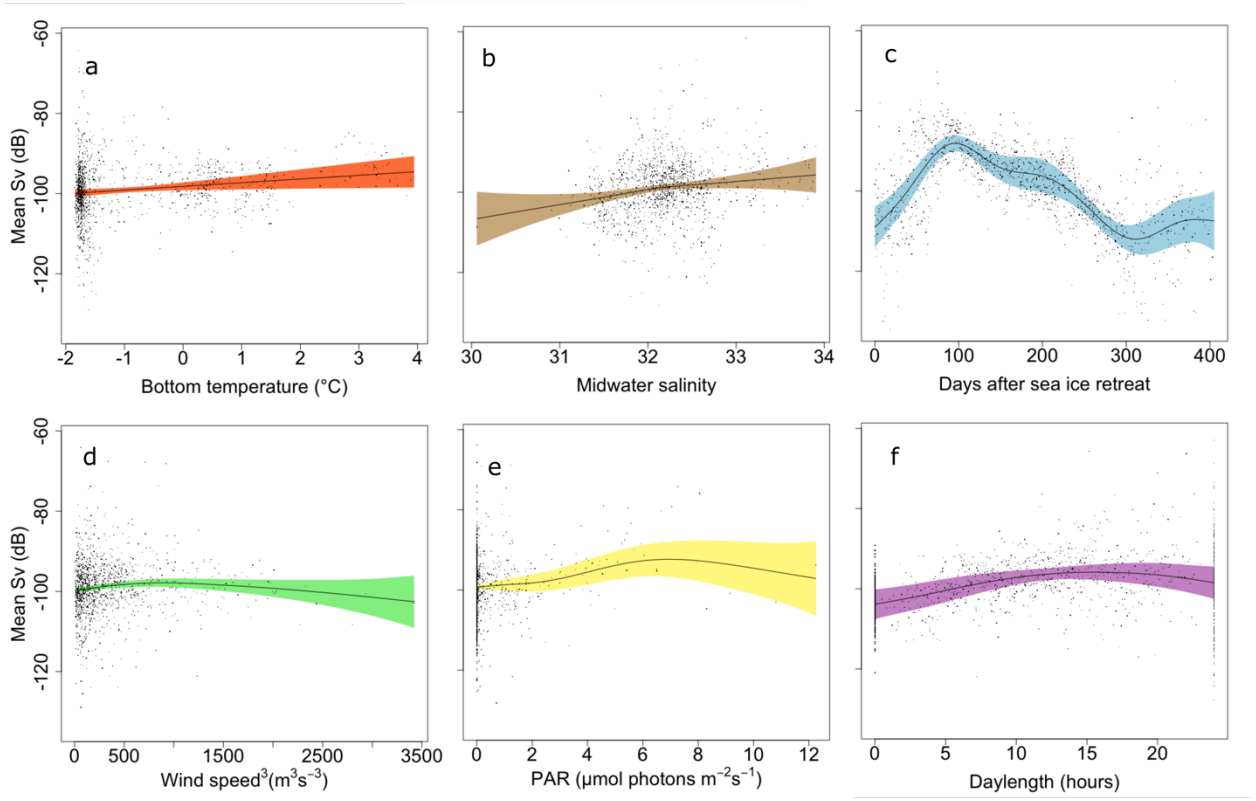

Figure 3.6. Partial effects of covariates included in the Arctic cod (*Boreogadus saida*) backscatter Generalized Additive Model. Grey areas indicate 95% confidence intervals. Points correspond to residual values.

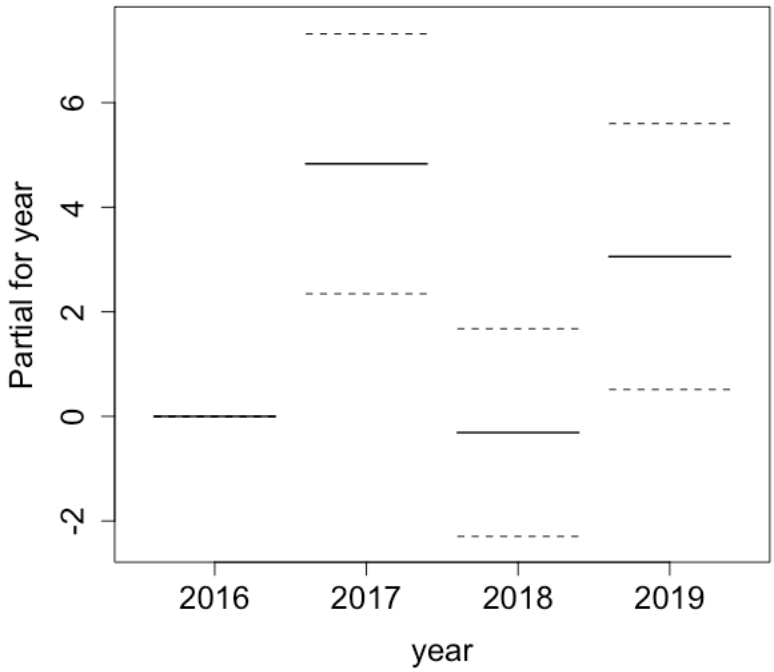

Figure 3.7. Partial effects of year in the Arctic cod (*Boreogadus saida*) backscatter Generalized Additive Model. The envelope encompassing the mean values indicates the standard error for each year.

3.4 DISCUSSION

3.4.1 *Temporal patterns in environmental variables and fish backscatter*

The two sets of sea ice and water temperature characteristics observed in 2016/2018 and 2017/2019 are attributed to differential northward heat fluxes through the Bering strait. Sea ice retreat and advance dates in the Chukchi Sea are mainly associated with mean northward transport of warmer Pacific waters through the Bering Strait during April–June and during the summer months, respectively (Serreze et al. 2019). In 2017, moorings in the Bering Strait recorded one of the highest heat inflows in the last three decades (Woodgate and Peralta-Ferriz 2021). This high heat inflow was a result of combined high water transport (~ 1.2 Sv) and temperatures of 4 °C as

early as June, ~ 0.2 Sv and two degrees higher than those recorded in 2016, 2018, and the climatological average for the same month (Woodgate and Peralta-Ferriz 2021). This upstream observation is consistent with the resulting early sea ice retreat and the long open water season in the Chukchi Sea during 2017 and probably 2019, the two years with lowest sea ice concentrations on record in the area (Serreze et al. 2019). Greater northward heat fluxes through the Bering Strait and longer exposure to solar radiation due to earlier retreat and later advance of sea ice are also consistent with the higher temperatures (1.7–2.7 °C more) recorded at the CEO in 2017 and 2019 than in 2016 and 2018.

Contrasting patterns in fish acoustic backscatter were observed between years with different sea ice and temperature conditions, emphasizing the important role of these physical factors on the Chukchi Sea ecosystem. Higher peaks in fish density and variance occurring earlier in the summer during years with early sea ice retreat and high temperatures is attributed to a combination of (1) earlier and increased transport of age-0 Arctic cod from spawning areas; (2) enhanced local primary production followed by increased secondary production due to an earlier sea ice retreat; and (3) increased growth rates of fish due to higher temperatures.

Arctic cod aggregations found in the NE Chukchi shelf are mainly comprised by small, age-0 individuals possibly advected from spawning areas located further South (De Robertis et al. 2017; Forster et al. 2020; Levine et al. 2021). Arctic cod potential spawning areas have been proposed near St. Lawrence Island in the northern Bering Sea, east of the Chukotka peninsula in western Bering Strait, and the Beaufort Sea (Kono et al. 2016; Vestfals et al. 2019; Mueter et al. 2020). Arctic cod spawn under sea ice during autumn and winter (Graham and Hop 1995), and early stages of Arctic cod are believed to be advected into the NE Chukchi shelf by ocean currents in the spring (Forster et al. 2020; Levine et al. 2021). Higher fish densities occurring earlier in the

summer at the CEO were associated with high northward water transport from the northern Bering and southern Chukchi Seas into the northern Chukchi Sea in 2017 and 2019. This water flux supports the hypothesis that early stages of Arctic cod could be advected into the study area by prevailing northward currents in the spring. Highest backscatter values were observed in Bering/Chukchi Summer Water (BCSW) (Figure 3.8 and see Figure 1 of Appendix D) that flows north into the Chukchi Sea from the northern Bering Sea shelf (Danielson et al. 2017a) providing further support for the hypothesis of Arctic cod advection from the south rather than advection from potential spawning sites in the Beaufort Sea.

Earlier sea ice retreat could, through earlier increases in water column light irradiance and stratification, have propitiated the earlier and extended periods of high chlorophyll concentrations and enhanced Arctic cod densities observed at the CEO in 2017 and 2019 (Figure 3.8 and see Figure 2 in Appendix D). Arctic cod larvae hatch under sea ice from January to July and develop in surface waters over spring and summer (Bouchard and Fortier 2011; Geoffroy et al. 2016). In general, early hatchers (i.e. those hatching during winter/early spring) have the advantage of an extended growing season that leads to larger pre-winter sizes (Fortier et al. 2006; Bouchard and Fortier 2011) at the end of the growth year. Large pre-winter sizes are associated with enhanced winter survival through increased lipid content, predator avoidance, resistance to starvation, and physiological tolerance (e.g. Hunt et al. 2011). Later hatching during times when temperature, light, and food are at their maximum would result in a shorter growing season and sizes too small to ensure winter survival (Bouchard et al. 2017). It has been observed that early sea ice breakup favors higher densities of larger pre-winter Arctic cod (Bouchard et al. 2017). In the Canadian Arctic, the biomass of juvenile Arctic cod in late September was 11 times greater for an early May ice breakup (< 50 % ice cover) compared to a late September ice breakup (Bouchard et al. 2017).

These observations are consistent with the 2–16 times greater fish densities for a May/June sea ice retreat (2017 and 2019) compared to a July sea ice retreat (2016 and 2018) observed at the CEO.

Earlier ice retreat and warmer waters enhance growth and survival of early hatchers by increasing food availability earlier in the year relative to years with late sea ice retreat (LeBlanc et al. 2019b). Earlier phytoplankton blooms and extended periods of primary productivity have been observed in association with decreased sea ice in the Chukchi Sea, northern Barents Sea, and the Canadian Arctic (Zhang et al. 2015; Kahru et al. 2016; LeBlanc et al. 2019b). An advanced and extended bloom results in an earlier and more intense production of copepod nauplii and copepodites (LeBlanc et al. 2019b), the preferred prey of age-0 Arctic cod (Bouchard et al. 2016). In this study I observed that early sea ice retreat in June 2017 was associated with earlier and extended periods of primary production and higher zooplankton densities (see Figure 2 and Figure 3 in Appendix D). However, an ice retreat before June in 2019 did not result in an earlier bloom and lower zooplankton densities were observed compared to 2017. These observations support previous studies in the Canadian Arctic (LeBlanc et al. 2019b) and in the Bering Sea (Hunt et al. 2002), and suggest a potential mismatch between copepods and their food when the ice breaks earlier than June (Leu et al. 2011). Arctic copepod species such as *Calanus glacialis*, time their seasonal migration, foraging, and reproduction to the ice algal and phytoplankton blooms (Leu et al. 2011). A mismatch between *C. glacialis* and its food can result in a fivefold lower biomass of *C. glacialis* in the summer that could in turn affect the recruitment of juvenile Arctic cod and upper trophic levels (Leu et al. 2011).

Higher temperatures at the CEO during 2017 and 2019 could have contributed to enhanced growth that resulted in earlier and higher Arctic cod acoustic backscatter in the summer. Temperature influences growth rates of juvenile Arctic cod (Laurel et al. 2017) with a relatively

high growth at 0 °C and near-maximal growth at 5 °C (Laurel et al. 2016). Highest backscatter values were observed in Bering/Chukchi Summer Waters in 2017 and 2019 when temperatures (0–4 °C) were closest to the reported temperature for near-maximal growth of Arctic cod. Levine et al. (2021) observed an 87% increase in fish backscatter throughout the summer associated with increases in fish length (i.e. backscattering cross section), suggesting that growth of individuals could also contribute to the large backscatter increases observed in the area.

Arctic cod typically disperse from nursery to adult habitats at higher depths (Geoffroy et al. 2016; Forster et al. 2020), likely the Beaufort and Chukchi slopes and Arctic basin (Levine et al. 2021), or colonize the ice pack as age-1 (David et al. 2016). Observed decreasing fish densities after October at the CEO could be due to a downward vertical movement of Arctic cod to depths below the transducer and/or to horizontal movement out of the Hanna Shoal area. In a previous study, we observed that fish targets descended to deeper waters after the summer where they stayed until February when they started moving upwards in the water column, reaching depths closest to the surface by the end of the summer (Chapter 1 and Gonzalez et al. 2021b). These observations suggest that not all individuals may leave the area in autumn, but that some may remain at depth until February when they move upwards closer to the sea ice, possibly as age-1.

Changes in mean Arctic cod density were paralleled by changes in variance throughout the year. As fish densities increased, variance in daily backscatter, a proxy for density, increased. Once the Arctic cod population was established in the area, variance decreased and remained low.

A summary of temporal patterns of Arctic cod and relevant environmental variables is presented in Figure 3.8.

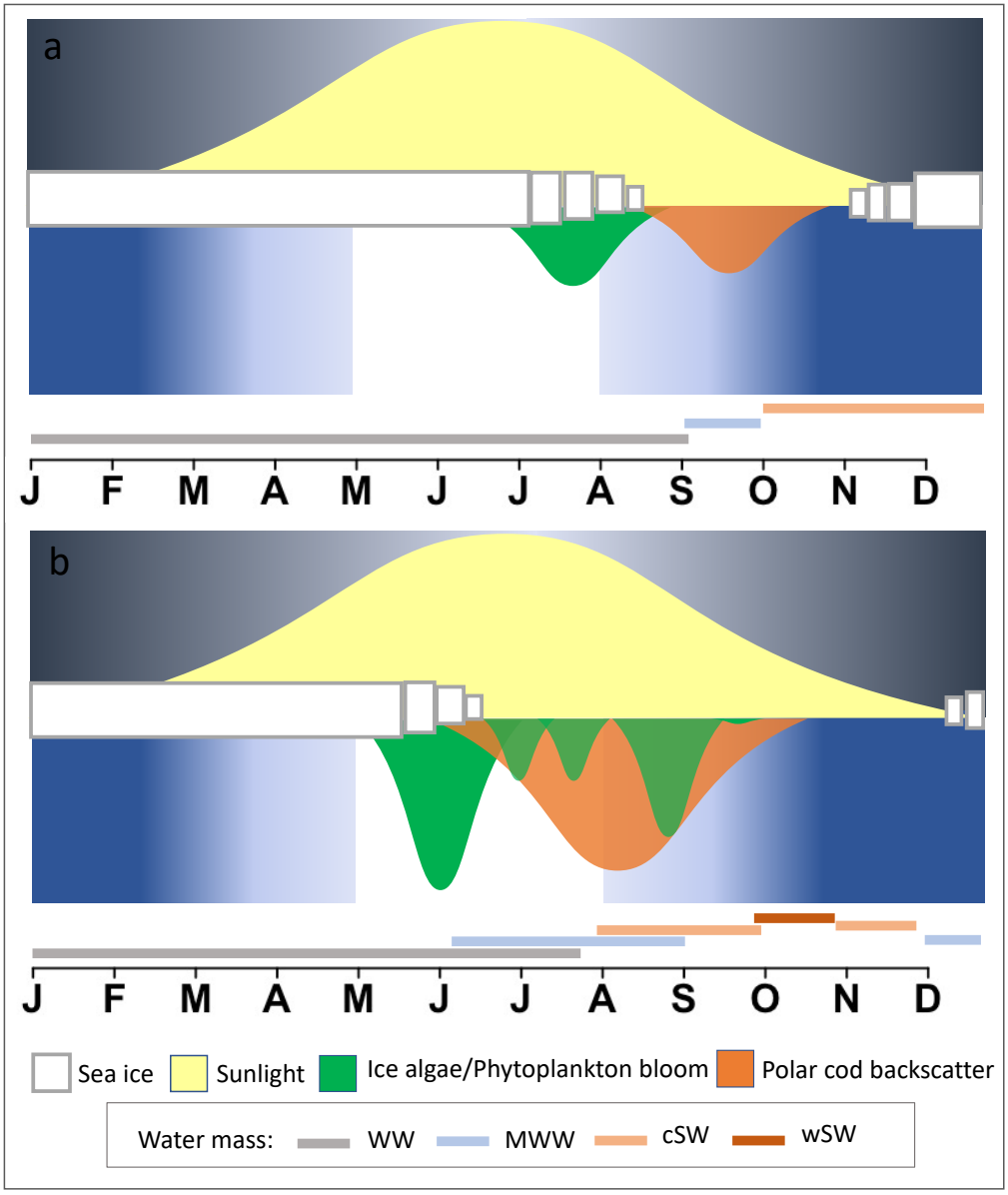

Figure 3.8. Summary of temporal pattens in biological and physical variables in (a) "cold" years (2017 and 2019) and (b) "warm" years (2016 and 2018) at the Chukchi Ecosystem Observatory. WW: Winter Water, MWW: Modified Winter Water, cSW: cool Shelf Water, wSW: warm Shelf water.

3.4.2 *Relationship between fish backscatter mean and variance: Taylor's power law*

Taylor's power law scaling exponents (i.e. log-log regression slopes) from this study were within the typical *b* value range of 1.5 to 2.5, agreeing with previous empirical work (see Eisler et al.,

2008) but varied among years with different environmental conditions. In "warm" years, TPL slopes were significantly below the theoretical value of $b = 2$ (Taylor 1961). Kilpatrick & Ives (2003) demonstrated how negative interactions among species in a community can produce TPL slopes smaller than 2, which may be relevant to the NE Chukchi Sea. In warmer years, enhanced northward movement of Bering Sea species, especially walleye pollock (Levine et al. 2021), could lead to increased interspecific competition and reductions of the TPL slope compared to "cold" years when Arctic cod is the dominant species (De Robertis et al. 2017). Increased abundance of Arctic cod in "warm" years could also increase intraspecific competition through cannibalism, a behavior previously reported for this species in the Beaufort and Chukchi Seas (e.g. Benoit et al., 2010; Gray et al., 2016) leading to reductions of the TPL slope. Observed lower fish temporal aggregation (i.e. lower temporal variability) at high fish densities in "warm" than in "cold" years are consistent with observations reported in a previous study at the CEO (Gonzalez et al. 2021, Chapter 1). Out-of-phase associations between water temperature and fish patchiness were observed with lowest fish and zooplankton aggregations occurring during months of highest fish and zooplankton densities (July–November).

In "cold" years, when seasonality at the CEO is more accentuated (i.e. greater temporal variability), the TPL slope was greater than the theoretical value of 2. Greater slopes suggest higher temporal aggregation (i.e. greater temporal fluctuations) in Arctic cod densities with shorter persistence. Overall, the TPL scaling exponent b seems sensitive enough to track changes in fish density fluctuations under different sea ice and temperature conditions in the NE Chukchi Sea supporting previous empirical studies suggesting that TPL exponents do contain ecologically relevant information (e.g. Cobain et al., 2019; Lagrue et al., 2015; Taylor & Woiwod, 1982) and can be useful ecosystem metrics (Cobain et al. 2019).

3.4.3 *Fish backscatter fluctuations*

Fish backscatter fluctuations at the CEO did not follow a Gaussian distribution and were better described by a t-distributions with low degrees of freedom (df ~ 3) characteristic of heavy tails. This suggests that large jumps in Sv from one day to the next are more likely than expected under a normal distribution. Heavy-tailed distributions have been recently reported for a range of taxa implying that extreme population fluctuations are more likely than previously expected and that a normal distribution underestimates the probability of extreme events (i.e. black-swan events, Segura et al. 2013; Anderson et al. 2017). However, Anderson et al. (2017) did not observe heavy-tailed distributions in fish populations. In the present study, density fluctuations were measured at a scale smaller than the reproduction rate, so we are looking at the effects of migrations or movements in and out the sampled area rather than the effects of local predation, competition, or drastic changes in the environment that drive die-offs (Anderson et al. 2017) or outbreaks (Segura et al. 2013) described at other scales. Also, the amount of data used to characterize fluctuations in Anderson et al 2017 were lower than in the present study, precluding the characterization of extreme events.

At the CEO, fluctuations of fish backscatter were symmetric and centered on zero (i.e. mean of the distribution ~ 0) indicating that large rate increases and decreases from one day to the next are equally likely. At the temporal resolution (daily) and the spatial extent of measurements (55 m^2) centered, heavy-tailed distributions in density fluctuations could be explained by Arctic cod foraging behaviors. Probabilistic search patterns described by a type of random walk models known as Lévy flights have been demonstrated to be the optimal search strategy for marine predators in environments with patchy prey distributions (Sims et al. 2008; Humphries et al. 2010) such as those of Arctic cod prey in the Arctic (e.g. Blachowiak-Samolyk et al. 2006). Lévy flights

describe a movement pattern characterized by many small steps connected by longer relocation steps that could result in movements into and away from the acoustic beam providing a potential explanation to the observed heavy-tailed, non-skewed distributions in density fluctuations (Viswanathan 2010). The standard deviation of density fluctuations distributions was greater in 2018 and smaller in 2019 compared to the rest of the years, suggesting that different foraging strategies could be in place. Variations in prey abundance and distribution (e.g. higher abundances distributed more uniformly) associated with changes in the physical environment could lead to changes in Arctic cod foraging strategies that may be reflected in daily or lower scale fluctuation distributions. A closer look at Arctic cod and zooplankton distributional patterns (e.g. mean location, dispersion, and aggregation in the water column) in association with Arctic cod density fluctuation distributions at daily and smaller scales under different environmental conditions could provide insight into this hypothesis.

3.4.4 *Environmental drivers of temporal patterns in Arctic cod backscatter*

Linkages between oceanographic variables and fish backscatter suggest that seasonal sea-ice dynamics and water mass advection are important for the ecology of Arctic cod. Sea ice conditions in winter and spring have been shown to explain Arctic cod densities in the summer (Bouchard et al. 2017; LeBlanc et al. 2019b). The timing of sea ice retreat affects the timing, amplitude, and duration of sea ice algae and phytoplankton blooms, which stimulates and supports secondary productivity, and ultimately determines available food resources for Arctic cod. LeBlanc et al. (2019) observed that zooplankton backscatter in August was more strongly correlated to ice breakup date and phytoplankton bloom onset date than to chlorophyll a concentration, indicating that the duration of the season of food availability rather than food abundance was likely the primary driver of zooplankton biomass in late summer. At the CEO, significance of days after sea

ice retreat, daylength, and PAR, but not of chlorophyll a concentration in this study also suggest that duration of food abundance rather than food abundance might be the primary driver of secondary production, and therefore of Arctic cod densities.

Temperature and salinity have been reported as important variables associated with Arctic cod abundances (De Robertis et al. 2017; Logerwell et al. 2018; Forster et al. 2020). In this study, a linear, slightly positive association between temperature (range -2–4 °C) and Arctic cod density was observed. This trend is consistent with other studies that report a bell-shaped association between temperature and Arctic cod abundances with highest abundances at 4–6 °C (Vestfals et al. 2019; Forster et al. 2020), the temperatures for Arctic cod optimal growth (Laurel et al. 2016). Positive linear associations between Arctic cod and salinities up to 34 psu have also been observed in other studies (De Robertis et al. 2017; Forster et al. 2020). Temperature and salinity can be used to define water masses with characteristic nutrient concentration and phytoplankton composition (Danielson et al. 2017a), which have been shown to influence the distribution of Arctic cod and their prey (Eisner et al. 2013). Highest Arctic cod densities were observed in BCSW, specifically cool Shelf Water (cSW) and warm Shelf Water (wSW), and in Modified Winter Water (MWW) (Figure 3.8 and Figure 1 in Appendix D), which are the prevalent water masses at the CEO during spring, summer, and autumn (Danielson et al. 2020). BCSW is a nutrient-rich water mass (Danielson et al. 2017a) with a zooplankton community composed of lipid-rich calanoid copepods and euphausiids (Eisner et al. 2013), which are prey for Arctic cod (Rand et al. 2013). Lowest Arctic cod densities were observed during winter when Winter Water (WW) is the dominant water mass present in the area (Danielson et al. 2020). WW is characterized by lower nutrient concentrations than BCSW (Danielson et al. 2017a) and is composed of smaller zooplankton including *Oithona similis* and *Pseudocalanus* spp. (Eisner et al. 2013). These zooplankton species

are a less advantageous prey for Arctic cod given their smaller lipid content (Falk-Petersen et al. 2009). Water mass distribution is influenced by advection and local changes in temperature and salinity driven by sea ice melt and formation cycles. Temporal variations in water masses influence nutrient and prey composition of the water column through time, ultimately affecting temporal patterns of Arctic cod densities at the CEO.

Wind patterns determine sea ice drift and water mass movement that, in turn, affects distributions of Arctic cod and their prey. Wind-driven variations in water flow direction can explain interannual changes in age-0 gadid backscatter in the Chukchi and western Beaufort seas (Vestfals et al. 2019; Levine et al. 2021). Flow reversals associated with strong southward winds in the summer were used to explain the retention of Arctic cod in the Chukchi shelf in the summer of 2018, whereas autumn northward winds were responsible for the northward advection of age-0 Arctic cod towards the Chukchi and Beaufort shelf breaks (Levine et al. 2021).

3.5 CONCLUSIONS

Four years of continuous biological and physical observations at the CEO provide evidence that sea ice is a key structuring factor of the Chukchi Sea ecosystem. This study supports previous observations that earlier sea ice retreat and increases in temperature associated with enhanced water transport from the NE Pacific could temporally benefit Arctic cod production in the NE Chukchi Sea. Earlier sea ice retreat results in greater and earlier peaks in Arctic cod densities and more stable populations (i.e. smaller fluctuations) by extending the growing season with favorable temperature and food conditions. Continuing changes in the physical environment could further alter the timing of biological processes that could lead to a mismatch of age-0 Arctic cod and their prey. Changes in water mass characteristics in the area could also alter the quality of Arctic cod

prey by replacing lipid-rich species such as *Calanus glacialis* and *Calanus hyperboreous* by smaller, relatively lipid-poor species such as the subarctic *Calanus finmarchicus* (Spear et al. 2020). These changes in food availability and quality would likely impact Arctic cod growth and survival rates in the NE Chukchi Sea (Bouchard and Fortier 2020). Increasing temperatures and earlier transport off the Chukchi shelf due to increased northward advection of warm Pacific waters could limit age-0 growth prior to their first winter and may increase competition and predation pressure by increasing abundances of subarctic pelagic fish such as walleye pollock (Fossheim et al. 2015; Huntington et al. 2020; Levine et al. 2021). Further increases in temperatures above optimal could also be detrimental for egg development and age-0 Arctic cod growth.

As high latitudes experience increased anthropogenic and climatological pressures, increased understanding of temporal patterns and environmental drivers of key components of the Arctic ecosystem, like Arctic cod, can be used to inform resource use and management decisions. This work provides baseline information on temporal patterns and environmental drivers of Arctic cod in the northeast Chukchi Sea and provides insight into the oceanographic processes and environmental characteristics that affect Arctic cod feeding, growth, and survival.

Chapter 4. REPRESENTATIVE RANGE OF ACOUSTIC POINT SOURCE MEASUREMENTS IN THE CHUKCHI SEA[2]

4.1 INTRODUCTION

Detecting and predicting biological responses to episodic perturbations (e.g. oil spills, marine heatwaves) and longer-term trends (e.g. global warming, ocean acidification) in marine environments requires a characterization and understanding of the ecosystem's "natural" or baseline variability. However, characterizing biological variability is not easy because marine ecosystems are comprised of numerous physical and biological processes operating over multiple spatial and temporal scales (Stommel 1963; Haury et al. 1978; Levin 1992; Schneider 1994).

Characterizing and monitoring biological variability in marine ecosystems requires high resolution, long-term (i.e. high scope) datasets that can be challenging to obtain due to limited resources or constrained accessibility. Such challenges are amplified in high latitude marine environments where the presence of sea ice during most of the year limits vessel-based sampling of the water column (e.g. Mueter et al. 2017; Spear et al. 2019). In these areas, data acquisition is typically limited in duration and/or resolution, fragmenting our understanding of important bio-physical processes over the annual cycle.

The use of echosounders attached to bottom-mounted platforms or moorings (i.e. stationary acoustics) provides a non-invasive technology to characterize and monitor temporal variability in abundance and behavior of pelagic organisms (e.g. Urmy et al. 2012; Horne and Jacques 2018; Gonzalez et al. 2021). Stationary acoustics can: (1) characterize "natural" or baseline conditions through continuous sampling of fish and zooplankton year-round; (2) quantify the amount of

[2] In press: Gonzalez S, Horne JK, Danielson SL, Lieber L, Lopez G. Representative range of acoustic point source measurements in the Chukchi Sea. Elementa.

change relative to baseline variability to help determine thresholds of environmental effects; and (3) monitor changes, episodic or trending, in pelagic organisms' abundance or behaviors. The inclusion of active acoustics in instrumented platforms (i.e. marine observatories; e.g. Godø et al. 2014) also allows the simultaneous and continuous collection of biological and physical data, which can be used to understand underlying mechanisms of observed biological patterns, a prerequisite to predicting biological responses to environmental change (Linder et al. 2017).

Despite covering a wide spectrum of temporal scales (e.g. seconds to years), acoustic measurements from stationary echosounders are point source measurements and are limited in their spatial coverage. Since fish and zooplankton distributions are heterogeneous (i.e. patchy), biological similarity is expected to decay with geographical distance (Soininen et al. 2007). Beyond a certain distance, known as the representative range, meaningful inferences cannot be derived as uncertainty and interpolation errors are expected to increase (Martin et al. 2005; Anttila et al. 2008; Milewska and Hogg 2010). When monitoring a large spatial domain, multiple point measurements within the representative range provide redundant information and a reallocation of sampling resources would lower sampling costs or could be used to expand the sampling domain. A better understanding of a site's representative range ensures appropriate characterization and monitoring of the environment, and at the same time, optimizes the cost-effectiveness of monitoring through the deployment of one or multiple sensor packages.

Located over the Northeast Chukchi shelf on the southern flank of Hanna Shoal, the Chukchi Ecosystem Observatory (CEO, Figure 4.1), is a set of instrumented moorings that has been collecting high-resolution, continuous biological, biogeochemical, and physical measurements since 2014 (Danielson et al. 2017b; Hauri et al. 2018; Lalande et al. 2020). The location of the CEO enables tracking of temporal variability and potential trends (i.e. ocean

monitoring, Danielson et al. 2017) in a biological hotspot (Grebmeier et al. 2015). In this study concurrent mobile and stationary acoustic data were used to: (1) characterize spatial variability in fish and zooplankton densities, and (2) quantify the representative range of CEO's point source, active acoustic sampling. Comparison of stationary acoustic data with data from surface, mobile surveys will further the understanding of spatiotemporal biological variability in Arctic ecosystems, and inform the design of effective monitoring networks to monitor and detect potential impacts of environmental change on pelagic communities.

4.2 METHODS

4.2.1 *Study area*

The seasonally ice-covered NE Chukchi Sea receives a nearly continual input of heat, nutrients, organic carbon, and organisms from Pacific-origin water flowing northward in response to an oceanic pressure head that results from an elevation difference between the Pacific and Arctic Oceans (Stigebrandt 1984) (Figure 4.1). This input from the Bering Sea, combined with shallow depths, enhances biological productivity in the Chukchi Sea (Grebmeier et al. 2015). A large phytoplankton bloom that occurs seasonally in late spring and summer (Questel et al. 2013) supports the largest soft bottom benthic faunal biomass in the world's ocean (Grebmeier et al. 2006a, 2015), and corresponding populations of zooplankton (Ershova et al. 2015), seabirds (Kuletz et al. 2015), and marine mammals (Hannay et al. 2013). The Chukchi continental shelf is also home to Arctic cod (*Boreogadus saida*), a fish species that plays a key role in the transfer of energy from lower to higher trophic levels in high latitudes (Lowry and Frost 1981; Whitehouse et al. 2014).

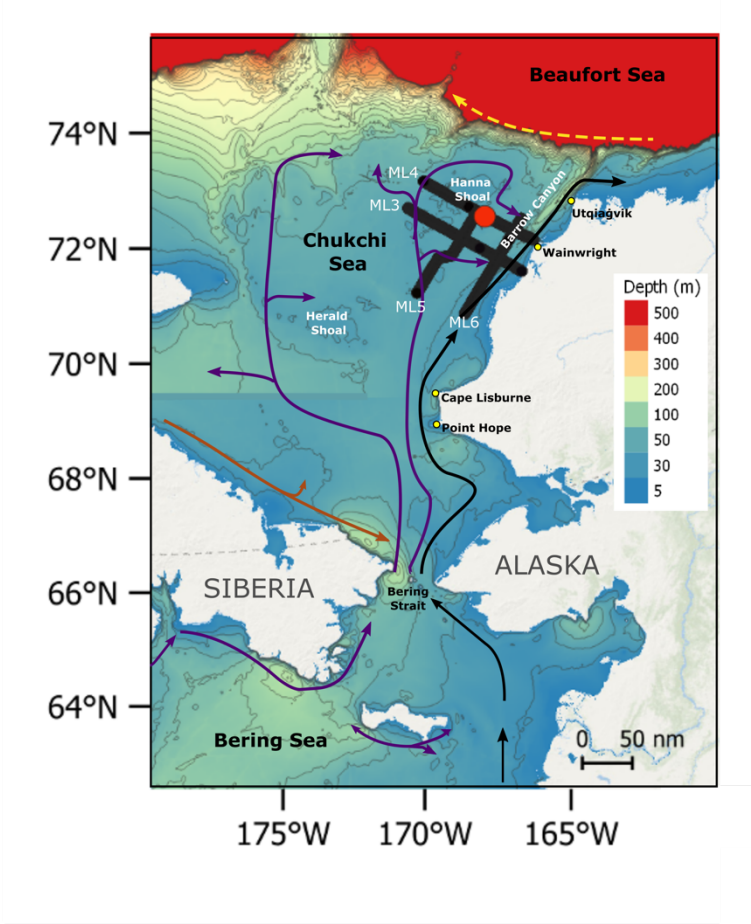

Figure 4.1. Map of the study region showing bathymetric depths, and main flow pathways. The yellow arrow represents the Beaufort Gyre, black arrows represent the Alaskan Coastal Current, the brown arrow represents the Siberian Coastal Current, and purple arrows represent pathways of Bering Shelf, Anadyr, and Chukchi shelf waters. The red circle indicates the location of the Chukchi Ecosystem Observatory (CEO) and selected transects (ML3–ML6) from the Arctic Marine Biodiversity Observing Network (AMBON) surveys are shown in black.

4.2.2 *Datasets*

To characterize spatial variability in fish and zooplankton densities in the study area and to quantify the representative range of CEO point measurements, active acoustic data from a stationary mooring (i.e. temporally indexed data) and coincident mobile surveys (i.e. spatially indexed data) conducted in proximity to the mooring (Figure 4.1) were analyzed.

4.2.2.1 Spatially indexed data

Spatial variability in fish and zooplankton density was characterized using acoustic data from four transects (ML3, ML4, ML5, and ML6) measured during two Arctic Marine Biodiversity Observing Network (AMBON) surveys that included coverage of Hanna Shoal (Figure 4.1). These surveys were conducted during August 8th–September 5th in 2015 and August 5–24th in 2017. Acoustic data were collected using a Teledyne 307 kHz Workhorse Mariner acoustic Doppler current profiler (ADCP) mounted to the survey vessel at a depth of ca. 3 m below the sea surface. Data were collected every 0.5 seconds (2 Hz) with a vertical resolution of 1 m. ADCPs can be used to measure acoustic backscatter (i.e. ensemble reflected energy) throughout the water column as a proxy for pelagic fish and zooplankton densities (e.g. Cochrane et al. 1994; Ressler 2002; Zedel et al. 2003) and have been used to describe diel migrations and distributions of biological scattering layers (e.g. Luo et al. 2000; Cisewski et al. 2010). ADCPs cannot be calibrated using standard reference targets (Demer et al. 2015) but comparisons of measurements by an ADCP and a calibrated scientific echosounder showed that data from the two instruments were highly correlated (Brierley et al. 1998).

All ADCP data were acquired using VMDas software (v. 1.46; RD Instruments, Inc.) and post-processed in WinADCP (v. 1.14; RD Instruments, Inc.) as part of standard quality control procedures. Data files were then exported and further processed in Matlab R2020a. Volume-backscattering strength (Sv measured in dB re 1 m^{-1}, hereafter dB) was calculated across a maximum of 25 vertical bins from the ADCP's recorded raw echo intensity data using the sonar equation as described in Deines (1999) and updated by Mullison (2017). The backscatter sonar equation accounts for two-way signal transmission loss (i.e. time-varying gain), sound absorption, and uses an instrument- and beam-specific Returned Signal Strength Indicator (RSSI) scaling factor to convert counts to decibels. This makes ADCP backscatter measurements more robust

compared to raw echo intensity measurements, which are more readily extracted from an ADCP. Mean Sv was calculated for each vertical bin along each of the four beams of the ADCP. The mean of the four beams (Sv_{mean}) was used to calculate mean backscatter in the water column for each along-track 4-ping (i.e. 2 second) bin (corresponding to 8 to 10 m at vessel speeds of 8–10 knots). A double pass 1x3 median filter was applied to the Sv data to reduce contamination/interference from the ship's echosounder.

4.2.2.2 Temporally indexed data

Temporally-indexed acoustic backscatter data was collected at the CEO (71° 35.976' N, 161° 31.621' W) using an upward-looking, Acoustic Zooplankton Fish Profiler (AZFP; ASL Environmental Sciences), deployed at 35 m depth (bottom depth: 45 m) (Figure 4.1). The instrument operated at 38 (12°), 125 (8°), 200 (8°), and 455 (7°) kHz (nominal beamwidths, measured between half power points in parenthesis) since September 9, 2014. The AZFP collected data every 15 seconds (0.067 Hz) at a vertical resolution of 4 cm.

Acoustic backscatter from the AZFP was processed using Echoview software (v. 9.0). Background noise was subtracted and a minimum signal-to-noise ratio filter of 6 dB was applied. Echoes within 3 m from the face of the transducer were excluded from analyses to avoid integration of echoes in the acoustic nearfield (Foote 2014). Sea water surface and sea ice edges were delimited using Echoview's bottom detection and linear offset operator algorithm followed by visual inspection and manual correction. A surface exclusion line was set 0.5 m below the corrected surface and echoes above the line were excluded to ensure that backscatter from surface turbulence or sea ice was not included in analyses.

I used the 125 kHz AZFP mooring backscatter data corresponding to August and September of 2015 and 2017 to match the timing of mobile surveys in the area. A threshold of -110 dB was applied and backscatter for the entire water column was integrated in 1-minute bins (i.e. 4 pings).

4.2.3 *Characterization of spatial variability*

To characterize spatial heterogeneity and spatial dependence in acoustic backscatter I quantified and compared spatial variability in across-shore (ML3 and ML4) and along-shore (ML5 and ML6) transects within years, and from 2015 and 2017 AMBON surveys using autocorrelation functions (Legendre 1993) and wavelets (Torrence and Compo 1998).

Autocorrelation is a property of ecological variables that occurs when measurements that are close together in space or time are more similar than measurements taken farther apart. Spatial autocorrelation manifests as patches or gradients in biological distributions that can result from physical forcing of environmental variables or community processes (Legendre 1993). Lagged Autocorrelation Functions quantify spatial dependency in acoustic backscatter by partitioning covariance over distance classes (Legendre and Fortin 1989). Lagged Pearson's product-moment correlation coefficients (ρ) define the correlation between all measurements at a given lag (h) and can be modeled using an exponential model:

$$\hat{\rho}(h) = \hat{\rho}(0)e^{-\alpha d} \tag{4.1}$$

where $\hat{\rho}(0)$ is the autocorrelation at lag 0, d is the number of lags, and α is the range at which the autocorrelation decays by a value of e. I calculated the isotropic (i.e. direction-independent) and anisotropic (i.e. direction-dependent) correlograms of acoustic backscatter from transects conducted in 2015 and 2017.

Wavelet analysis can be used to explore spatial structure along one-dimensional transects (e.g. Torgersen et al. 2004; Grados et al. 2012; McGowan et al. 2019). A wavelet transform decomposes a data series as a function of scale and position through the convolution of a waveform—the wavelet—that is stretched or compressed (i.e. scaled) and slid through the series (i.e. translation). In this way, the wavelet decomposition identifies dominant spatial scales that

account for variance throughout the series (Torrence and Compo 1998). A continuous Morlet mother wavelet function (Torrence and Compo 1998) was applied to each transect. Wavelet power was calculated using the R package *WaveletComp* (v. 1.1, Roesch & Schimidbauer 2018). Statistical significance in localized wavelet power was evaluated through comparison to a white noise (constant value, equal to the time series variance) null hypothesis at a 95% confidence level (Torrence and Compo 1998) using 100 simulations. Edge effects were minimized by adding zeroes at the beginning and end of each data series to increase the total length of the series to the next power of two (Torrence and Compo 1998). Horizontal integration of wavelet power at each scale over the entire series—the global wavelet spectrum—allows the measurement of variance contributed by each scale across the entire transect. The global wavelet spectrum was calculated using the R package *WaveletComp* (v. 1.1, Roesch & Schimidbauer 2018). Significance of this time-averaged variance was tested against white noise at a 95% confidence level (Torrence and Compo 1998).

4.2.4 *Quantification of representative range*

Six different methods described in Horne and Jacques (2018) were used to quantify the representative range of point measurements from the CEO AZFP. The use of multiple methods enables assessment of consistency among calculated ranges and facilitates generation of guidelines to design the spatial distribution of monitoring sensors. All methods estimate the representative range of the mean or variance of a quantity. Both mean and variance are considered appropriate monitoring metrics to track changes in biological variables (Underwood 1991; Osenberg et al. 1994). The six methods can be categorized into four approaches: (1) distance between sensors based on spatial correlation; (2) sample size calculations assuming random sampling to detect a minimum threshold of change; (3) maximization of spatial variance; and (4) scales at which spatial

and temporal variability are equivalent. The first approach calculates the optimum distance between sensors based on the relationship of spatial measurements. Using the decay of spatial correlation with distance (e.g. Anttila et al. 2008), the representative range corresponds to the distance at which measurements become independent. The second approach quantifies the number of sensors needed to detect change using a paired t-test, sample size calculation assuming a random sampling framework (e.g. Rycroft 1949). Three methods that use this random sampling approach include: the number of replicates using a derivative of minimum sample size calculations for a paired t-test (Gray et al. 1992), a paired t-test, repeated measures ANOVA (Sullivan 2006), and a sample size calculation for a paired t-test including statistical power (Zar 2010). The third and fourth approaches quantify representative ranges of temporal variance rather than the mean. The third approach models the theoretical power spectrum as a function of the spatial autocorrelation (modeled in the first approach). The spatial period at which 95% of the maximum observed variance in fish density is set as the representative period of variance (e.g. Gilman et al. 1962). The final approach compares empirically derived spatial and temporal power-spectra to identify equivalent scales of spatial and temporal variability by identifying periods at which identical magnitudes of spatial and temporal variability are observed (e.g. Wiens 1976).

4.3 RESULTS

4.3.1 *Characterization of spatial variability*

4.3.1.1 Spatial autocorrelation

The autocorrelation structure of each of the four transects surveyed in 2015 and 2017 is presented in Figure 4.2. The spatial distribution of pelagic organisms' densities, described by the distance at which samples become independent (ρ=0) and the % of variance associated with spatial autocorrelation (ρ(1)), varied widely among transects. Differences between calculated ranges

within across and along-shore transect pairs were typically larger than differences observed between transects of different orientation. Across-shore measurements became independent ($\rho(2/\sqrt{l})$) at distances of 14,880–53,296 m whereas along-shore measurements became independent at 10,856–73,960 m. In 2015, more than half (58–89%) of the variability observed between sequential observations was explained by autocorrelation ($\rho(1)$) whereas autocorrelation explained a smaller proportion of this variability (30–38%) in 2017.

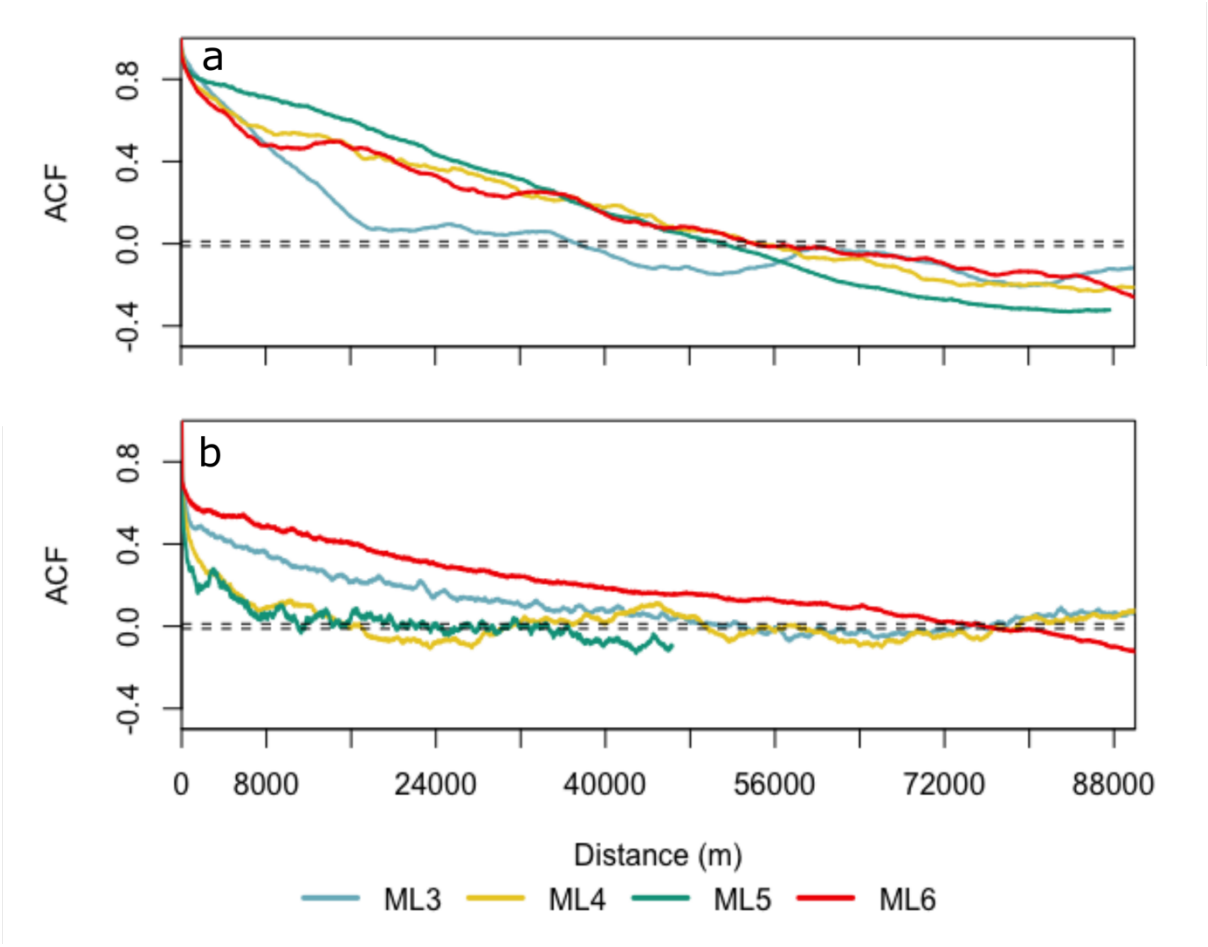

Figure 4.2. Autocorrelation function for across-shore (ML3 and ML4) and along-shore (ML5 and ML6) acoustic transects conducted in 2015 (a) and 2017 (b). Dashed lines indicate the 95% threshold of significance.

4.3.1.2 Wavelets

Scales of spatial variability differed among transects and between years (Figure 4.3). In general, spatial variability was concentrated at fewer scales in 2015 than in 2017. Peaks in averaged wavelet power were observed at scales ranging from 1024 m to 73,500 m in 2015 and from 64 m to 73,500 m in 2017. In 2015, the largest peaks in averaged wavelet power were observed at large scales (greater than 30 km) in ML3 and ML5 and at intermediate (10–30 km) scales in transects ML4 and ML6. In 2017, largest peaks in averaged wavelet power were observed at smaller scales (1–4 km) compared to 2015 for ML3 and ML5 and at large scales (greater than 40 km) for ML4 and ML6 transects.

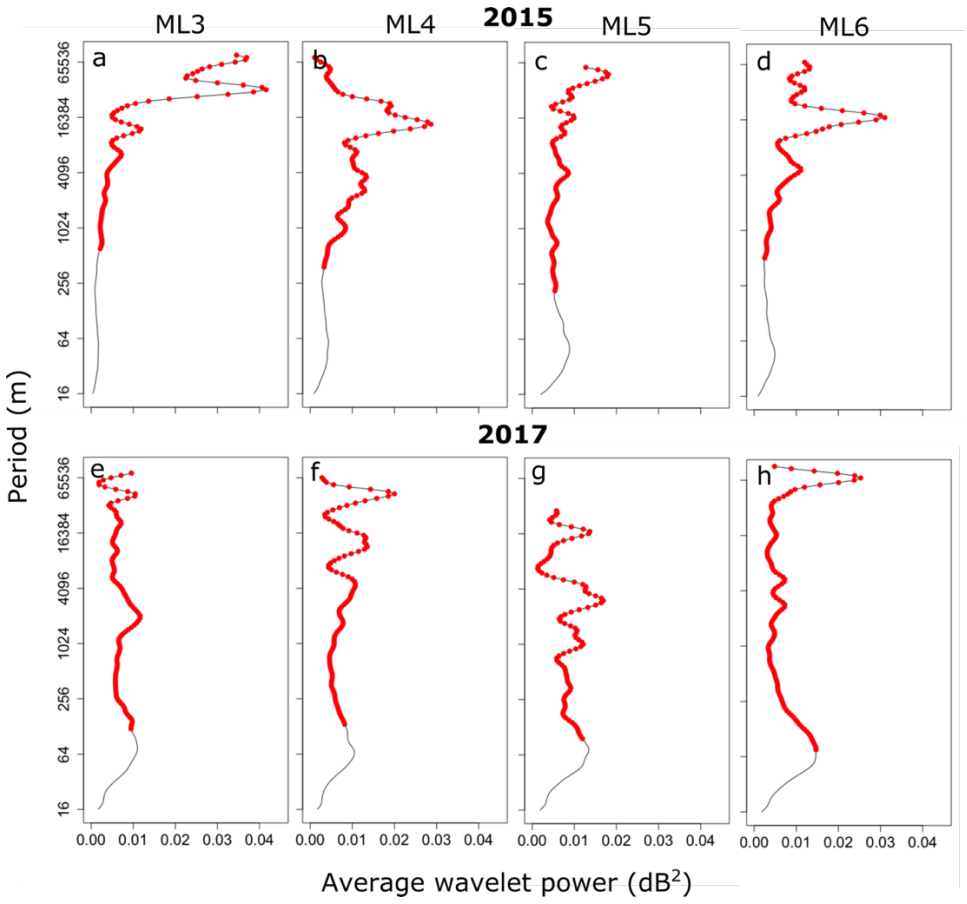

Figure 4.3. Averaged wavelet power for across- (ML3 and ML4) and along-shore (ML5 and ML6) acoustic transects conducted during 2015 (a–d) and 2017 (e–h) surveys. Significant scales (95% confidence against white noise) are shown in red.

4.3.2 *Quantification of representative range*

4.3.2.1 Spatial autocorrelation

Spatial autocorrelation decayed exponentially as a function of distance (Figure 4.4). Exponential decay models fit to the lagged coefficient of determination (squared correlation coefficient, R^2) followed $y = 0.685e^{-0.0006456x}$ in 2015 and $y = 0.229e^{-0.0007704x}$ in 2017. The coefficient of determination at lag 1 ($\rho(1)$) indicated that more than half of the variability between sequential observations was explained by autocorrelation in 2015 ($\rho(1) = 0.68$) whereas a smaller proportion of this variability could be attributed to autocorrelation in 2017 ($\rho(1) = 0.23$). The mean number of observations per transect (26,488 in 2015 and 25,179 in 2017) was used to calculate a 95% confidence interval for the lagged coefficients of determination. Based on calculated thresholds of significance (0.012 in 2015 and 0.013 in 2017) the representative range was estimated to be 49,817 m in 2015 (Figure 4.4a) and 30,101 m in 2017 (Figure 4.4b). The representative area, defined as a circle of radius equal to the representative range, was 7797 km^2 in 2015 and 2846 km^2 in 2017.

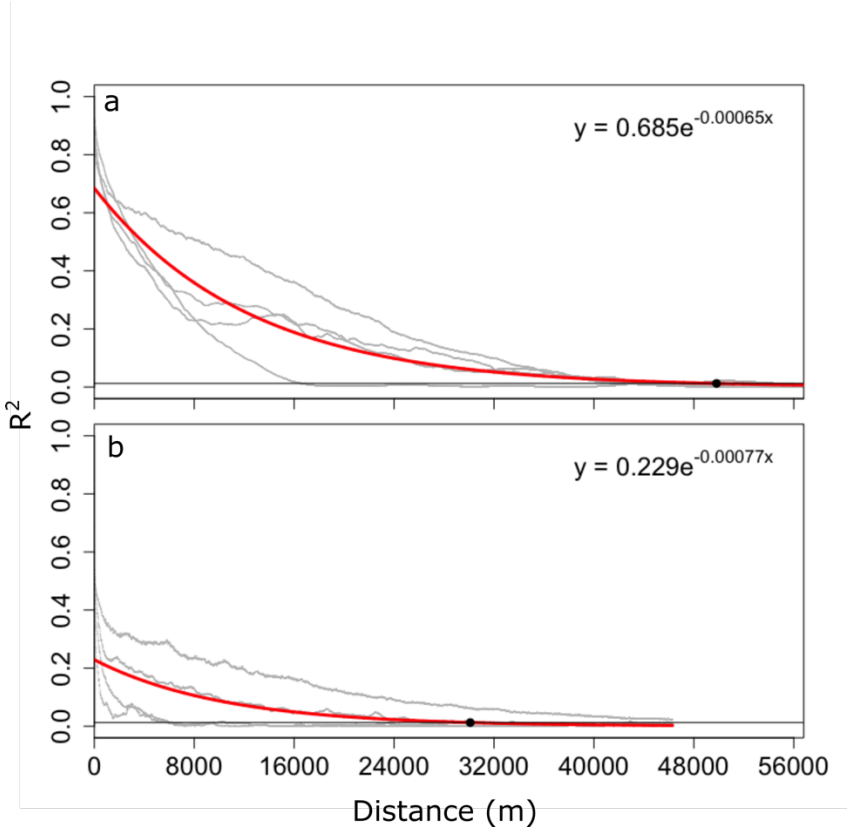

Figure 4.4. Lagged coefficient of determination (R^2) model for 2015 (a) and 2017 (b) datasets. Squared correlation values for each individual transect are shown in grey and model fit is shown in red. The black point indicates the representative range at the 95% threshold of significance (black line).

Representative ranges calculated using this method were highly dependent on the length of the transects used in the analysis (Figure 4.5). To examine the relationship between representative range and transect length I calculated the representative range for each of the four transects surveyed in 2015 using transect lengths from 1.6 km (200 observations) to ~ 250 km in 0.8 km (100 observations) increments. Representative ranges increased with transect length with values ranging from 16 m to ~ 70,000 m and constituted 11–32% of the transect length in average. In general, representative ranges were similar for all transects up to a transect length of 18 km after which ranges increased at different rates. Representative ranges reached an asymptote at different

transect lengths for each transect (Figure 4.5). Minimal changes in representative range (i.e. rate change smaller than 0.5%) were observed for transect lengths greater than 100 km for ML3, 144 km for ML4, 149 km for ML5, and 165 km for ML6.

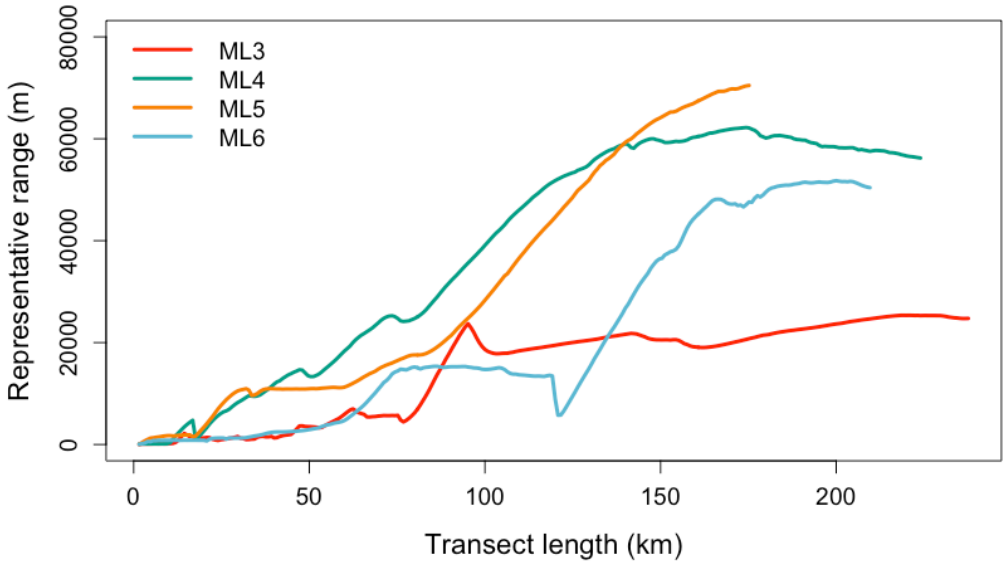

Figure 4.5. Representative ranges of acoustic backscatter for different transect lengths using the Autocorrelation method for the 2015 dataset.

4.3.2.2 Sample size calculations

The number of required sensors to detect a minimum threshold of change was calculated for the 2015 and 2017 acoustic grids using the Gray et al. (1992) equation and derived paired t-test and power test equations. To meet independence requirements of sample size calculations, data were averaged into 49,817 m bins for the 2015 and 30,101 m bins for the 2017 data. These bin sizes corresponded to representative ranges calculated using the spatial autocorrelation method in Section 4.2.1. This coarser data resolution resulted in only 4–6 observations per transect. However, no significant differences in sample size calculations were observed when using at least 30 observations (~ 375 m bins) per transect (results not shown).

Representative ranges varied among sample size calculation methods and between years (Table 2.1). The representative range using the Gray et al. (1992) equation was 12,271 m in 2015 and 19,325 m in 2017. Paired t-test calculations resulted in representative ranges of 305 m in 2015 and 756 m in 2017. Representative ranges calculated using the power test equation for a significance level $\alpha = 0.05$ and a probability of type II error $\beta = 0.90$ were 2,677 m in 2015 and 4,215 m in 2017. Since choice of α and β are arbitrary, representative ranges for different combinations of α and β are presented in Figure 4.6. Setting $\alpha = 0.05$ and the effect size E = 1 dB constant, the representative range increased 30% when decreasing beta from 0.90 to 0.70, from 2677 m to 3492 m in 2015 (Figure 4.6a) and from 4,215 m to 5,500 m in 2017 (Figure 4.6b). If beta is held constant at a conservative value $\beta = 0.90$ and α is increased from 0.05 to 0.1, the representative range increases from 2,677 m to 2,965 m in 2015 (Figure 4.6a) and from 4,215 m to 4,670 m in 2017 (Figure 4.6b).

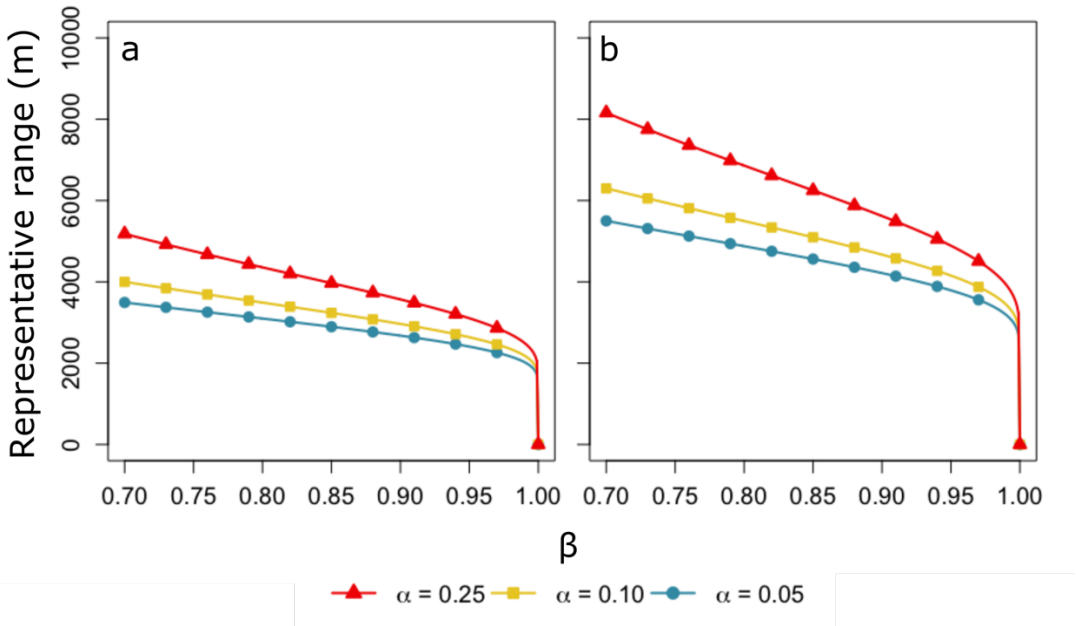

Figure 4.6. Representative ranges of acoustic backscatter calculated using power analysis for different combinations of α (0.05, 0.1, and 0.25) and β for 2015 (a) and 2017 (b) surveys.

4.3.2.3 Theoretical power spectra

The representative range of backscatter variance corresponds to the scale at which 95% of the maximum variance (21.9 dB^2 in 2015 and 2.4 dB^2 in 2017) was measured. Differences of one order of magnitude were observed in representative ranges between years (Figure 4.7). The relative variance exceeded the 95% maximum threshold at a period of 2,524 m in 2015 (Figure 4.7a) and 259 m in 2017 (Figure 4.7b) and negligible increases in variance are expected beyond these distances.

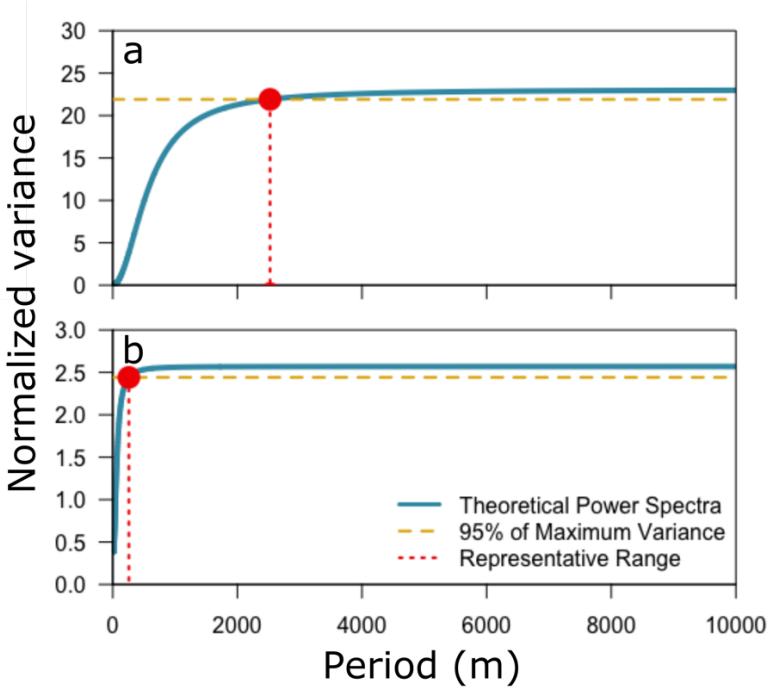

Figure 4.7. Theoretical power spectra for 2015 (a) and 2017 (b) acoustic backscatter datasets.

4.3.2.4 Equivalent scales of spatial and temporal variability

Spatial and temporal spectral power increased with period (Figure 8). Units of space and time were set relative to the 8 m and 1 minute resolution of the spatial and temporal datasets. In both years the spatial spectra ($y_{2015} = -0.58 + 1.25x$ and $y_{2017} = 0.30 + 0.99x$) increased more rapidly than the

temporal spectra ($y_{2015} = 0.16 + 0.96x$ and $y_{2017} = -0.197 + 0.92x$). In 2015, the modeled maximum temporal variance at the Nyquist frequency, equivalent to a period of 21 days, was 4.46 $\log_{10}(dB^2)$. The corresponding spatial variability was observed at a period of 86,152 m. Equal spatial and temporal variance was observed at a range of 1.5–3 units (250–8000 m) (Figure 4.8a). In 2017, the modeled maximum temporal variance was 3.92 $\log_{10}(dB^2)$ and the corresponding spatial variability was observed at a period of 35,780 m (Figure 4.8b).

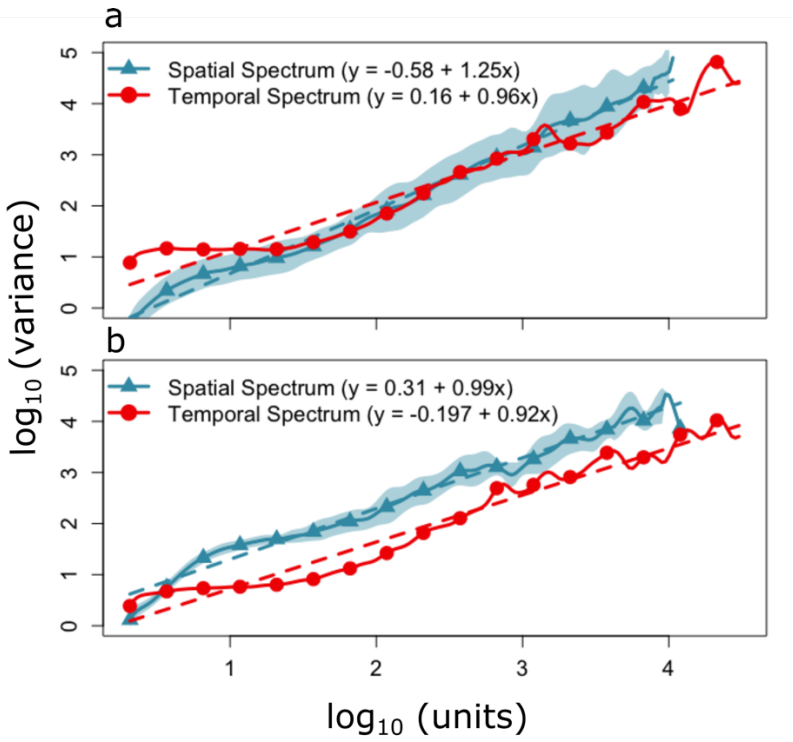

Figure 4.8. Equivalent scales of spatial and temporal variability of acoustic backscatter for 2015 (a) and 2017 (b) datasets.

4.3.2.5 Representative ranges of CEO's acoustic measurements

The spatial representative range of point source acoustic measurements at the CEO was dependent on the metric property (mean or variance), analytic method, and year (Table 4.1). The representative range of mean backscattering strength varied over one to two orders of magnitude

among methods with values ranging from 305 to 49,817 m in 2015 and from 756 to 30,101 m in 2017. Similar magnitude differences were observed for the representative range of backscattering strength variance with values ranging from 2,524 to 86,152 m and from 258 m and 35,780 m for 2015 and 2017 datasets, respectively. Variations in representative range were also observed between years but these differences were smaller (two to tenfold differences between years) than those observed among methods.

Table 4.1. Summary of spatial representative ranges of the mean and variance of backscattering strength measured at the Chukchi Ecosystem Observatory in 2015 and 2017. Representative range values for power test correspond to α=0.05 and β=0.09.

Method	**Description and reference**	**Metric property**	**Representative range 2015 (m)**	**Representative range 2017 (m)**
1. Spatial autocorrelation	Distance for independent samples. Anttila et al. (2008)	mean	49817	30101
2. Sample size calculations	Required sample size to detect minimum threshold of change.			
2.1. Gray's sample size calculation	Gray et al. (1992)	mean	12271	19325
2.2. T-test sample size calculation	Sullivan (2006)	mean	305	756
2.3. T-test power analysis	Zar (2010)	mean	2677	4215
3. Theoretical power spectra	Scale with maximum spatial variance from modeled power spectra. Gilman et al. (1962)	variance	2524	258
4. Equivalent spatial and temporal scales	Spatial and temporal scales with equal variance from wavelet decomposition. Wiens (1989)	variance	86152	35780

4.4 DISCUSSION

The approach comparing two data years and multiple methods to calculate spatial representative ranges at the CEO illustrates the occurrence of: (1) relatively large representative ranges (up to ~ 90 km), (2) variations in range estimates between years (1–10-fold differences), and (3) large variations in range estimates among methods (1–2 orders of magnitude differences). Each of these observations impacts the choice of representative range calculation method and the interpretation and application of results derived from point source observing systems such as the CEO in the Chukchi Sea.

Relatively large representative ranges of CEO's acoustic measurements, compared to similar studies, could be a result of low spatial heterogeneity in physical and/or biological characteristics, low abundance of organisms, and/or potential limitations of the sampling approach. Representative ranges calculated by Horne and Jacques (2018) for a stationary echosounder deployed in Admiralty Inlet, WA were much smaller (representative ranges of up to 1.4 km) than those observed in this study (representative ranges up to ~ 90 km) but were calculated over a much smaller area (8 km^2), in an environment with different physical characteristics and dynamics (temperate latitude, high tidal current speeds, estuarine dynamics) and at a much higher spatial resolution (transects placed every 0.25–0.5 km).

Large representative ranges observed in this study could be expected in environments with tight bio-physical associations and large characteristic environmental length scales. For instance, large representative ranges may occur when spatial variability of physical characteristics that shape biological distributions is low, or in environments characterized by weak bio-physical associations when biological distributions are homogeneous and independent of the spatial structure of the physical environment. In the Chukchi Sea, fish and zooplankton distributions are tightly coupled

with environmental factors that vary over scales consistent with calculated representative ranges. In particular, zooplankton abundances, species compositions, and spatial distributions are primarily influenced by water mass properties (e.g. Hopcroft et al. 2010; Ershova et al. 2015; Pinchuk and Eisner 2017; Spear et al. 2019). Water masses in the study region often retain distinguishing characteristics over scales ranging from ~ 20 to 100 km (Day et al. 2013; Gong and Pickart 2015; Danielson et al. 2020) and depend in part on the inflow of water masses from lower latitudes and the presence of sea ice and melt water in the summer (Spear et al. 2019). The length scale of lateral boundaries between oceanic water masses is set by the internal Rossby radius of deformation, which in the Chukchi Sea is often on the order of 1–5 km (Nurser and Bacon 2014). Frontal zones in the Chukchi are found between water masses associated with sea ice melt, winter water, and summer shelf water (Lu et al. 2020). Fish distributions in the Chukchi Sea are also influenced by physical environmental factors including bottom depth, water temperature, and salinity (Norcross et al. 2010; De Robertis et al. 2017; Iken et al. 2019; Forster et al. 2020). Iken et al. (2019) observed that distributions of demersal fish assemblages contained little spatial structure with variations in species composition and abundances observed mainly between coastal and offshore areas from samples collected during the 2015 AMBON survey. Day et al. (2013) reported variability in zooplankton and fish biomass across three regions located ~ 40 km apart in the NE Chukchi Sea. Large representative ranges could also be a result of weak spatial patterns due to low abundances and diversity of pelagic organisms in the benthic-dominated Chukchi Sea (Grebmeier et al. 2006a).

Limitations of the sampling approach might also contribute to large representative ranges observed in this study. The lower sensitivity of ADCPs, compared to scientific echosounders, could result in weak biological spatial patterns that result in large representative ranges. In

addition, acoustic backscatter measured using a 300 kHz ADCP includes small particle aggregates, bubbles, and electrical or mechanical noise that would reduce signal to noise ratios, and potentially obscure biological patterns. I observed strong biological scattering layers throughout all transects and biological patterns are not expected to be affected by the ADCP's sensitivity or by the inclusion of non-biological backscatter sources in this study. Finally, acoustic backscatter measurements integrate all sources of energy reflected from particles and animals in the water column. These values correspond to assemblages of zooplankton and fish species of different age/size classes where each category potentially has a different spatial distribution. As a result, strong heterogeneous spatial patterns of some species could be masked by homogeneous distributions of abundant species. A higher discrimination of integrated backscatter measurements into species and/or groups of species using calibrated, multi-frequency scientific echosounders could enable a more accurate characterization of spatial patterns and provide representative ranges specific for taxa of interest.

Differences in representative range values between years are expected due to changes in the timing and spatial distribution of environmental structure (e.g. sea ice melt fronts) and processes (e.g. water inflow from the Bering Sea) that determine water mass characteristics and associated species assemblages in the region (Spear et al. 2019). Interannual variations in sea ice extent and water inflow from the Bering Sea (Chen and Zhao 2017; Zhang et al. 2020) results in interannual variations in water mass spatial distributions (Yang and Bai 2020). Zooplankton assemblages in the Chukchi Sea can vary from predominance of small zooplankton species of Pacific origin (e.g. copepods *Neocalanus* spp., *Eucalanus bungii*) to large lipid-rich Arctic zooplankton species (e.g. *Calanus hyperboreus*) depending on interannual changes in advection pathways into the Arctic (Pinchuk and Eisner 2017). Variations in water mass distributions and

associated species composition result in changes in acoustic backscatter spatial patterns that affect calculated representative range values. In the study area, differences were observed in current direction and water column characteristics (e.g. surface and near-bottom temperatures and salinity, primary production, (Danielson 2021) between the two survey years which could be contributing to differences in the spatial distribution of pelagic organisms and estimated representative ranges.

Differences in estimated representative ranges among methods are attributed to differences in the methodologies, rationale and associated assumptions of each approach. Variations of 1–2 orders of magnitude in the estimates are consistent with differences of up to 2 orders of magnitude (~ 30 to 1400 m) observed by Horne and Jacques (2018) in a much smaller study domain. A comparison of methods to calculate representative ranges of air quality monitoring stations in EU countries also resulted in variations of 1–3 orders of magnitude in estimated ranges that were attributed to differences in the basic principles of the methods, in the definitions of similarity criteria and thresholds, and in the underlying definitions of representative ranges (Kracht et al. 2017). The choice of method will depend on the purpose of the study and the available data. Horne and Jacques (2018) provide a decision tree for method selection depending on the study/monitoring objective including detection of change (sample size calculation approach), mapping of spatial distributions (autocorrelation function approach), characterization of spatial variance (maximization of spatial variance approach), and interpolation of temporal variability over space (equivalent scales of spatial and temporal variability approach).

Monitoring programs using stationary platforms in the Arctic will play a key role in the detection of biological responses to climate change, oil and gas exploration and exploitation, increased marine traffic and other ongoing environmental changes in high latitudes. Biological monitoring in remote areas needs to be efficient and cost-effective in order to be sustainable in the

long term. Stationary sensors are assumed to be more cost-effective than repeated, mobile surveys and enable year-round sampling in areas with limited access due to seasonal sea ice cover. Quantifying the representative range removes uncertainty in the monitoring network design and reduces monitoring costs by identifying the minimum number of sensor packages for complete coverage of a site and provides a quantitative measure of the spatial scope of ongoing monitoring efforts. Stationary acoustic measurements at the CEO are representative of circular areas up to 7000 nm^2, depending on the calculation method, which correspond to areas of up to 46% of that covered by the spatial surveys. The study/monitoring goals, including the extent of the spatial domain, will determine the number of monitoring packages and their spatial distribution.

Representative range calculation and monitoring network system design are best completed as part of a baseline characterization of spatial and temporal biological patterns in the study domain. All methods used in this study require a synchronous spatial and temporal characterization of biological distributions prior to the calculation of representative range(s). Spatial datasets used in this study come from surveys conducted in the vicinity of the CEO but were not explicitly designed for the purpose of this study. One of the methods (equivalent spatial and temporal scales) requires a temporal characterization of the variable of interest. In that case, spatial and temporal data should be collected simultaneously. In this study, representative ranges were calculated based on spatiotemporal patterns of biological characteristics and did not consider physical features (e.g. depth, water mass characteristics) that may influence biological distributions. Also, best practice dictates that temporal and spatial data should be collected using instruments with the same characteristics, in the case of acoustic data, using calibrated, scientific echosounders operating at the same frequencies. In all cases, a prior delineation of the study domain and a definition of what constitutes “similar” or “representative” should be defined to meet the purpose of the study.

Although there has been considerable interest in understanding spatial and temporal biological patterns, little attention has been paid to the consequences of observed patterns for monitoring design (Rhodes and Jonzén 2011). The concept of representative ranges was initiated and predominantly used in association with meteorological (e.g. Ciach and Krajewski 2006; Milewska and Hogg 2010) and air quality (e.g. Piersanti et al. 2015; Yatkin et al. 2020) monitoring. Attempts to evaluate and standardize methods to calculate representative ranges have been advocated in air quality measurements (Martín et al. 2015; Kracht et al. 2017). However, this renewed interest is not evident within the oceanographic community. Despite continued use of moorings and increased use of ocean observing systems, quantifying spatial representative ranges of stationary sensors is not commonly used to optimize sensor layout nor to quantify the spatial scope of monitoring measurements. The results emphasize the importance of defining the study/monitoring spatial domain in conjunction with study objectives to ensure that representative samples are obtained for analyses. A calculation of representative ranges improves monitoring and characterization of biological communities and enables the design of cost-effective monitoring including the number, location, and spacing of sensors. Understanding how representative ranges of point measurements change depending on the timing of the survey, the location of stationary platforms, and the design of baseline spatial characterization (e.g. grid resolution and extent) is key to ensure the collection of representative samples and/or data. Research to understand how spatial representative ranges are affected by these factors could be achieved using simulated sampling schemes. Ensuring the collection of representative samples in a cost-efficient way becomes even more relevant in the face of environmental changes that are driving shifts in species distributions in high latitude environments.

Chapter 5. TEMPORAL VARIABILITY IN PELAGIC BIOMASS DISTRIBUTIONS AT WAVE AND TIDAL SITES AND IMPLICATIONS FOR STANDARDIZATION OF BIOLOGICAL MONITORING[3]

5.1 INTRODUCTION

Effects of Marine Renewable Energy (MRE) wave and tidal development and operation on biological communities remain uncertain (Boehlert and Gill 2010; Frid et al. 2012; Copping et al. 2016), and the ecology of many MRE sites has been traditionally understudied due to dynamic environmental conditions. As a result, regulators have taken a precautionary approach and evidence of no (or minor) measurable effects associated with MRE development is required before approval of a MRE license (Copping 2018). As part of the permitting/consenting process, biological characterization of pre-installation conditions (e.g. abundance, diversity, and fluctuations of biological communities), and post-installation monitoring that ensures detection of change in biological attributes are mandatory conditions for every MRE project.

Environmental monitoring plans are industry sector, site, and project specific. No standard monitoring requirements exist for wave or tidal energy projects in the world. This makes it difficult to assess environmental impacts (i.e. detection of change above a threshold), impedes permitting/consenting, and hampers industry development (Maclean et al. 2014; Wright 2014). Standardized monitoring goals and methods would expedite project development, enable assessment of MRE device effects on the environment, and facilitate comparisons of impacts among sites and sectors to evaluate if changes are site/device specific.

[3] Published as: Gonzalez S, Horne JK, Ward EJ (2019) Temporal variability in pelagic biomass distributions at wave and tidal sites and implications for standardization of biological monitoring. Int Mar Energy J 2:15–28

Within MRE sectors, sites are primarily chosen by similarities in their physical characteristics such as current velocities for tidal sites, and favorable wind conditions for wave sites, but this does not mandate that biological characteristics (e.g. fish and zooplankton biomass and biomass distributions) among sites are also similar. A comparison of fish and zooplankton densities and vertical distributions at two tidal sites showed that similarities exist and that a common method to determine thresholds for environmental monitoring is possible (Wiesebron et al. 2016b). To establish if standard methods could be applied across MRE industry sectors, comparisons of sites with different physical environments are needed. The next logical step is to compare biological characteristics at wave (open coastal area) and tidal (tidally dynamic) MRE sites. Observations from this comparison will highlight general similarities and site/sector-specific differences that can be considered when developing monitoring strategies for the MRE industry.

Stationary active acoustic methods can be used to monitor the water column in a wide range of environmental conditions. Wave and tidal energy sites are typically located in relatively shallow water (<60 m), that maximize amplitudes of ocean surface waves and tidal currents. Traditional biological sampling (i.e. vessel-based net deployments) can be operationally challenging in these environments due to high flows, turbulence, and the presence of energy conversion devices. Deployment of active acoustic packages overcomes these sampling challenges and is not subject to net availability/selectivity, increased sampling mortality, or large investments in time and resources.

The objectives of this study were to: (1) characterize and compare temporal variability in densities and distributions of fish and macrozooplankton at a wave and a tidal energy test site; (2) identify environmental variables influencing observed patterns; and (3) discuss the potential for standardizing analytic methods to acoustically monitor biomass across MRE industrial sectors.

5.2 METHODS

5.2.1 *Study area*

I investigated the dynamics of marine animals living in the water column (i.e. pelagic organisms) at two sites that have been selected for testing and developing MRE from tidal currents and waves in the United States (Figure 5.1). The tidal site was selected by the Snohomish Public Utility District 1 (SnoPUD) for the deployment of two OpenHydro (http://openhydro.com/home.html) turbines in northern Admiralty Inlet, the main entrance to Puget Sound, Washington, characterized by currents reaching circa 3 ms-1 (Gooch et al. 2009; Jacques 2014). This project obtained a Federal Energy Regulatory Agency (FERC) license in 2014 but due to funding constraints it was discontinued that same year.

The second site is at the PacWave test site (formerly known as the Pacific Marine Energy Center South Energy Test Site) (Figure 5.1). PacWave is a planned grid-connected test facility for wave energy converters (WECs), located circa 11 km off the coast of Newport, Oregon. This wave energy pilot site (hereafter wave site) is currently in the permitting process and is expected to be available for device testing in 2019.

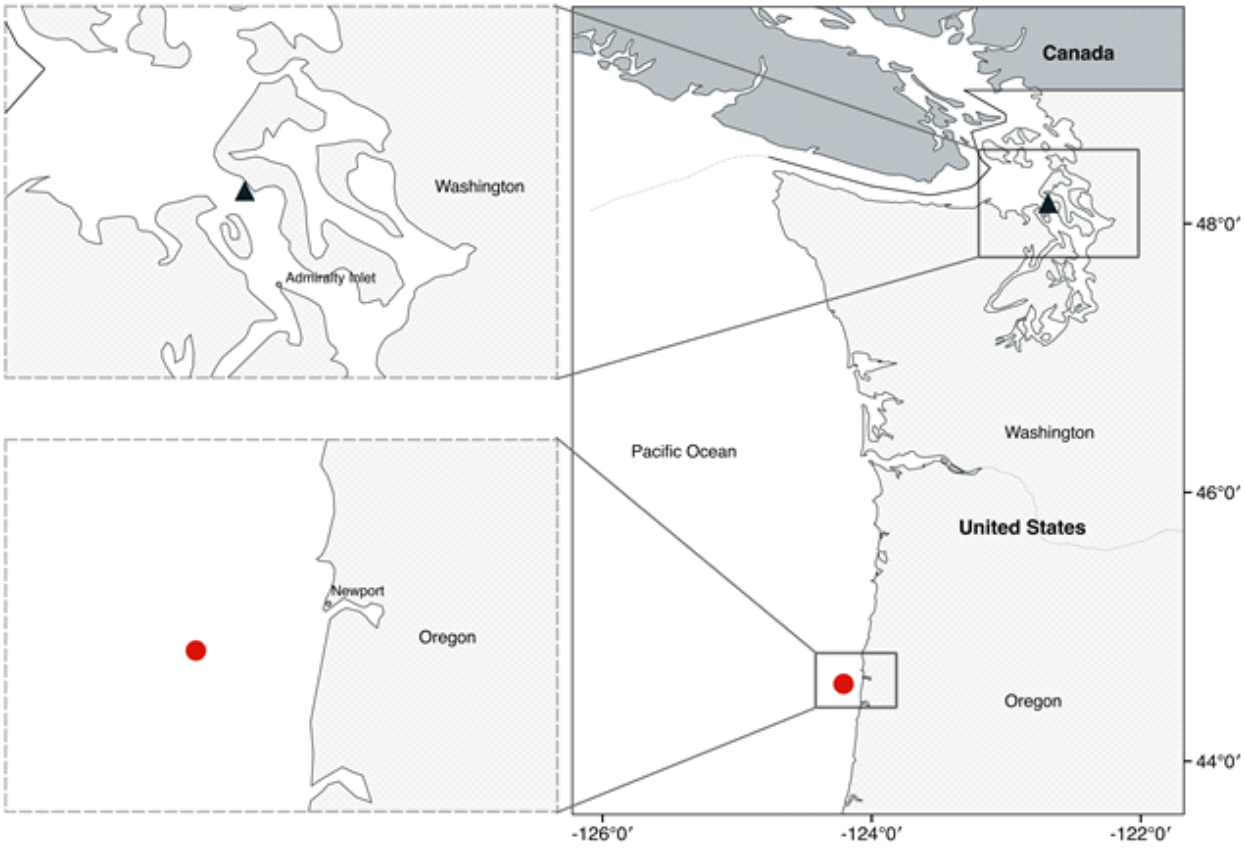

Figure 5.1. Study sites showing locations of the acoustic deployments at SnoPUD's tidal energy pilot site in Admiralty Inlet, WA (triangle) and PacWave test site (circle), a wave energy test site off the coast of Newport, OR.

5.2.2 *Data acquisition*

Active acoustic data collected at fixed locations were used to quantify temporal variability of pelagic fish and macrozooplankton at both study sites. The approach focused on communities in the area of a site rather than on individual animals in the area of a device, as impacts to populations will affect long term viability of MRE sites. Acoustic backscatter (i.e. ensemble reflected energy) data were collected using bottom-mounted Sea Spider platforms (http://www.teledynemarine.com/sea-spider) with upward looking echosounders. Tidal site data were collected using a BioSonics DTX echosounder operating at 120 kHz with a 7° (between half

power points) beam. The echosounder was placed at 55m depth about 750 m to the west of Admiralty Head at the SnoPUD tidal turbine site from May 9th to June 8, 2011. The echosounder sampled at 5 Hz for 12 minutes every 2 hours. The bottom package located at the wave site consisted of a Simrad WBAT (www.simrad.com) operating at 70 kHz, with an 18° beam at a depth of 61 m. The WBAT echosounder sampled 175 pings at 1 Hz (~ 3 min) every hour from April 19th to September 30, 2016. Acoustic sampling parameters are listed in Table 5.1. Both echosounders were calibrated prior to deployment following standard procedures outlined by Demer et al. (2015).

Table 5.1. Echosounder sampling parameters used in Admiralty Inlet (tidal site) and at PacWave (wave site) deployments.

	Tidal site	Wave site
Manufacturer	BioSonics	Kongsberg/Simrad
Model	DTX	WBAT
Frequency	120 kHz	70 kHz
Pulse form	CW	CW
Pulse length	500 µs	512 µs
Pulse rate	5 Hz	1 Hz

At both sites, no energy conversion devices were deployed during field measurements. Therefore, collected data characterize pre-installation conditions and may be used in the future to assess biological changes associated with the installation and operation of energy devices.

5.2.3 *Data processing*

Processing of tidal site backscatter data were completed prior to this study and is described in (Jacques 2014). A threshold of -75 dB re 1 m-1 (hereafter dB) (MacLennan et al. 2002) was applied to remove background noise and data were limited to 25 m from the bottom to minimize backscatter from surface turbulence. The original 12-minute samples collected at the tidal site were subsampled to match the ~ 3 min samples acquired at the wave site. From each 12 min sample, 4

different data sections can be analyzed. Using continuous acoustic data from a tidal site in the Fall of Warness, Scotland, Wiesebron et al. (2016) demonstrated that there were no significant differences between equal length subsets from the original series. Thus, the first 875 pings (175 pings x 5 Hz) were selected and analyzed from each data series.

Acoustic data from the wave site was processed in Echoview (version 7.1). The data range was also constrained to 25 m from the bottom and a threshold of -75 dB was applied to match the Admiralty Inlet data. Echoes within 3 m from the face of the transducer were excluded from the analysis to avoid the integration of echoes in the acoustic nearfield. Background noise was estimated from passive acoustic measurements collected during a mobile surface survey conducted in the area. Noise level was obtained by finding the value that minimized the sum of the squared differences between observed and expected mean volume backscattering strength (mean Sv). Noise was estimated using (1) where NL is the noise level at 1 m (dB), r the range in m, and α the absorption coefficient (dB/m). The estimated noise level at 1 m (-136.24 dB) was then used to subtract noise from the water column:

$$NL(r) = NL + 20log_{10}(r) + 2\alpha(r - 1) \quad (5.1)$$

To align sampling density at both sites, one of the two samples collected in a 2-hour period at the wave site (i.e. hourly samples) was selected to match the sampling frequency of the tidal site (a sample every 2 hours). A t-test was performed between mean acoustic backscatter when selecting the 1st versus the 2nd hour of each 2-hour period. No significant difference was found so the 1st hour was arbitrarily selected for analysis. A one-month period (May 8th to June 9th) from the wave site dataset was used to match calendar dates of the tidal site.

5.2.4 *Data analysis*

5.2.4.1 Biological descriptors: echometrics

A suite of metrics derived from acoustic data, collectively referred to as echometrics (Burgos and Horne 2008; Urmy et al. 2012), was used to describe temporal variations in density and vertical distributions of fish and macrozooplankton in the water column. The echometrics suite includes: (1) mean Sv, proportional to mean density of organisms (MacLennan et al. 2002); (2) center of mass (units: m), the mean weighted location of backscatter in the water column relative to the bottom; (3) inertia (units: m2), a measure of organism dispersion (i.e. variance) from the center of mass; and (4) an aggregation index (units: m-1), which measures vertical patchiness of backscatter through the water column. The aggregation index is calculated over a scale from 0 to 1, with 0 being evenly distributed throughout the water column and 1 being aggregated.

Echometrics can be used to summarize temporal (and spatial) variability in abundance and behavior in large datasets and to detect and quantify variability in animal densities across temporal scales (e.g. transient events, diel vertical migrations, interannual changes).

Time series of metrics were tabulated to summarize biological characteristics at each site. Mean density (i.e. mean Sv) was obtained by integrating backscatter through the entire water column within 3 min bins. Computed metrics for each 3 min sample resulted in a time series with 1 datapoint every 2 hours (n=362 datapoints). Mean and variance of normally-distributed metrics (mean Sv, center of mass, and inertia) were compared using t-tests and F-tests ($\alpha = 0.05$). For the non-normally distributed aggregation index, non-parametric Kolmogorov-Smirnov (Massey 1951) and Bartlett's (Bartlett 1947) tests were used to compare means and variances.

5.2.4.2 Scales of variation in biological characteristics

Wavelet analysis (Torrence and Compo 1998) was used to describe and compare dominant periodicities in biological characteristics (i.e. density and vertical distribution of pelagic organisms) at both study sites. A wavelet transform decomposes a time series across time and frequency domains. The result is a 2-dimensional heat-map, called a scalogram, that represents the wavelet power (i.e. variance) contributed by each temporal period (i.e. scale) at each time step. Therefore, a wavelet transform allows, not only the detection of constituent periods or frequencies (analogous to a Fourier Transform), but also the location of frequency components in the time series (Torrence and Compo 1998; Cazelles et al. 2008).

A continuous Morlet mother wavelet function (Torrence and Compo 1998) was applied to each time series from both sites. Continuous wavelets enable the localization of transient patterns in variance and have been previously used for the analysis of temporally-indexed acoustic data (e.g. Urmy 2012; Jacques 2014; Viehman and Zydlewski 2017)). Temporal scales analyzed ranged from 4 hours (2 times the data resolution) to 256 hours. Wavelet power was calculated using the R package *biwavelet* (version 0.20.11, Gouhier et al. 2016). Statistical significance in localized wavelet power was tested against a white noise (constant value, equal to the time series variance) null hypothesis at a 95% confidence level (Torrence and Compo 1998).

Horizontal integration of wavelet power at each scale over the entire deployment—the global wavelet spectrum—allows the measurement of variance contributed by each scale across the entire series. Significance of this time-averaged variance was tested against both white and red (modelled as a first order autoregressive process with the variance and autocorrelation empirically derived from the time series) noise at a 95% confidence level (Torrence and Compo 1998).

Wavelet coherence was calculated to compare dominant periodicities in biological descriptors of density and vertical distributions between the two study sites. Coherence is a measure of the

local correlation between two time series in the time-frequency domain, taking values between 0 and 1 (Grinsted et al. 2004). Statistical significance in wavelet coherence was tested against a white noise null hypothesis at a 95% confidence level.

5.2.4.3 Selection of environmental predictors and time series models

To select environmental predictors for temporal patterns in density and vertical distribution of pelagic organisms at both study sites, linear regression models were fit using different sets of covariates. Mean Sv, center of mass, inertia, and a log10-transformed aggregation index were used as response variables. Only covariates available for both sites were included in the regression models: Julian day, daily tidal range (daily difference between high and low tide), 24-hour periodicity introduced as a Fourier series, and day-tidal range interactions representing the phase of the moon. Tidal data were obtained from the NOAA tide and current database (https://tidesandcurrents.noaa.gov/stations.html?type=Water+Levels). The best fit model was identified using the corrected Akaike Information Criterion (AICc) (Akaike 1987). Residual plots and the variance inflation factor (VIF) (Belsley et al. 1980) were examined to evaluate model fit and multicollinearity.

Autoregressive Moving Average (ARMA) models (Box and Jenkins 1976; Chatfield 1989) were used to model density and vertical distribution of pelagic organisms over time at both study sites. These models include an autoregressive, AR(p), component which regresses a process on p past values, and a moving average, MA(q), component which models the error based on q previous values (Box and Jenkins 1976). Modelling the errors with MA(q) components is often used to model unexplained variability in the environment.

ARMA models can be formatted as a Regression-ARMA model (Reg-ARMA)—a linear regression with autocorrelated errors—to model dependent data using environmental predictors in

addition to lagged dependent values (Hyndman et al. 2017). Linder et al. (2017) used Reg-ARMA models as candidate models for the characterization of acoustic data from the Admiralty Inlet tidal energy site. These models are structured as shown in (2) and (3), where nt is the error remaining from the linear regression model, $b1$-bp represents the parameters multiplied by the autoregressive error terms, and $\theta 1{-}\theta q$ represents the parameters multiplied by the moving-average error term.

$$y_t = a + b_1 x_{1t} + \cdots b_p x_{pt} + n_t \tag{5.2}$$

$$n_t = b_1 n_{t-1} + \cdots b_p n_{t-p} + e_t + \theta_1 e_{t-1} + \cdots \theta_q e_{t-q};\ e_t \sim Normal(0, \sigma) \tag{5.3}$$

The auto.arima function of the R package *forecast*, version 8.2 (Hyndman et al. 2017), was used to fit and select Reg-ARMA models for each metric and site. Environmental predictors from the selected linear regression model (see section D3) were included in the Reg-ARMA model selection. Response variables and covariates were standardized using a z-score transformation to enable comparison of relative effects of the variables at both sites. The non-normally distributed aggregation index was log10 transformed prior to being transformed to a z-score.

Autocorrelation plots of model residuals were visually inspected for statistically significant values (i.e. autocorrelation values outside the 95% critical value bounds). A seasonal component was included in the Reg-ARMA model when significance was observed at a lag of 12 hours that corresponds to daily cycles in the data.

5.3 RESULTS

5.3.1 *Echometrics time series*

There were both similarities and clear differences in density and vertical distributions of pelagic organisms between wave and tidal sites (Figure 5.2 and Table 5.2). Mean density values (mean

Sv) were lower at the tidal site than at the wave site, where an increasing trend was present. Location of organisms in the water column (i.e. center of mass) was, on average, higher off bottom at the wave site than at the tidal site but there were no significant differences in the dispersion (i.e. inertia) from the mean location between sites. Standard deviations for all metrics except the aggregation index were significantly ($p < 0.05$) greater at the wave site than at the tidal site (Table 5.2). The aggregation index remained close to zero throughout most of the time series for both sites, punctuated by episodic occurrences of high aggregation values at the tidal site.

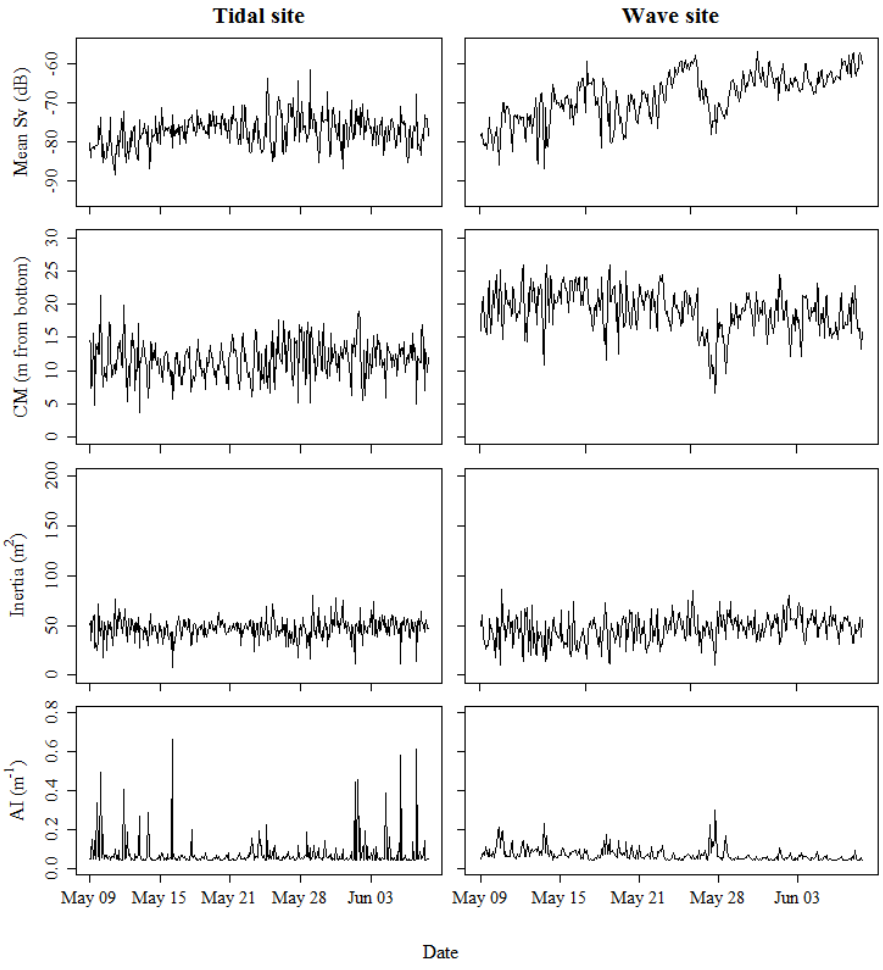

Figure 5.2. Time series (N=362) of mean volume backscattered energy (mean Sv), center of mass (CM), inertia, and aggregation index (AI) from a tidal energy pilot site located in Admiralty Inlet (WA) (left panel) and a wave energy pilot site located off the coast of Newport (OR) (right panel).

Table 5.2. Means and standard deviations of four metrics representing biological characteristics and tidal range at the Admiralty Inlet (WA) tidal site and the PacWave (OR) wave energy site.

	Mean			Standard Deviation		
	Tidal Site	Wave Site	p-Value	Tidal Site	Wave Site	p-Value
Mean Sv (dB)	-77.26	-68.36	< 2.20e–16	4.06	6.18	4.00e–15
Center of mass (m)	11.62	19.05	< 2.20e–16	2.76	3.24	2.26e–03
Inertia (m2)	46.94	46.16	0.38	10.48	13.56	1.13e–06
Aggregation Index (m-1)	0.074	0.070	1.00e–07	0.08	0.03	< 2.20e–16
Tidal range (m)	8.88	8.43	5.09e–03	2.37	1.91	5.24e–05

5.3.2 *Scales of variation in biological characteristics*

Dominant periodicities in density and vertical distributions of pelagic organisms were observed at both sites (Figure 5.3). All metrics varied at the 24-hour diel period at both sites but the significance of this periodicity was more consistent through time in mean Sv and center of mass at the tidal site (Figure 5.3, left panel). Significance at a 12-hour periodicity was also detected at the tidal and wave sites suggesting the importance of tidal processes in both environments. Site-specific periodicities were also observed. Longer-period variability—between 64 and 256-hour (~2 weeks) periods—was observed at the wave site in mean Sv, center of mass and aggregation index (Figure 5.3, right panel). At the tidal site, there was variability at the 128 and 256-h periods in mean Sv, corresponding to lunar phase and neap-spring tidal cycles (Figure 5.3, left panel). Inertia had significant variability at the 64 and 128-hour (~1 week) periods at both sites.

Significant peaks in the global wavelet spectrum were observed at the 24-hour period for density and center of mass at the tidal site only (Figure 5.4, left panel) suggesting a major influence of diel cycles at the tidal site. Significant peaks at longer periods (128-256 hours) were observed

when contrasted with white noise for mean Sv, aggregation index, and center of mass at the wave site (Figure 5.4, right panel), and only mean Sv at the tidal site (Figure 5.4, left panel).

Both sites were in phase (i.e. high coherence) at 12-h and 24-h periods in all metrics and at the 64-h period for inertia (Figure 5.5). These periods are consistent with observations from the wavelet analyses for each site (Figure 5.3).

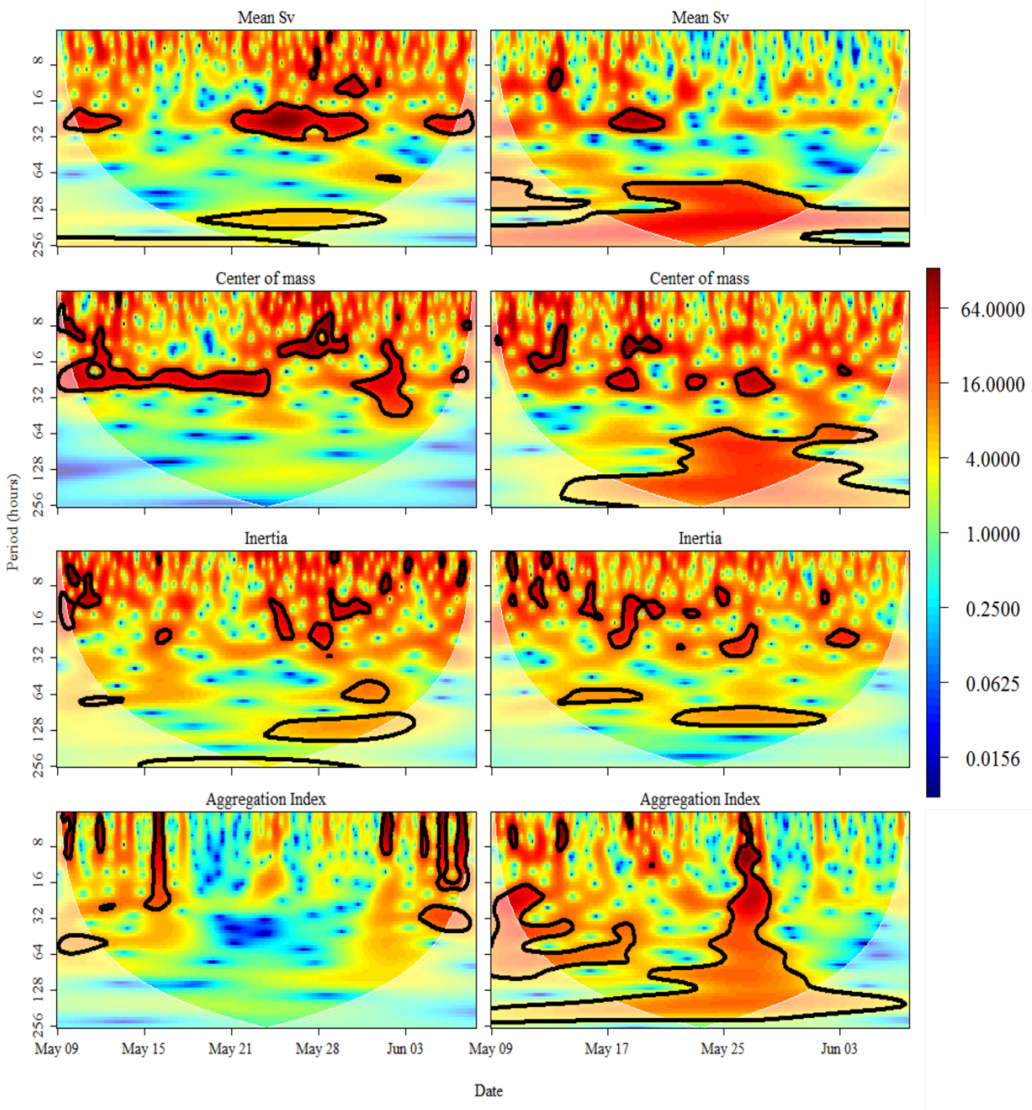

Figure 5.3. Wavelet decomposition of the temporal variability in pelagic fish and macrozooplankton characteristics (Mean Sv, center of mass, inertia, and aggregation index) at Admiralty Inlet (WA) tidal site (left panel) and the PacWave energy site (right panel). Areas of significance are traced with a black line. Color bar represents wavelet power (σ^2).

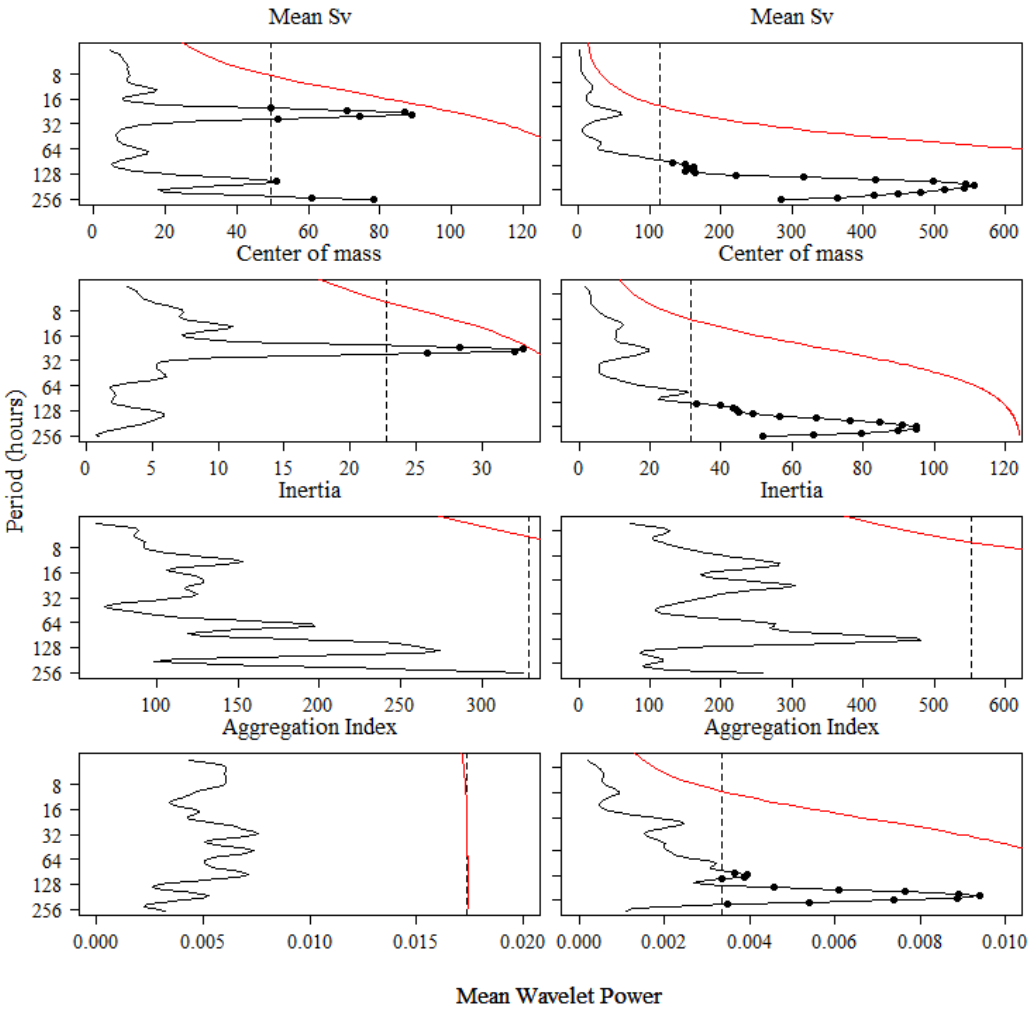

Figure 5.4. Time averaged variance (global wavelet spectrum) of biological descriptors at the Admiralty Inlet (WA) tidal site (left panel) and the PacWave Energy Test Site (OR) wave energy site (right panel). Dashed black line represents white noise and the red solid line represents red noise.

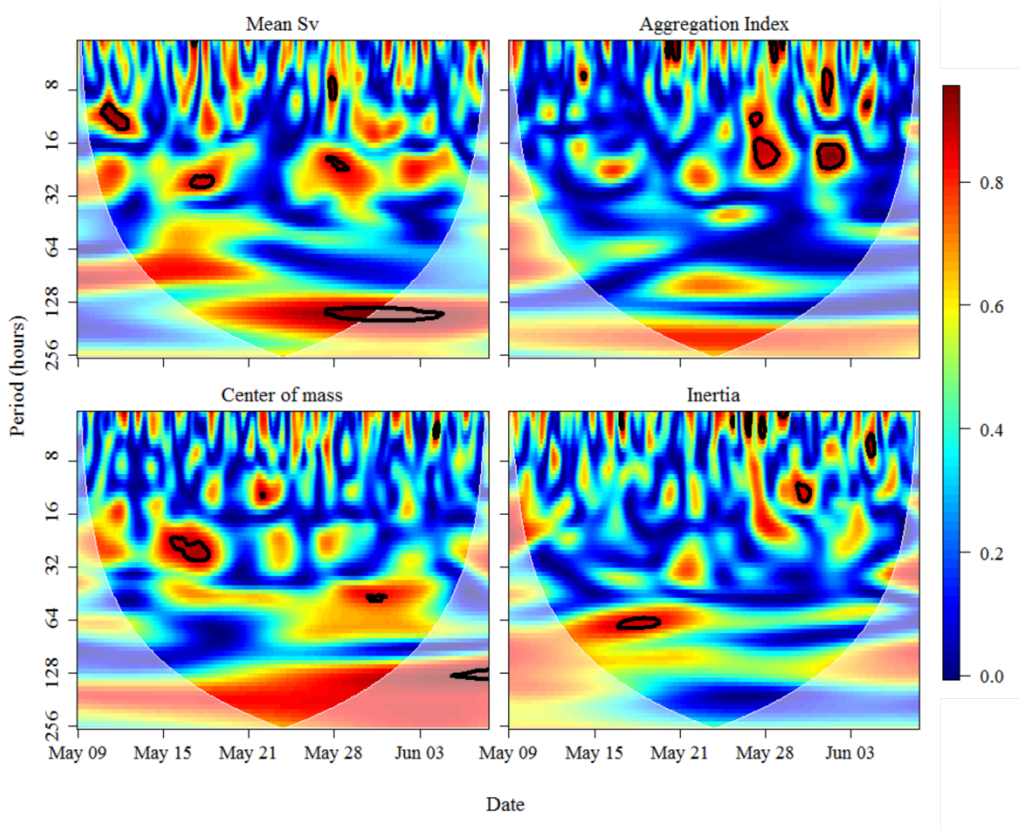

Figure 5.5. Wavelet coherence in biological characteristics (Mean Sv, center of mass, inertia, and aggregation index) between the Admiralty Inlet (WA) tidal site and the PacWave energy site. Areas of significance are traced with a black line. Color bar represents coherence.

5.3.3 *Selection of environmental predictors and time series models*

Common environmental predictors explained patterns in metrics at tidal and wave sites (Table 5.3). The regression model selected for mean Sv as the response variable included all covariates at both sites (Table 5.3). Tidal range and moon phase (tidal range-Julian day interaction; TR:D) were included in regression models for center of mass and inertia of both sites. Aggregation index models for both sites included the 24-hour period. Selected models for all metrics at the wave site included day of year as a predictor, whereas tidal range was included in all selected models for the tidal site (Table 5.3).

Reg-ARMA orders and standardized coefficients that best explained the structure of the time series are presented in Table 5.4 and fits of the selected models are shown in Figure 5.6. Overall, selected models accurately described periodicity and amplitude of mean Sv and center of mass values at both sites. The amplitude of inertia values for both sites and aggregation index for the tidal site were not well described by the models. AR and MA orders differed for each metric and site. In general, higher AR orders at the wave site suggest smoother changes and longer 'memory' (i.e. dependence on 1-5 previous time steps) in biological characteristics than at the tidal site (i.e. generally dependent only on the previous time step). Higher MA orders were observed at the tidal site compared to the wave site (MA components generally explain autocorrelation in the unexplained residual variation of the model). Seasonal components (1-day lag) were only included in mean Sv models, indicating the presence of daily cycles in organism density at both sites.

Table 5.3. Covariates and p-values from linear regressions for Admiralty Inlet tidal site and the PacWave site time series. * indicates significant p-values (< 0.05). TR:D is the interaction between tidal range and Julian day, and represents the moon phase. 24H sin and cos are the sine and cosine components of a 24-hour periodicity.

	Tidal site		Wave site	
	Estimate	p-value	Estimate	p-value
Mean Sv				
Tidal range	4.22e–02	4.16e–09*	-1.53e–02	0.034*
Julian day	3.33e–01	6.07e–12*	4.42e–01	4.53e–16*
TR:D	-2.91e–04	8.61e–09*	9.38e–05	0.05*
24H sin	-1.30	3.48e–07*	-1.044	0.000732*
24H cos	2.13	6.05e–16*	1.47	2.42e–06*
Center of mass				
Tidal range	-8.14e–03	0.000483*	-1.84e–02	0.000517*
Julian day	–	–	-2.39e–01	9.25e–10*
TR:D	5.34e–05	0.000908*	1.25e–04	0.000501*
24H sin	-1.40	2.87e–13*	–	–
24H cos	7.57e–01	4.94 e–05*	–	–
Inertia				

Tidal range	-2.44e–02	0.01*	4.95e–02	0.0273*
Julian day	–	–	7.03e–01	1.76e–05*
TR:D	1.74e–04	0.0099*	-3.25e–04	0.0320*
24H sin	–	–	-1.48	0.1215
24H cos	–	–	2.4	0.0124*
Aggregation index				
Tidal range	-9.72e–05	0.05*	–	–
Julian day	–	–	-0.02	<2e-16*
TR:D	–	–	–	–
24H sin	7.58e–02	3.44e–02*	0.04	0.07447
24H cos	-9.82e–02	6.20e–03*	-0.13	2.27e–08*

Table 5.4. Estimated significant coefficients for Regression Autoregressive Moving Average models that describe biological characteristics of tidal and wave energy pilot sites.

	Mean Sv		Center of Mass		Inertia		Aggregation Index	
	Tidal Site	Wave Site	Tidal Site	Wave Site	Tidal Site	Wave Site	Tidal Site	Wave Site
ARMA coefficients								
AR1	0.15	1.33	–	1.28	0.10	0.20	–	0.70
AR2	–	-0.62	–	-0.42	–	0.00	–	–
AR3	–	0.23	–	-0.03	–	-0.07	–	–
AR4	–	–	–	0.10	–	-0.06	–	–
AR5	–	–	–	–	–	0.14	–	–
MA1	–	-0.66	-0.87	-0.77	–	–	-0.05	-0.31
MA2	–	–	-0.21	–	–	–	0.08	–
MA3	–	–	-0.07	–	–	–	0.09	–
MA4	–	–	0.17	–	–	–	0.11	–
SAR1	0.25	0.18	–	–	–	–	–	–
Covariate coefficients								
Tidal range	0.05	-0.12	-0.06	-0.05	0.07	0.08	0.00	–
Julian day	0.18	0.71	–	-0.37	–	0.30	–	-0.45
TR:D	-0.29	0.03	0.08	0.11	0.17	-0.09	–	–
24H sin	-0.32	-0.17	-0.50	–	–	-0.11	0.15	0.12
24H cos	0.53	0.24	0.28	–	–	0.18	-0.20	-0.36
24H total	0.62	0.29	0.58	–	–	0.21	0.25	0.38

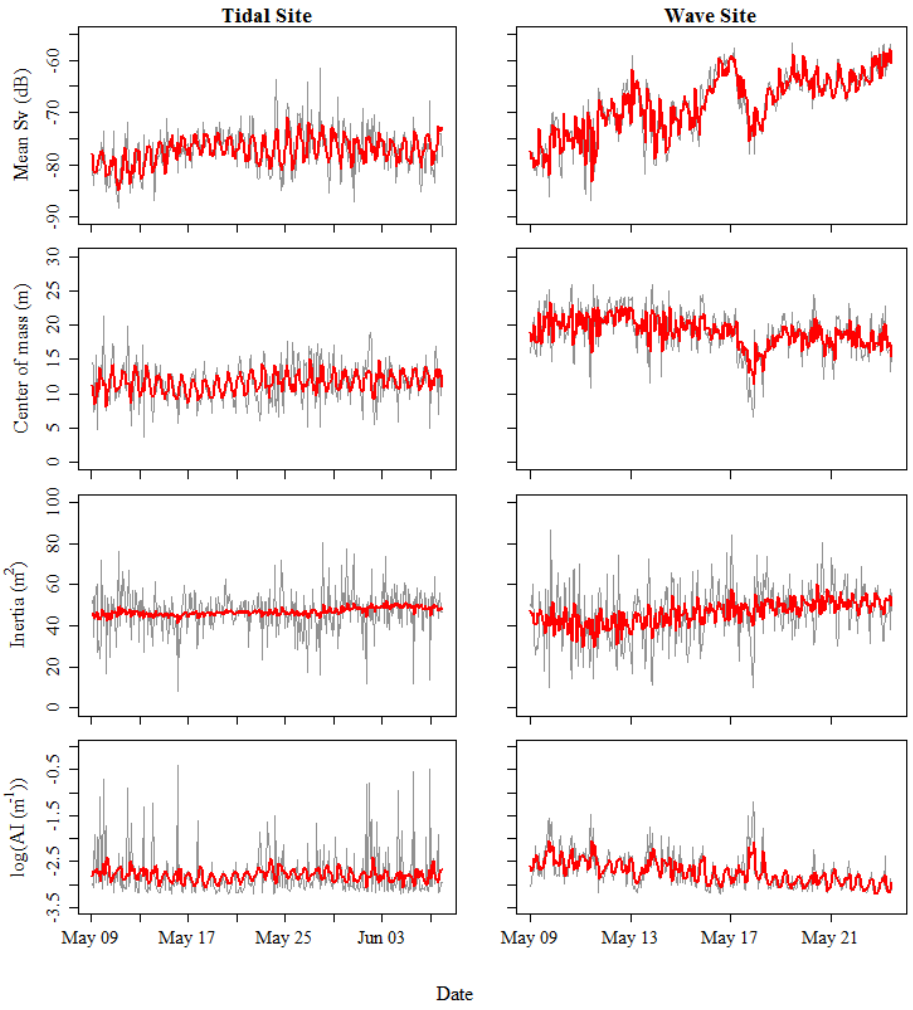

Figure 5.6. Regression Autoregressive Moving Average models for mean Sv, center of mass, inertia and aggregation index for a tidal and a wave energy site. Raw data are in grey and in red are shown the mean model predictions.

5.4 DISCUSSION

Understanding temporal patterns in changes to biological characteristics at wave and tidal energy sites is essential to inform MRE development and operation. Monitoring strategies that ensure detection of biological changes associated with the installation, operation, and decommissioning of MRE devices are required to ensure sustainable development of the industry and to meet

regulatory requirements (Copping 2018). But, detecting biological changes in highly variable aquatic environments is challenging. Densities and distributions of aquatic populations vary across a wide range of spatial and temporal scales as a result of multiple physical and biological processes acting and/or interacting across an equally wide range of scales (e.g. Stommel 1963; Haury et al. 1978). Therefore, characterization of "natural" or pre-installation variability in the biological characteristics of a site (e.g. abundance, diversity, vertical distributions) maximizes the probability of detecting changes associated with MRE deployment and operations from natural variability (Linder et al. 2017). After installation of MRE devices, departures from expected variations in biological characteristics based on pre-installation data can be detected, and quantified; after which action plans to modify, mitigate, or cease operations can be developed and implemented. Quantification of temporal patterns in biological characteristics and the identification of environmental drivers can be used to design environmental monitoring plans. To ensure detection of biological changes, monitoring plans should include all relevant variables and corresponding sample designs. Understanding temporal biological patterns is therefore essential to establishing appropriate sampling resolutions, regulations, and reporting requirements for MRE environmental monitoring.

Despite differences in physical characteristics of tidal and wave site environments, similarities in biological characteristics were observed. A primary criterion for wave and tidal energy development site selection is their physical attributes: high tidal flows at tidal sites and open coastal areas with favorable wind conditions at wave energy sites. Since biological communities are shaped by the physical characteristics of their environment (Stommel 1963), it is expected that biological characteristics of two MRE sites with distinctive physical attributes would differ. I found numerous common biological characteristics at the studied wave and tidal sites. Dispersion

(i.e. inertia) magnitudes and dominant periodicities were similar at both sites, and at least one regression covariate was shared between the sites for all metrics. For example, density and location of fish and microzooplankton metrics indicated common diel and/or tidal cycles at both sites. Diel and tidal patterns have also been reported as dominant variables in studies of fish density in the Fall of Warness (Scotland) (Wiesebron et al. 2016b) and fish counts at Cobscook Bay (Maine, US) (Viehman and Zydlewski 2017) tidal sites.

Differences in biological characteristics between tidal and wave energy sites (i.e. sector-specific characteristics) were also observed. One major difference between sites was the dominant periods of variation in biological characteristics. At the tidal site, dominant periodicities were shorter and more consistent through time compared to the wave site. In contrast, longer period processes dominated at the wave site as shown by significant peaks at longer periodicities and higher order autoregressive component in ARMA models. This difference in temporal variability is attributed to differences in the hydrodynamics of the sites. Admiralty Inlet is located at the confluence of waters with different oceanographic properties coming from Deception Pass, the Hood Canal basin, and the Puget Sound main basin (Moore et al. 2008). Each of these water masses potentially carries distinctive species assemblages, so differences in biological characteristics could be expected between ebb and flood tides when different water masses are transported through the study site. The PacWave site is located in an open coastal area where water masses are more uniform during tidal cycles and changes in water masses occur over longer periods in response to changes in wind-driven circulation patterns (Kosro 2005; Sigleo et al. 2005). Diel patterns in density and location of organisms were relatively more important than tidal cycles at both sites as illustrated by greater wavelet power at the 24- compared to the 12-hour period. Fish and zooplankton species undergo vertical and horizontal diel (24-hour) migrations for feeding and

predator avoidance in response to environmental cues such as changes in light intensity (e.g. Axenrot et al. 2004; Benoit-Bird and Au 2006; Kaltenberg and Benoit-Bird 2009).

Although diel patterns were dominant at both sites, the influence of diel cycles on biological characteristics was not consistent within or between sites through the deployment. Density changes were more intermittent and lower in magnitude at the wave site compared to the tidal site. Changes in the relative importance of diel fluctuations could be due to multiple factors such as episodic decreases in light intensity (e.g. cloud cover), or occurrence of storms that can mix the water column and attenuate diel migration patterns. Diel patterns are species and life-stage specific (Nilsson et al. 2003; Becker et al. 2011), so changes in species and size composition of the community could also explain changes in dominant periodicities of biological fluctuations observed in this study. At the wave site an increasing trend in biomass density suggests that sampling may have occurred during a transition with new species or size groups entering the study area. Sampling at the wave site (May-June) corresponds to the formation (April-May) and establishment (May-July) of seasonal upwelling off the Oregon coast (Peterson et al. 1979). Occurrence of seasonal coastal upwelling enhances nutrient availability and primary productivity, which ultimately translates into increased zooplankton and fish abundances (Cury et al. 1995; Parrish and Mallicoate 2007). Acoustic observations of species ensembles may obscure the detection of diel patterns of individual species (Viehman and Zydlewski 2017).

The study of temporal variability using stationary platforms including acoustic and other environmental sensors has great potential for biological monitoring at MRE sites (e.g. Jacques 2014). Stationary active acoustics can detect biological changes and trends in short (e.g. diel migrations) to long (e.g. tidal dynamics, seasonal) period fluctuations at highly variable and energetic environments where traditional sampling is constrained. Autonomous acoustic sensors

also provide advantages over shipboard spatial surveys by reducing or eliminating: (1) long term cost and effort required to acquire data; (2) bias in measurements due to ship avoidance behaviors by marine animals; and (3) convolution of temporal and spatial variability that occurs during mobile, spatial surveys (Godø et al. 2014). A previous comparison of active acoustic technologies showed that scientific echosounders can identify patterns not present in data from ADCPs or acoustic cameras, and were therefore recommended to monitor fish density at tidal energy sites (Jacques 2014). Internationally accepted calibration protocols for scientific echosounders (Foote et al. 1987; Demer et al. 2015) ensure equivalency among datasets, which is crucial to make progress in understanding effects of the MRE industry on marine environments. For instance, if effects are not site-specific but device-specific, then alternate device designs can be selected or mitigation measures can be regulated to minimize impacts.

Acoustic sampling technologies are constrained like any other sampling device. Acoustic data alone rarely provides sufficient information for species identification (Horne 2000). For the MRE industry, species discrimination and identification are particularly relevant when addressing regulations for species of special status. Supplementary information from literature, increased acoustic frequency spectrum, direct net sampling, and optical sampling can be used to verify acoustic targets. The quality of acoustic data can also be affected by entrained air (Simmonds and MacLennan 2005) in surface layers typically found in the high velocity environments of tidal energy sites. Although automated methods to remove turbulence are being developed (e.g. Fraser et al. 2017), methods to filter or predict backscatter in turbulent areas are still needed to allow a full characterization of the water column using acoustics. Despite covering a wide spectrum of temporal scales (e.g. seconds to months or years), point source measurements using stationary acoustics do not include a large range of spatial scales when characterizing variability in animal

densities or behaviors. By quantifying the spatial area that is represented by a point source measurement (i.e. representative range, Horne and Jacques 2018), I can ensure an appropriate characterization and monitoring of biological communities, and at the same time, optimize the cost-effectiveness of remote monitoring. Pre-installation spatial characterization through concurrent acoustic mobile surveys and point source measures can be used to calculate the spatial representative range and define the number of monitoring packages needed to optimize sampling for environmental monitoring goals.

Data processing that reduces acoustic data volumes and automates analysis is required to ensure timely responses to changes in biomass distributions during MRE monitored operations. Storage, processing, and analysis of large volumes of acoustic data over long-term deployments can be challenging (Godø et al. 2014). Advantages of using distributional metric suites include the reduction of large acoustic data volumes into a manageable and informative form. Metric suites can be used as ecological indicators. Ecological indicators are intended to examine composition (e.g. number and variety of species), structure (e.g. vertical distribution pattern) and function (e.g. ecological processes) of ecosystems to assess the magnitude of stress, degree of exposure, and ecological responses to stress (Dale and Beyeler 2001; Niemi and McDonald 2004). Mean Sv and center of mass monitor ecosystem structure whereas inertia and the aggregation index track changes in ecosystem function (Wiesebron et al. 2016b). These metrics can also be used to detect and describe potential responses of fish and macrozooplankton to MRE devices. Moving devices generate noise and electromagnetic fields that can be evaded or avoided by fish (Boehlert and Gill 2010; Viehman and Zydlewski 2014). Aggregation behaviours can also be expected as new structure in a homogeneous seascape can potentially act as fish aggregation devices (FADs) and can provide refuge from high speed currents in the wake of the device (Inger et al. 2009; Boehlert

and Gill 2010; Cada and Bevelhimer 2011). Removal of hydrokinetic energy may change local hydrodynamics affecting turbulence and stratification patterns that in turn, can affect vertical movements of organisms (Boehlert and Gill 2010). Avoidance and aggregation effects can be measured as a decrease or increase in mean Sv values, and changes in vertical distribution patterns can be measured as changes in center of mass, inertia, and aggregation index.

Wavelets and Reg-ARMA enabled the detection of generic and specific biological features of the MRE sites and are therefore recommended as standard tools for the analysis of biological monitoring data. Wavelet analysis detected differences in biological patterns across sites, which illustrates its potential for detecting changes before and after the installation of MRE devices—a required attribute to be an effective tool for environmental monitoring. Reg-ARMA models were used to identify relevant environmental factors that shape biological patterns and are important in the forecast of biological responses (e.g. Linder and Horne 2018). These models quantified amplitudes and periodicities of all metrics except inertia (at both sites) and amplitudes of the aggregation index (at the tidal site). Other environmental covariates (e.g. current speed, temperature, stratification) or alternate models may be needed to capture amplitudes of all biological fluctuations. A set of models have been recommended to quantify pre-installation conditions (Linder et al. 2017) and measure environmental change (Linder and Horne 2018), based on the statistical properties of ecological indicators (normal and non-normal distributions), quantity of interest (mean or variance), and application (detection, quantification, or forecast of change).

A standard approach for pre-installation characterization and post-installation monitoring enables comparisons among sites, and will streamline the current, long and expensive MRE permitting process (Polagye et al. 2011; Wright 2014; Magagna and Uihlein 2015; Fox et al. 2018).

To date, monitoring plans have been designed for individual sites and species of special status (e.g. harbor seal populations at the SeaGen tidal site and southern resident killer whales at Snohomish Public Utility District 1 tidal site). Moreover, choices of monitoring technologies and sampling resolutions have differed among tidal energy sites within the U.S. (e.g. Coobscook Bay (MA) (Viehman and Zydlewski 2014) vs Admiralty Inlet (WA) (Jacques 2014). Near identical acoustic sampling used at the Admiralty Inlet (US) and the Fall of Warness (UK) tidal energy sites enabled the characterization and comparison of fish and macrozooplankton densities, with results suggesting that standardization of biological monitoring within the tidal MRE sector is feasible (Wiesebron et al. 2016b). In this study a comparison of wave and tidal energy sites representing two sectors of the MRE industry suggests that standard remote sensing technologies (stationary active acoustics), biological indicators (echometrics), and analytic methods (wavelets and Reg-ARMA models) could be used for biological monitoring across all sectors in the MRE industry.

While standard monitoring practices are desirable to facilitate sustainable development of the MRE industry, site-specific characteristics should be used to tailor monitoring plans. Pre-installation characterization data are needed to identify dominant temporal scales in biological characteristics and then used to set sampling resolutions to minimize monitoring costs while maximizing the quality of monitoring data (i.e. optimization). Timing of post-installation sampling can also be determined using pre-installation characterization data. For instance, if natural variations in a monitoring metric are associated with tidal states, then sampling should occur at the same tidal state or averaged across tidal states to detect change rather than patterns being convolved over time due to sampling. This approach using continuous acoustic data can also be used to design discrete sampling (e.g. net tows) (Blauw et al. 2012). Identification of environmental covariates is important when forecasting and discriminating sources of biological

change. During pre-installation monitoring, environmental variables believed to influence biological temporal patterns should be measured and included in data analyses to identify environmental forcing of natural variability at each site. Identified variables should then be monitored along with response variables during post-installation monitoring to help distinguish biological changes associated with MRE from natural variability. Assuming that representative data are obtained, pre-installation acoustic data can be used to define thresholds of change in monitored variables at a site (Wiesebron et al. 2016a).

5.5 CONCLUSION

Stationary active acoustics is a cost-effective tool to sample biological communities through the entire water column over long periods of time in variable or high-energy aquatic environments. Acoustic-derived density measurements are a strong candidate as a common/standard data stream to be used for biological monitoring across sectors of the MRE industry. Standard practices (e.g. sampling methods and analytic approaches) are possible for biological monitoring at MRE sites but should be adapted to site/sector-specific characteristics (e.g. major influencing covariates and periodicity). Pre-installation characterization is important to quantify natural variability and to tune monitoring strategies to include site-specific characteristics for post-installation monitoring. This approach will maximize cost-effective detection, understanding, and prediction of MRE development impacts on the environment. Current climate change and declines in non-renewable energy sources accentuate the need for alternatives to fossil fuels to meet energy demands. Monitoring strategies that facilitate the development of MRE industry while preserving aquatic ecosystems are required to sustain environmental viability.

Chapter 6. SYNTHESIS

6.1 SYNTHESIS AND SIGNIFICANCE

Marine environments are changing, and further changes are expected in response to climate change, industry development (e.g. oil and gas explorations and marine renewable energy), pollution, and fishing (e.g. Halpern et al. 2008; Duarte et al. 2012; Doney et al. 2012). There is an urgent need to understand impacts of these stressors on marine ecosystems and to adopt effective management measures that minimize detrimental effects. Accomplishing this goal requires a comprehensive understanding of "natural" or baseline temporal patterns of biological components and underlying processes that influence observed patterns.

High-latitude environments and marine renewable energy (MRE) sites have been particularly understudied due to sampling challenges (e.g. presence of sea ice, and high current velocities). This lack of baseline information required to measure biological responses to environmental change has increased the difficulty to document impacts and to predict effects of further change. This dissertation provides a high-resolution, continuous characterization of fish and zooplankton dynamics in the Chukchi Sea and at sites selected for marine renewable energy development. This characterization increases the ability to detect and predict biological responses to environmental change, ensure the collection of representative samples, and to assist the design of standard strategies for biological monitoring of aquatic ecosystems. Comparison of multi-year, high resolution, stationary acoustic data from the Chukchi Ecosystem Observatory (CEO) and concurrent measurements from a large set of environmental sensors (Chapters 2 and 3) increased our understanding of temporal variability in the abundance and behavior of fish and zooplankton in the Chukchi Sea. Increased understanding of temporal patterns and environmental drivers of key components of Arctic ecosystems, including Arctic cod, increases our ability to predict

biological responses to further changes in high latitude environments. Quantification of the spatial area that is represented by point source measurements (Chapter 4) informs design of cost-efficient, distributed monitoring networks (i.e. maximizing the amount of data collected while minimizing the cost of collecting measurements) that can be used to monitor any aquatic ecosystem. Comparisons of temporal variability in biological characteristics at sites selected for tidal and wave energy, with very distinct environmental characteristics (Chapter 5), allows us to assess the potential for applying standard methods and analytic tools for biological monitoring, and to tune standard strategies to specific characteristics of the system. Identifying and defining standard monitoring goals and sampling methods is necessary to expedite Marine Renewable Energy projects development, reduce monitoring costs, detect environmental impacts, and to enable comparison of impacts among sites.

In summary, this dissertation provides knowledge and tools that can be used to assess biological responses to climate change, to design cost-effective ecosystem assessment of aquatic resources, and to define monitoring strategies for MRE, oil and gas exploration or other projects with potential impacts on aquatic ecosystems.

6.2 IMPLICATIONS FOR BIOLOGICAL MONITORING AND RESOURCE ASSESSMENT

This dissertation provides baseline information and methodological approaches that can be used to optimize sampling (i.e. minimizing sampling costs while maximizing data quality) in monitoring and resource assessment efforts. The calculation of representative ranges (Chapter 4) quantifies the spatial scope of measurements from stationary sensors and informs strategies for monitoring programs and sampling designs. Method selection to quantify representative ranges is key and should be tied to the study/monitoring objective(s). A delineation of the study domain and a definition of what constitutes “similar” or “representative” must be aligned to meet

study/monitoring goals. Once goals are defined, concurrent stationary and mobile measurements should be conducted using comparable technologies (e.g. calibrated scientific echosounders with the same frequencies). After representative ranges are calculated, we can use those ranges/areas to define the number and spacing of sensors in a study domain.

The comparison of wave and tidal energy sites representing two sectors of the MRE industry demonstrated that a combination of stationary active acoustics, echometrics, wavelets and Regression-Autoregressive Moving Average models can be used as a standard approach for biological monitoring across sectors of the MRE industry. A standardization of sampling techniques, biological metrics, and analytic methods reduces monitoring costs and streamlines permitting process for MRE projects. Observations from this comparison also highlight similarities and site/sector-specific differences that should be considered when developing monitoring strategies for the MRE industry. Dominant scales of variation and autocorrelation of biological characteristics assessed pre-device installation can be used to set sampling resolutions to minimize monitoring costs while maximizing the quality of monitoring data. Sample timing during post-device installation monitoring, including collection of direct samples using nets or other tools, can also be determined using pre-device installation data. To illustrate by example, if natural variation in a monitoring metric is associated with tidal states, then sampling should occur at the same tidal state or averaged across tidal states to detect change. Identifying environmental drivers of observed biological patterns is important when forecasting and discriminating sources of biological change. Candidate environmental variables believed to influence biological temporal patterns should be measured during pre-device installation sampling and included in data analyses to identify dominant environmental drivers of natural variability at each site. Identified variables should then be monitored along with response variables during post-device installation monitoring to

distinguish biological changes associated with MRE development from natural variability. Assuming that representative samples are collected, pre-device installation acoustic data can be used to define thresholds of change in monitored variables at a site (Wiesebron et al. 2016b). Additionally, concurrent acoustic mobile and stationary measurements during pre-device site characterization can be used to calculate the spatial representative range of point source observations and to define the number of monitoring packages needed to optimize sampling for environmental goals (see Chapter 4). These approaches and procedures are recommended in the context of the MRE developing industry but are applicable to monitoring efforts associated with numerous activities that are conducted over a range of environments; oil and gas exploration, offshore mining, fishing. To date, mandated MRE environmental monitoring plans have been typically specified within industry sector, at a specific site, and for a specific project. This approach precludes industry and project development, assessment of MRE device effects on the environment, and comparison of impacts among sites and industry sectors.

Quantifying temporal patterns in fish and zooplankton densities and their environmental drivers can also be used to optimize sampling. A thorough characterization of temporal patterns can be used to inform appropriate timing, frequency, and extent of continuous and discrete sampling needed to effectively monitor patterns and processes at any location. Dominant scales of temporal biological variability can be used to define sampling periodicity to quantify variability in any process of interest. For instance, observed differences in the duration of "seasons" for fish and zooplankton in the NE Chukchi Sea should be considered when defining the timing and frequency of sampling if the goal is to characterize changes within annual patterns in each community. Also, the timing and amplitude of key environmental processes (e.g. phytoplankton blooms, fish production) can be used to define the timing of sampling surveys. As an example, the amplitude

and timing of peaks in Arctic cod density in the summer, a proxy of gadid annual recruitment (Bouchard et al. 2017), has been strongly linked to the timing of sea ice retreat, which is associated with transport of water through the Bering Strait (Chapter 3). Therefore, time of sea ice retreat can be used to define the appropriate timeframe for summer surveys to provide accurate estimations of Arctic cod production and recruitment that can be used to inform resource management decisions.

6.3 PREDICTING BIOLOGICAL RESPONSES TO ENVIRONMENTAL CHANGE: MANAGEMENT AND CONSERVATION PLANNING OF MARINE ECOSYSTEMS.

The characterization of fish and zooplankton temporal patterns and environmental drivers in the NE Chukchi Sea advances the mechanistic understanding of high-latitude marine ecosystem dynamics. This mechanistic understanding can be used to predict potential impacts of climate change and inform ecosystem-based management and conservation planning for the Arctic. Potential shifts in biomass, species compositions, phenology, and distribution of endemic Arctic species along with northward expansion of subarctic populations may result in the displacement and/or replacement of current subsistence food resources for coastal human communities (cf. Grebmeier et al. 2006b). Northward expansion of subarctic fish species may lead to the northward extension of commercial boreal fisheries and introduce the potential for both spatial and temporal conflicts with traditional subsistence activities, environmental disturbance (e.g. bottom trawling), and overfishing of target stocks (Thorson et al. 2021). Timely understanding of ecosystem responses to current environmental change and examination of potential changes given future climate scenarios enables identification of sustainable activities and the planning of conservation or management responses to help ensure food security, cultural continuity, and economic well-being of Artic Indigenous People (Huntington et al. 2021). Characterization of current

environmental patterns in the Chukchi Sea within this dissertation can be combined with projected climate trajectories to identify and increase understanding of potential ecosystem spatiotemporal shifts that may require changes to current ecosystem-based management and conservation planning at local and regional scales.

BIBLIOGRAPHY

Akaike H (1987) Factor analysis and AIC. Psychometrika 52:317–332

Amano K, Abe Y, Matsuno K, Yamaguchi A (2019) Yearly comparison of the planktonic chaetognath community in the Chukchi Sea in the summers of 1991 and 2007. Polar Sci 19:112–119. https://doi.org/10.1016/j.polar.2018.11.011

Anderson SC, Branch TA, Cooper AB, Dulvy NK (2017) Black-swan events in animal populations. Proc Natl Acad Sci U S A 114:3252–3257. https://doi.org/10.1073/pnas.1611525114

Anttila S, Kairesalo T, Pellikka P (2008) A feasible method to assess inaccuracy caused by patchiness in water quality monitoring. Environ Monit Assess 142:11–22. https://doi.org/10.1007/s10661-007-9904-y

Ardyna M, Arrigo KR (2020) Phytoplankton dynamics in a changing Arctic Ocean. Nat Clim Chang 10:892–903. https://doi.org/10.1038/s41558-020-0905-y

Arrigo KR, Perovich DK, Pickart RS, et al (2014) Phytoplankton blooms beneath the sea ice in the Chukchi sea. Deep Res Part II Top Stud Oceanogr 105:1–16. https://doi.org/10.1016/j.dsr2.2014.03.018

Arrigo KR, Perovich DK, Pickart RS, et al (2012a) Massive phytoplankton blooms under arctic sea ice. Science (80-) 336:1408. https://doi.org/10.1126/science.1215065

Arrigo KR, Perovich DK, Pickart RS, et al (2012b) Under Arctic Sea Ice. Science (80-) 336:. https://doi.org/10.1126/science.1215065

Arrigo KR, van Dijken GL (2015) Continued increases in Arctic Ocean primary production. Prog Oceanogr 136:60–70. https://doi.org/10.1016/j.pocean.2015.05.002

Ashjian CJ, Campbell RG, Gelfman C, et al (2017) Mesozooplankton abundance and distribution in association with hydrography on Hanna Shoal, NE Chukchi Sea, during August 2012 and 2013. Deep Res Part II Top Stud Oceanogr 144:21–36. https://doi.org/10.1016/j.dsr2.2017.08.012

Ashjian CJ, Campbell RG, Welch HE, et al (2003) Annual cycle in abundance, distribution, and

size in relation to hydrography of important copepod species in the western Arctic Ocean. Deep Res Part I Oceanogr Res Pap 50:1235–1261. https://doi.org/10.1016/S0967-0637(03)00129-8

Assmy P, Fernández-Méndez M, Duarte P, et al (2017) Leads in Arctic pack ice enable early phytoplankton blooms below snow-covered sea ice. Sci Rep 7:1–9. https://doi.org/10.1038/srep40850

Axenrot T, Didrikas T, Danielsson C, Hansson S (2004) Diel patterns in pelagic fish behaviour and distribution observed from a stationary, bottom-mounted, and upward-facing transducer. ICES J Mar Sci 61:1100–1104. https://doi.org/10.1016/j.icesjms.2004.07.006

Barber DG, Hop H, Mundy CJ, et al (2015) Selected physical, biological and biogeochemical implications of a rapidly changing Arctic Marginal Ice Zone. Prog Oceanogr 139:122–150. https://doi.org/10.1016/j.pocean.2015.09.003

Barber WE, Smith RL, Vallarino M, Meyer RM (1997) Demersal fish assemblages of the northeastern Chukchi Sea, Alaska. Fish Bull 95:195–209

Bartlett MS (1947) The use of transformations. Biometrics 3:39–52

Becker A, Cowley PD, Whitfield AK, et al (2011) Diel fish movements in the littoral zone of a temporarily closed South African estuary. J Exp Mar Bio Ecol 406:63–70. https://doi.org/10.1016/j.jembe.2011.06.014

Belsley D, Kuh E, Welsch R (1980) Detecting and assessing collinearity. John Wiley & Sons, Inc

Benaglia T, Chauveau D, Hunter D, Young D (2009) mixtools: An R Package for Analyzing Finite Mixture Models. J Stat Softw 32:1–29

Benoit-Bird KJ, Au WWL (2006) Extreme diel horizontal migrations by a tropical nearshore resident micronekton community. Mar Ecol Prog Ser 319:1–14. https://doi.org/10.3354/meps319001

Benoit D, Simard Y, Fortier L (2014) Pre-winter distribution and habitat characteristics of polar cod (Boreogadus saida) in southeastern Beaufort Sea. Polar Biol 37:149–163. https://doi.org/10.1007/s00300-013-1419-0

Benoit D, Simard Y, Fortier L (2008) Hydroacoustic detection of large winter aggregations of Arctic cod (Boreogadus saida) at depth in ice-covered Franklin Bay (Beaufort Sea). J Geophys Res Ocean 113:1–9. https://doi.org/10.1029/2007JC004276

Benoit D, Simard Y, Gagné J, et al (2010) From polar night to midnight sun: Photoperiod, seal predation, and the diel vertical migrations of polar cod (Boreogadus saida) under landfast ice in the Arctic Ocean. Polar Biol 33:1505–1520. https://doi.org/10.1007/s00300-010-0840-x

Berge J, Cottier F, Last KS, et al (2009) Diel vertical migration of Arctic zooplankton during the polar night. Biol Lett 5:69–72. https://doi.org/10.1098/rsbl.2008.0484

Berge J, Renaud PE, Darnis G, et al (2015) In the dark: A review of ecosystem processes during the Arctic polar night. Prog Oceanogr 139:258–271. https://doi.org/10.1016/j.pocean.2015.08.005

Bivand R, Lewin-Koh N (2019) maptools: Tools for Handling Spatial Objects

Blachowiak-Samolyk K, Kwasniewski S, Richardson K, et al (2006) Arctic zooplankton do not perform diel vertical migration (DVM) during periods of midnight sun. Mar Ecol Prog Ser 308:101–116. https://doi.org/10.3354/meps308101

Blauw AN, Benincà E, Laane RWPM, et al (2012) Dancing with the Tides: Fluctuations of Coastal Phytoplankton Orchestrated by Different Oscillatory Modes of the Tidal Cycle. PLoS One 7:. https://doi.org/10.1371/journal.pone.0049319

Bluhm BA, Gradinger R (2008) Regional Variability in Food Availability for Arctic Marine Mammals. Ecol Appl 18:S77–S96. https://doi.org/http://dx.doi.org/10.1890/06-0562.1

Bluhm BA, Iken K, Hopcroft RR (2010) Observations and exploration of the Arctic's Canada Basin and the Chukchi Sea: The Hidden Ocean and RUSALCA expeditions. Deep Res Part II Top Stud Oceanogr 57:1–4. https://doi.org/10.1016/j.dsr2.2009.08.001

Boehlert GW, Gill AB (2010) Environmental and ecological effects of ocean renewable energy development. Oceanography 23:68–81. https://doi.org/10.5670/oceanog.2010.46

Born EW, Teilmann J, Acquarone M, Riget FF (2004) Habitat Use of Ringed Seals (Phoca hispida) in the North Water Area (North Baffin Bay). Arctic 57:129–142

Bouchard C, Fortier L (2011) Circum-arctic comparison of the hatching season of polar cod Boreogadus saida: A test of the freshwater winter refuge hypothesis. Prog Oceanogr 90:105–116. https://doi.org/10.1016/j.pocean.2011.02.008

Bouchard C, Fortier L (2020) The importance of Calanus glacialis for the feeding success of young polar cod: a circumpolar synthesis. Polar Biol. https://doi.org/10.1007/s00300-020-02643-0

Bouchard C, Geoffroy M, LeBlanc M, et al (2017) Climate warming enhances polar cod recruitment, at least transiently. Prog Oceanogr 156:121–129. https://doi.org/10.1016/j.pocean.2017.06.008

Bouchard C, Mollard S, Suzuki K, et al (2016) Contrasting the early life histories of sympatric Arctic gadids Boreogadus saida and Arctogadus glacialis in the Canadian Beaufort Sea. Polar Biol 39:1005–1022. https://doi.org/10.1007/s00300-014-1617-4

Box GEP, Jenkins GM (1976) Time series analysis-forecasting and control. Holden-Day, San Francisco, CA

Brierley AS, Brandon MA, Watkins JL (1998) An assessment of the utility of an acoustic Doppler current profiler for biomass estimation. Deep Res Part I Oceanogr Res Pap 45:1555–1573. https://doi.org/10.1016/S0967-0637(98)00012-0

Burgos JM, Horne JK (2008) Characterization and classification of acoustically detected fish spatial distributions. ICES J Mar Sci 65:1235–1247. https://doi.org/10.1093/icesjms/fsn087

Cada GF, Bevelhimer MS (2011) Attraction to and Avoidance of Instream Hydrokinetic Turbines by Freshwater Aquatic Organisms. Prepared for the U.S. Department of Energy, Office of Energy Efficiency and Renewable Energy, Wind and Water Power Program, ORNL/TM-2011/131. Washington, D.C.

Campbell HA, Fraser KPP, Bishop CM, et al (2008) Hibernation in an Antarctic fish: On ice for winter. PLoS One 3:e1743. https://doi.org/10.1371/journal.pone.0001743

Cazelles B, Chavez M, Berteaux D, et al (2008) Wavelet analysis of ecological time series. Oecologia 156:287–304. https://doi.org/10.1007/s00442-008-0993-2

Chatfield C (1989) The analysis of time series: an introduction, 4th edn. Chapman and Hall, New York

Chen P, Zhao J (2017) Variation of sea ice extent in different regions of the Arctic Ocean. Acta Oceanol Sin 36:9–19. https://doi.org/10.1007/s13131-016-0886-x

Ciach GJ, Krajewski WF (2006) Analysis and modeling of spatial correlation structure in small-scale rainfall in Central Oklahoma. Adv Water Resour 29:1450–1463. https://doi.org/10.1016/j.advwatres.2005.11.003

Cisewski B, Strass VH, Rhein M, Krägefsky S (2010) Seasonal variation of diel vertical migration of zooplankton from ADCP backscatter time series data in the Lazarev Sea, Antarctica. Deep Res Part I Oceanogr Res Pap 57:78–94.

https://doi.org/10.1016/j.dsr.2009.10.005

Cobain MRD, Brede M, Trueman CN (2019) Taylor's power law captures the effects of environmental variability on community structure: An example from fishes in the North Sea. J Anim Ecol 88:290–301. https://doi.org/10.1111/1365-2656.12923

Cochrane NA, Sameoto DD, Belliveau DJ (1994) Temporal variability of euphausiid concentrations in a Nova Scotia shelf basin using a bottom-mounted acoustic doppler current profiler. Mar Ecol Prog Ser 107:55–66. https://doi.org/10.3354/meps107055

Cohen JE, Plank MJ, Law R (2012) Taylor's law and body size in exploited marine ecosystems. Ecol Evol 2:3168–3178. https://doi.org/10.1002/ece3.418

Cohen JH, Berge J, Moline MA, et al (2015) Is ambient light during the high Arctic polar night sufficient to act as a visual cue for zooplankton? PLoS One 10:1–12. https://doi.org/10.1371/journal.pone.0126247

Cohen JH, Forward RBJ (2009) Zooplankton Diel Vertical Migration — A Review of Proximate Control. Oceanogr Mar Biol An Annu Rev 47:77–110

Comiso JC, Parkinson CL (2004) Satellite-Observed Changes in the Arctic. Phys Today 57:38–44

Copping A (2018) The State of Knowledge for Environmental Effects Driving Consenting/Permitting for the Marine Renewable Energy Industry. Report by Pacific Northwest National Laboratory (PNNL).

Copping AE, Sather NK, Hanna L, et al (2016) Annex IV 2016 State of the Science Report: Environmental effects of marine renewable energy development around the world. 199. https://doi.org/10.1097/JNN.0b013e3182829024

Cottier FR, Tarling GA, Wold A, Falk-Petersen S (2006) Unsynchronized and synchronized vertical migration of zooplankton in a high arctic fjord. Limnol Oceanogr 51:2586–2599. https://doi.org/10.4319/lo.2006.51.6.2586

Cury PM, Roy C, Mendelssohn R, et al (1995) Moderate is better: exploring nonlinear climatic effects on the Californian northern anchovy (Engraulis mordax). Can J Fish Aquat Sci 121:417–424

Daase M, Falk-Petersen HHS (2016) Small-scale diel vertical migration of zooplankton in the High Arctic. Polar Biol 39:1213–1223. https://doi.org/10.1007/s00300-015-1840-7

Dale T, Kaartvedt S (2000) Diel patterns in stage-specific vertical migration of Calanus

finmarchicus in habitats with midnight sun. ICES J Mar Sci 57:1800–1818. https://doi.org/10.1006/jmsc.2000.0961

Dale VH, Beyeler SC (2001) Challenges in the development and use of ecological indicators. Ecol Indic 1:3–10. https://doi.org/10.1016/S1470-160X(01)00003-6

Danielson S, Ahkinga O, Ashjian C, et al (2020) Manifestation and consequences of warming and altered heat fluxes over the Bering and Chukchi Sea continental shelves. Deep Sea Res Part II Top Stud Oceanogr 177:104781. https://doi.org/10.1016/j.dsr2.2020.104781

Danielson SL (2021) Water velocity and other parameters taken by ADCP from the research vessel Norseman II during Arctic Marine Biodiversity Observing Network, AMBON, cruise in the Chukchi Sea from 2017-08-06 to 2017-08-25 (NCEI Accession 0227757). NOAA National Centers for

Danielson SL, Eisner L, Ladd C, et al (2017a) A comparison between late summer 2012 and 2013 water masses, macronutrients, and phytoplankton standing crops in the northern Bering and Chukchi Seas. Deep Res Part II Top Stud Oceanogr 135:7–26. https://doi.org/10.1016/j.dsr2.2016.05.024

Danielson SL, Iken K, Hauri C, et al (2017b) Collaborative approaches to multi-disciplinary monitoring of the Chukchi shelf marine ecosystem: Networks of networks for maintaining long-term Arctic observations. In: MTS/IEEE Oceans17 conference proceedings, Anchorage, AK, USA, 18–21 September 2017. pp 1–7

Darnis G, Fortier L (2014) Temperature, food and the seasonal vertical migration of key arctic copepods in the thermally stratified Amundsen Gulf (Beaufort Sea, Arctic Ocean). J Plankton Res 36:1092–1108. https://doi.org/10.1093/plankt/fbu035

Darnis G, Hobbs L, Geoffroy M, et al (2017) From polar night to midnight sun: Diel vertical migration, metabolism and biogeochemical role of zooplankton in a high Arctic fjord (Kongsfjorden, Svalbard). Limnol Oceanogr 62:1586–1605. https://doi.org/10.1002/lno.10519

Darnis G, Robert D, Pomerleau C, et al (2012) Current state and trends in Canadian Arctic marine ecosystems: II. Heterotrophic food web, pelagic-benthic coupling, and biodiversity. Clim Change 115:179–205. https://doi.org/10.1007/s10584-012-0483-8

David C, Lange B, Krumpen T, et al (2016) Under-ice distribution of polar cod Boreogadus saida in the central Arctic Ocean and their association with sea-ice habitat properties. Polar

Biol 39:981–994. https://doi.org/10.1007/s00300-015-1774-0

Day RH, Weingartner TJ, Hopcroft RR, et al (2013) The offshore northeastern Chukchi Sea, Alaska: A complex high-latitude ecosystem. Cont Shelf Res 67:147–165. https://doi.org/10.1016/j.csr.2013.02.002

De Robertis A, McKelvey DR, Ressler PH (2010) Development and application of an empirical multifrequency method for backscatter classification. Can J Fish Aquat Sci 67:1459–1474. https://doi.org/10.1139/F10-075

De Robertis A, Taylor K, Wilson CD, Farley E V (2017) Abundance and distribution of Arctic cod (Boreogadus saida) and other pelagic fishes over the U.S. Continental Shelf of the Northern Bering and Chukchi Seas. Deep Sea Res Part II Top Stud Oceanogr 135:51–65. https://doi.org/10.1016/j.dsr2.2016.03.002

Deines KL (1999) Backscatter estimation using broadband acoustic Doppler current profilers. Proc IEEE Work Conf Curr Meas 249–253. https://doi.org/10.1109/ccm.1999.755249

Demer DA, Berger L, Bernasconi M, et al (2015) Calibration of acoustic instruments

Doney SC, Ruckelshaus M, Emmett Duffy J, et al (2012) Climate Change Impacts on Marine Ecosystems. Ann Rev Mar Sci 4:11–37. https://doi.org/10.1146/annurev-marine-041911-111611

Drinkwater KF, Mueter FJ, Saitoh SI (2018) Shifting boundaries of water, ice, flora, fauna, people, and institutions in the Arctic and Subarctic. ICES J Mar Sci 75:2293–2298. https://doi.org/10.1093/icesjms/fsy179

Duarte CM, Agustí S, Wassmann P, et al (2012) Tipping elements in the Arctic marine ecosystem. Ambio 41:44–55. https://doi.org/10.1007/s13280-011-0224-7

Eisler Z, Bartos I, Kertész J (2008) Fluctuation scaling in complex systems: Taylor's law and beyond. Adv Phys 57:89–142. https://doi.org/10.1080/00018730801893043

Eisner L, Hillgruber N, Martinson E, Maselko J (2013) Pelagic fish and zooplankton species assemblages in relation to water mass characteristics in the northern Bering and southeast Chukchi seas. Polar Biol 36:87–113. https://doi.org/10.1007/s00300-012-1241-0

Elliott SM, Ashjian CJ, Feng Z, et al (2017) Physical control of the distributions of a key Arctic copepod in the Northeast Chukchi Sea. Deep Res Part II Top Stud Oceanogr 144:37–51. https://doi.org/10.1016/j.dsr2.2016.10.001

Ershova EA, Hopcroft RR, Kosobokova KN, et al (2015) Long-term changes in Summer

zooplankton communities of the Western Chukchi Sea, 1945–2012. Oceanography 28:100–115. https://doi.org/10.5670/oceanog.2015.60

Falk-Petersen S, Leu E, Berge J, et al (2008) Vertical migration in high Arctic waters during autumn 2004. Deep Res Part II Top Stud Oceanogr 55:2275–2284. https://doi.org/10.1016/j.dsr2.2008.05.010

Falk-Petersen S, Mayzaud P, Kattner G, Sargent JR (2009) Lipids and life strategy of Arctic Calanus. Mar Biol Res 5:18–39. https://doi.org/10.1080/17451000802512267

Feurer M, Klein A, Eggensperger K, et al (2015) Efficient and robust automated machine learning. Adv Neural Inf Process Syst 2962–2970

Foote KG (2014) Discriminating between the nearfield and the farfield of acoustic transducers. J Acoust Soc Am 136:1511–1517. https://doi.org/10.1121/1.4895701

Foote KG, Knudsen HP, Vestnes G, et al (1987) Calibration of acoustic instruments for fish density estimation: a practical guide. J Acoust Soc Am 83:

Forster CE, Norcross BL, Mueter FJ, et al (2020) Spatial patterns, environmental correlates, and potential seasonal migration triangle of polar cod (Boreogadus saida) distribution in the Chukchi and Beaufort seas. Polar Biol 43:1073–1094. https://doi.org/10.1007/s00300-020-02631-4

Fortier L, Sirois P, Michaud J, Barber D (2006) Survival of Arctic cod larvae (Boreogadus saida) in relation to sea ice and temperature in the Northeast Water Polynya (Greenland Sea). Can J Fish Aquat Sci 63:1608–1616. https://doi.org/10.1139/F06-064

Fortier M, Fortier L, Hattori H, et al (2001) Visual predators and the diel vertical migration of copepods under Arctic sea ice during the midnight sun. J Plankton Res 23:1263–1278

Fossheim M, Primicerio R, Johannesen E, et al (2015) Recent warming leads to a rapid borealization of fish communities in the Arctic. Nat Clim Chang 5:673–677. https://doi.org/10.1038/nclimate2647

Fox CJ, Benjamins S, Masden EA, Miller R (2018) Challenges and opportunities in monitoring the impacts of tidal-stream energy devices on marine vertebrates. Renew Sustain Energy Rev 81:1926–1938. https://doi.org/10.1016/j.rser.2017.06.004

Fraser S, Nikora V, Williamson BJ, Scott BE (2017) Automatic active acoustic target detection in turbulent aquatic environments. Limnol Oceanogr Methods 15:184–199. https://doi.org/10.1002/lom3.10155

Fraterrigo JM, Rusak JA (2008) Disturbance-driven changes in the variability of ecological patterns and processes. Ecol Lett 11:756–770. https://doi.org/10.1111/j.1461-0248.2008.01191.x

Frid C, Andonegi E, Depestele J, et al (2012) The environmental interactions of tidal and wave energy generation devices. Environ Impact Assess Rev 32:133–139. https://doi.org/10.1016/j.eiar.2011.06.002

Fujiwara A, Nishino S, Matsuno K, et al (2018) Changes in phytoplankton community structure during wind-induced fall bloom on the central Chukchi shelf. Polar Biol 41:1279–1295. https://doi.org/10.1007/s00300-018-2284-7

Fujiwara M, Cohen JE (2015) Mean and variance of population density and temporal Taylor's law in stochastic stage-structured density-dependent models of exploited fish populations. Theor Ecol 8:175–186. https://doi.org/10.1007/s12080-014-0242-8

Gaston KJ, McArdle BH (1994) The temporal variability of animal abundances: measures, methods and patterns. Philos Trans R Soc London 345:335–358

Geoffroy M, Cottier FR, Berge J, Inall ME (2017) AUV-based acoustic observations of the distribution and patchiness of pelagic scattering layers during midnight sun. ICES J Mar Sci 74:2342–2353. https://doi.org/10.1093/icesjms/fsw158

Geoffroy M, Majewski A, LeBlanc M, et al (2016) Vertical segregation of age-0 and age-1+ polar cod (Boreogadus saida) over the annual cycle in the Canadian Beaufort Sea. Polar Biol 39:1023–1037. https://doi.org/10.1007/s00300-015-1811-z

Geoffroy M, Robert D, Darnis G, Fortier L (2011) The aggregation of polar cod (Boreogadus saida) in the deep Atlantic layer of ice-covered Amundsen Gulf (Beaufort Sea) in winter. Polar Biol 34:1959–1971. https://doi.org/10.1007/s00300-011-1019-9

Gilman DL, Fuglister FJ, Mitchell JM (1962) Further Remarks on the Power Spectrum of "Red Noise." J. Atmos. Sci. 20:182–184

Gjelland KØ, Bøhn T, Horne JK, et al (2009) Planktivore vertical migration and shoaling under a subarctic light regime. Can J Fish Aquat Sci 66:525–539. https://doi.org/10.1139/F09-014

Goddard P, Lauth R, Armistead C (2014) Results of the 2012 Chukchi Sea bottom trawl survey of bottomfishes, crabs, and other demersal macrofauna. U.S. Dep. Commer., NOAA Tech. Memo. NMFS-AFSC-278. Seattle

Godø OR, Handegard NO, Browman HI, et al (2014) Marine ecosystem acoustics (MEA):

Quantifying processes in the sea at the spatio-temporal scales on which they occur. ICES J Mar Sci 71:2357–2369. https://doi.org/10.1093/icesjms/fsu116

Gong D, Pickart RS (2015) Summertime circulation in the eastern Chukchi Sea. Deep Res Part II Top Stud Oceanogr 118:18–31. https://doi.org/10.1016/j.dsr2.2015.02.006

Gonzalez S, Horne JK, Danielson SL (2021) Multi-scale temporal variability in biological-physical associations in the NE Chukchi Sea. Polar Biol. https://doi.org/10.1007/s00300-021-02844-1

Gonzalez S, Horne JK, Ward EJ (2019) Temporal variability in pelagic biomass distributions at wave and tidal sites and implications for standardization of biological monitoring. Int Mar Energy J 2:15–28

Gooch S, Thomson J, Polagye B, Meggitt D (2009) Site characterization for tidal power. MTS/IEEE Biloxi - Mar Technol Our Futur Glob Local Challenges, Ocean 2009. https://doi.org/10.23919/OCEANS.2009.5422134

Gouhier TC, Grinsted A, Simko V (2016) biwavelet: Conduct univariate and bivariate wavelet analyses

Gradinger R (2009) Sea-ice algae: Major contributors to primary production and algal biomass in the Chukchi and Beaufort Seas during May/June 2002. Deep Res Part II Top Stud Oceanogr 56:1201–1212. https://doi.org/10.1016/j.dsr2.2008.10.016

Grados D, Fablet R, Ballón M, et al (2012) Multiscale characterization of spatial relationships among oxycline depth, macrozooplankton, and forage fish off Peru using geostatistics, principal coordinates of neighbour matrices (PCNMs), and wavelets. Can J Fish Aquat Sci 69:740–754. https://doi.org/10.1139/f2012-017

Graham M, Hop H (1995) Aspects of Reproduction and Larval Biology of Arctic Cod (Boreogadus saida). Arct Inst North Am 48:130–135

Gray BP, Norcross BL, Blanchard AL, et al (2016) Variability in the summer diets of juvenile polar cod (Boreogadus saida) in the northeastern Chukchi and western Beaufort Seas. Polar Biol 39:1069–1080. https://doi.org/10.1007/s00300-015-1796-7

Gray JS, McIntyre AD, Stirn J (1992) Manual of Methods in Aquatic Environment Research: Biological assessment of marine pollution. FAO Tech Pap 324:

Grebmeier JM (2012) Shifting patterns of life in the Pacific Arctic and sub-Arctic seas. Ann Rev Mar Sci 4:63–78. https://doi.org/10.1146/annurev-marine-120710-100926

Grebmeier JM, Bluhm BA, Cooper LW, et al (2015) Ecosystem characteristics and processes facilitating persistent macrobenthic biomass hotspots and associated benthivory in the Pacific Arctic. Prog Oceanogr 136:92–114. https://doi.org/10.1016/j.pocean.2015.05.006

Grebmeier JM, Cooper LW, Feder HM, Sirenko BI (2006a) Ecosystem dynamics of the Pacific-influenced Northern Bering and Chukchi Seas in the Amerasian Arctic. Prog Oceanogr 71:331–361. https://doi.org/10.1016/j.pocean.2006.10.001

Grebmeier JM, Overland JE, Moore SE, et al (2006b) A major ecosystem shift in the northern Bering sea. Science (80-) 311:1461–1464. https://doi.org/10.1126/science.1121365

Grinsted A, Moore JC, Jevrejeva S (2004) Application of the cross wavelet transform and wavelet coherence to geophysical time series. Nonlinear Process Geophys 11:561–566. https://doi.org/10.5194/npg-11-561-2004

Halley J, Inchausti P (2002) Lognormality in ecological time series. Oikos 99:518–530. https://doi.org/10.1034/j.1600-0706.2002.11962.x

Halpern BS, Walbridge S, Selkoe KA, et al (2008) A Global Map of Human Impact on Marine Ecosystems. Science (80-) 319:948–952. https://doi.org/10.1126/science.1149345

Hampton SE, Strasser CA, Tewksbury JJ, et al (2013) Big data and the future of ecology. Front Ecol Environ 11:156–162. https://doi.org/10.1890/120103

Hannay DE, Delarue J, Mouy X, et al (2013) Marine mammal acoustic detections in the northeastern Chukchi Sea, September 2007-July 2011. Cont Shelf Res 67:127–146. https://doi.org/10.1016/j.csr.2013.07.009

Harter BB, Elliott KH, Divoky GJ, Davorem GK (2013) Arctic Cod (Boreogadus saida) as Prey : Fish Length-Energetics Relationship in the Beaufort Sea and Hudson Bay. Arct Inst North Am 66:191–196

Hastie T, Tibshirani R (1990) Generalized Additive Models. Chapman and Hall, London

Hauri C, Danielson S, McDonnell AMP, et al (2018) From sea ice to seals: A moored marine ecosystem observatory in the Arctic. Ocean Sci Discuss 14:1423–1433. https://doi.org/10.5194/os-2018-82

Haury LR, McGowan JA, Wiebe PH (1978) Patterns and processes in the time-space scales of plankton distributions. In: Steele JH (ed) Spatial Pattern in Plankton Communities, NATO Confe. New York, pp 277–327

Hays GC (2003) A review of the adaptive significance and ecosystem consequences of

zooplankton diel vertical migrations. Hydrobiologia 503:163–170. https://doi.org/10.1023/B:HYDR.0000008476.23617.b0

Hersbach H, Bell B, Berrisford P, et al (2018) ERA5 hourly data on single levels from 1979 to present. Copernicus Climate Change Service (C3S) Climate Data Store (CDS).

Hewitt JE, Thrush SF, Dayton PK, Bonsdorff E (2007) The effect of spatial and temporal heterogeneity on the design and analysis of empirical studies of scale-dependent systems. Am Nat 169:398–408. https://doi.org/10.1086/510925

Hill V, Ardyna M, Lee SH, Varela DE (2018a) Decadal trends in phytoplankton production in the Pacific Arctic Region from 1950 to 2012. Deep Res Part II Top Stud Oceanogr 152:82–94. https://doi.org/10.1016/j.dsr2.2016.12.015

Hill VJ, Light B, Steele M, Zimmerman RC (2018b) Light availability and phytoplankton growth beneath arctic sea ice: Integrating observations and modeling. J Geophys Res Ocean 123:3651–3667. https://doi.org/10.1029/2017JC013617

Hobbs L, Cottier F, Last K, Berge J (2018) Pan-Arctic diel vertical migration during the polar night. Mar Ecol Prog Ser 605:61–72. https://doi.org/10.3354/meps12753

Hop H, Falk-Petersen S, Svendsen H, et al (2006) Physical and biological characteristics of the pelagic system across Fram Strait to Kongsfjorden. Prog Oceanogr 71:182–231. https://doi.org/10.1016/j.pocean.2006.09.007

Hopcroft RR, Day RH (2013) Introduction to the special issue on the ecology of the northeastern Chukchi Sea. Cont Shelf Res 67:1–4. https://doi.org/10.1016/j.csr.2013.06.017

Hopcroft RR, Kosobokova KN, Pinchuk AI (2010) Zooplankton community patterns in the Chukchi Sea during summer 2004. Deep Res Part II Top Stud Oceanogr 57:27–39. https://doi.org/10.1016/j.dsr2.2009.08.003

Horne JK (2000) Acoustic approaches to remote species identification: A review. Fish Oceanogr 9:356–371. https://doi.org/10.1046/j.1365-2419.2000.00143.x

Horne JK, Jacques DA (2018) Determining representative ranges of point sensors in distributed networks. Environ Monit Assess 190:. https://doi.org/10.1007/s10661-018-6689-0

Horne JK, Schneider DC (1994) Analysis of Scale-Dependent Processes with Dimensionless Ratios. Oikos 70:201–211. https://doi.org/10.2307/3545631

Humphries NE, Queiroz N, Dyer JRM, et al (2010) Environmental context explains Lévy and Brownian movement patterns of marine predators. Nature 465:1066–1069.

https://doi.org/10.1038/nature09116

Hunt GL, Coyle KO, Eisner LB, et al (2011) Climate impacts on eastern Bering Sea foodwebs: a synthesis of new data and an assessment of the Oscillating Control Hypothesis. ICES J Mar Sci 68:1230–1243. https://doi.org/10.1093/icesjms/fsr036

Hunt GL, Stabeno P, Walters G, et al (2002) Climate change and control of the southeastern Bering Sea pelagic ecosystem. Deep Res Part II Top Stud Oceanogr 49:5821–5853. https://doi.org/10.1016/S0967-0645(02)00321-1

Huntington HP, Danielson SL, Wiese FK, et al (2020) Evidence suggests potential transformation of the Pacific Arctic ecosystem is underway. Nat Clim Chang. https://doi.org/10.1038/s41558-020-0695-2

Huntington HP, Zagorsky A, Kaltenborn BP, et al (2021) Societal implications of a changing Arctic Ocean. Ambio. https://doi.org/10.1007/s13280-021-01601-2

Hyndman R, O-Hara-Wild M, Bergmeir C, et al (2017) Forecast: forecasting functions for time series and linear models R package

Iken K, Mueter F, Grebmeier JM, et al (2019) Developing an observational design for epibenthos and fish assemblages in the Chukchi Sea. Deep Res Part II Top Stud Oceanogr 162:180–190. https://doi.org/10.1016/j.dsr2.2018.11.005

Inger R, Attrill MJ, Bearhop S, et al (2009) Marine renewable energy: Potential benefits to biodiversity? An urgent call for research. J Appl Ecol 46:1145–1153. https://doi.org/10.1111/j.1365-2664.2009.01697.x

Jacques DA (2014) Describing and Comparing Variability of Fish and Macrozooplankton Density at Marine Hydrokinetic Energy Sites. Dissertation. University of Washington

Janout MA, Hölemann J, Waite AM, et al (2016) Sea-ice retreat controls timing of summer plankton blooms in the Eastern Arctic Ocean. Geophys Res Lett 43:12,493-12,501. https://doi.org/10.1002/2016GL071232

Jay C V., Fischbach AS, Kochnev AA (2012) Walrus areas of use in the Chukchi Sea during sparse sea ice cover. Mar Ecol Prog Ser 468:1–13. https://doi.org/10.3354/meps10057

Ji R, Jin M, Varpe Ø (2013) Sea ice phenology and timing of primary production pulses in the Arctic Ocean. Glob Chang Biol 19:734–741. https://doi.org/10.1111/gcb.12074

Kahru M, Lee Z, Mitchell BG, Nevison CD (2016) Effects of sea ice cover on satellite-detected primary production in the Arctic Ocean. Biol Lett 12:20160223.

https://doi.org/10.1098/rsbl.2016.0223

Kaltenberg AM, Benoit-Bird KJ (2009) Diel behavior of sardine and anchovy schools in the California Current System. Mar Ecol Prog Ser 394:247–262. https://doi.org/10.3354/meps08252

Kang M, Furusawa M, Miyashita K (2002) Effective and accurate use of difference in mean volume backscattering strength to identify fish and plankton. ICES J Mar Sci 59:794–804. https://doi.org/10.1006/jmsc.2002.1229

Kelley D, Richards C (2021) oce: Analysis of oceanographic data. R package version 1.3-0

Kilpatrick AM, Ives AR (2003) Species interactions can explain Taylor's power law for ecological time series. Nature 422:65–68. https://doi.org/10.1038/nature01471

Kitamura M, Amakasu K, Kikuchi T, Nishino S (2017) Seasonal dynamics of zooplankton in the southern Chukchi Sea revealed from acoustic backscattering strength. Cont Shelf Res 133:47–58. https://doi.org/10.1016/j.csr.2016.12.009

Kono Y, Sasaki H, Kurihara Y, et al (2016) Distribution pattern of Polar cod (Boreogadus saida) larvae and larval fish assemblages in relation to oceanographic parameters in the northern Bering Sea and Chukchi Sea. Polar Biol 39:1039–1048. https://doi.org/10.1007/s00300-016-1961-7

Korneliussen RJ, Ona E (2003) Synthetic echograms generated from the relative frequency response. ICES J Mar Sci 60:636–640. https://doi.org/10.1016/S1054-3139(03)00035-3

Kosobokova KN (1999) The reproductive cycle and life history of the Arctic copepod Calanus glacialis in the White Sea. 254–263

Kosro PM (2005) On the spatial structure of coastal circulation off Newport, Oregon during spring and summer 2001 in a region of varying shelf width. J Geophys Res C Ocean 110:1–16. https://doi.org/10.1029/2004JC002769

Kracht O, Santiago JL, Martin F, et al (2017) Spatial Representativeness of Air Quality Monitoring Sites - Outcomes of the FAIRMODE/AQUILA intercomparison exercise, EUR 28987 EN, Publications Office of the European Union, Luxembourg

Kuletz KJ, Ferguson MC, Hurley B, et al (2015) Seasonal spatial patterns in seabird and marine mammal distribution in the eastern Chukchi and western Beaufort seas: Identifying biologically important pelagic areas. Prog Oceanogr 136:175–200. https://doi.org/10.1016/j.pocean.2015.05.012

Kuo TC, Mandal S, Yamauchi A, Hsieh CH (2016) Life history traits and exploitation affect the spatial mean-variance relationship in fish abundance. Ecology 97:1251–1259. https://doi.org/10.1890/15-1270.1/suppinfo

Kwok R (2018) Arctic sea ice thickness, volume, and multiyear ice coverage: Losses and coupled variability (1958-2018). Environ Res Lett 13:. https://doi.org/10.1088/1748-9326/aae3ec

Lagrue C, Poulin R, Cohen JE (2015) Parasitism alters three power laws of scaling in a metazoan community: Taylor's law, density-mass allometry, and variance-mass allometry. Proc Natl Acad Sci U S A 112:1791–1796. https://doi.org/10.1073/pnas.1422475112

Lalande C, Grebmeier JM, Hopcroft RR, Danielson SL (2020) Annual cycle of export fluxes of biogenic matter near Hanna Shoal in the northeast Chukchi Sea. Deep Res Part II Top Stud Oceanogr 104730. https://doi.org/10.1016/j.dsr2.2020.104730

Lane PVZ, Llinás L, Smith SL, Pilz D (2008) Zooplankton distribution in the western Arctic during summer 2002: Hydrographic habitats and implications for food chain dynamics. J Mar Syst 70:97–133. https://doi.org/10.1016/j.jmarsys.2007.04.001

Last KS, Hobbs L, Berge J, et al (2016) Moonlight Drives Ocean-Scale Mass Vertical Migration of Zooplankton during the Arctic Winter. Curr Biol 26:244–251. https://doi.org/10.1016/j.cub.2015.11.038

Laurel BJ, Copeman LA, Spencer M, Iseri P (2017) Temperature-dependent growth as a function of size and age in juvenile Arctic cod (Boreogadus saida). ICES J Mar Sci 74:1614–1621. https://doi.org/10.1093/icesjms/fsx028

Laurel BJ, Spencer M, Iseri P, Copeman LA (2016) Temperature-dependent growth and behavior of juvenile Arctic cod (Boreogadus saida) and co-occurring North Pacific gadids. Polar Biol 39:1127–1135. https://doi.org/10.1007/s00300-015-1761-5

LeBlanc M, Gauthier S, Garbus SE, et al (2019a) The co-distribution of Arctic cod and its seabird predators across the marginal ice zone in Baffin Bay. Elementa 7:1–18. https://doi.org/10.1525/elementa.339

LeBlanc M, Geoffroy M, Bouchard C, et al (2019b) Pelagic production and the recruitment of juvenile polar cod Boreogadus saida in Canadian Arctic seas. Polar Biol. https://doi.org/10.1007/s00300-019-02565-6

Legendre P (1993) Spatial autocorrelation: trouble or new paradigm? Ecology 74:1659–1673.

https://doi.org/10.2307/1939924

Legendre P, Fortin M-J (1989) Spatial Pattern and Ecological Analysis. Vegetatio 80:107–138

Leu E, Mundy CJ, Assmy P, et al (2015) Arctic spring awakening - Steering principles behind the phenology of vernal ice algal blooms. Prog Oceanogr 139:151–170. https://doi.org/10.1016/j.pocean.2015.07.012

Leu E, Søreide JE, Hessen DO, et al (2011) Consequences of changing sea-ice cover for primary and secondary producers in the European Arctic shelf seas: Timing, quantity, and quality. Prog Oceanogr 90:18–32. https://doi.org/10.1016/j.pocean.2011.02.004

Levin SA (1992) The problem of pattern and scale. Ecology 73:1943–1967

Levine RM, De Robertis A, Grünbaum D, et al (2021) Autonomous vehicle surveys indicate that flow reversals retain juvenile fishes in a highly advective high-latitude ecosystem. Limnol Oceanogr 66:1139–1154. https://doi.org/10.1002/lno.11671

Lewis KM, Van Dijken GL, Arrigo KR (2020) Changes in phytoplankton concentration now drive increaseLewis, K. M., Van Dijken, G. L., & Arrigo, K. R. (2020). Changes in phytoplankton concentration now drive increased Arctic Ocean primary production. Science, 369(6500), 198–202. https://doi.org/10.1. Science (80-) 369:198–202

Li WKW, McLaughlin FA, Lovejoy C, Carmack EC (2009) Smallest algae thrive as the arctic ocean freshens. Science (80-) 326:539. https://doi.org/10.1126/science.1179798

Lin II (2012) Typhoon-induced phytoplankton blooms and primary productivity increase in the western North Pacific subtropical ocean. J Geophys Res Ocean 117:. https://doi.org/10.1029/2011JC007626

Linder HL, Horne JK (2018) Evaluating statistical models to measure environmental change: A tidal turbine case study. Ecol Indic 84:765–792. https://doi.org/10.1016/j.ecolind.2017.09.041

Linder HL, Horne JK, Ward EJ (2017) Modeling baseline conditions of ecological indicators: Marine renewable energy environmental monitoring. Ecol Indic 83:178–191. https://doi.org/10.1016/j.ecolind.2017.07.015

Logerwell E, Rand K, Danielson S, Sousa L (2018) Environmental drivers of benthic fish distribution in and around Barrow Canyon in the northeastern Chukchi Sea and western Beaufort Sea. Deep Res Part II Top Stud Oceanogr 152:170–181. https://doi.org/10.1016/j.dsr2.2017.04.012

Lorenzen CJ (1972) Extinction of light in the ocean by phytoplankton. ICES J Mar Sci 34:262–267. https://doi.org/10.1093/icesjms/34.2.262

Lowry LF, Frost KJ (1981) Distribution, growth, and foods of Arctic cod (Boreogadus saida) in the Bering, Chukchi and Beaufort Seas. Can Field-Naturalist 95:186–191

Lu K, Danielson S, Hedstrom K, Weingartner T (2020) Assessing the role of oceanic heat fluxes on ice ablation of the central Chukchi Sea Shelf. Prog Oceanogr 184:102313. https://doi.org/10.1016/j.pocean.2020.102313

Luo J, Ortner PB, Forcucci D, Cummings SR (2000) Diel vertical migration of zooplankton and mesopelagic fish in the Arabian Sea. Deep Res Part II Top Stud Oceanogr 47:1451–1473. https://doi.org/10.1016/S0967-0645(99)00150-2

Maclean IMD, Inger R, Benson D, et al (2014) Resolving issues with environmental impact assessment of marine renewable energy installations. Front Mar Sci 1:1–5. https://doi.org/10.3389/fmars.2014.00075

MacLennan D, Fernandes PG, Dalen J (2002) A consistent approach to definitions and symbols in fisheries acoustics. ICES J Mar Sci 59:365–369. https://doi.org/10.1006/jmsc.2001.1158

Madureira LSP, Ward P, Atkinson A (1993) Differences in backscattering strength determined at 120 and 38 kHz for three species of Antarctic macroplankton. Mar Ecol Prog Ser 93:17–24. https://doi.org/10.3354/meps093017

Magagna D, Uihlein A (2015) Ocean energy development in Europe: Current status and future perspectives. Int J Mar Energy 11:84–104. https://doi.org/10.1016/j.ijome.2015.05.001

Majaneva S, Berge J, Renaud PE, et al (2013) Aggregations of predators and prey affect predation impact of the Arctic ctenophore Mertensia ovum. Mar Ecol Prog Ser 476:87–100. https://doi.org/10.3354/meps10143

Martin AP, Zubkov M V, Burkill PH, Holland RJ (2005) Extreme spatial variability in marine picoplankton and its consequences for interpreting Eulerian time-series. Biol Lett 1:366–369. https://doi.org/10.1098/rsbl.2005.0316

Martín F, Santiago JL, Kracht O, et al (2015) FAIRMODE Spatial representativeness feasibility study. JRC Technical Report EUR 27385 EN, Joint Research Centre - European Commission

Maslanik J, Stroeve J (1999) Near-Real-Time DMSP SSMIS Daily Polar Gridded Sea Ice Concentrations, Version 1. In: Boulder, Color. USA. NASA Natl. Snow Ice Data Cent.

Distrib. Act. Arch. Cent.

Massey FJJ (1951) The Kolmogorov-Smirnoc Test for Goodness of Fit. J Am Stat Assoc Stat Assoc 46:68–78

Matley JK, Crawford RE, Dick TA (2012) Summer foraging behaviour of shallow-diving seabirds and distribution of their prey, Arctic cod (Boreogadus saida), in the Canadian Arctic . Polar Res 31:15894. https://doi.org/10.3402/polar.v31i0.15894

Matsuno K, Yamaguchi A, Hirawake T, Imai I (2011) Year-to-year changes of the mesozooplankton community in the Chukchi Sea during summers of 1991, 1992 and 2007, 2008. Polar Biol 34:1349–1360. https://doi.org/10.1007/s00300-011-0988-z

Maurer BA (1999) Untangling ecological complexity: the macroscopic perspective. University of Chicago Press, Chicago, IL

McGowan DW, Horne JK, Parker-Stetter SL (2019) Variability in species composition and distribution of forage fish in the Gulf of Alaska. Deep Res Part II Top Stud Oceanogr 165:221–237. https://doi.org/10.1016/j.dsr2.2016.11.019

McIntire EJB, Fajardo A (2009) Beyond description: The active and effective way to infer processes from spatial patterns. Ecology 90:46–56. https://doi.org/10.1890/07-2096.1

Mellin C, Huchery C, Caley MJ, et al (2010) Reef size and isolation determine the temporal stability of coral reef populations. Ecology 91:3138–3145

Milewska E, Hogg WD (2010) Spatial representativeness of a long-term climate network in Canada. Atmosphere-Ocean 39:145–161. https://doi.org/10.1080/07055900.2001.9649671

Møller EF, Nielsen TG (2019) Borealization of Arctic zooplankton—smaller and less fat zooplankton species in Disko Bay, Western Greenland. Limnol Oceanogr 1–14. https://doi.org/10.1002/lno.11380

Moore SE, Stabeno PJ (2015) Synthesis of Arctic Research (SOAR) in marine ecosystems of the Pacific Arctic. Prog Oceanogr 136:1–11. https://doi.org/10.1016/j.pocean.2015.05.017

Moore SJ, Mantua NJ, Newton JA, et al (2008) A descriptive analysis of temporal and spatial patterns of variability in Puget Sound oceanographic properties. Estuar Coast Shelf Sci 80:545–554

Mueter F, Bouchard C, Hop H, et al (2020) Arctic gadids in a rapidly changing environment. Polar Biol. https://doi.org/10.1007/s00300-020-02696-1

Mueter FJ, Nahrgang J, John Nelson R, Berge J (2016) The ecology of gadid fishes in the

circumpolar Arctic with a special emphasis on the polar cod (Boreogadus saida). Polar Biol 39:961–967. https://doi.org/10.1007/s00300-016-1965-3

Mueter FJ, Weems J, Farley E V., Sigler MF (2017) Arctic Ecosystem Integrated Survey (Arctic Eis): Marine ecosystem dynamics in the rapidly changing Pacific Arctic Gateway. Deep Res Part II Top Stud Oceanogr 135:1–6. https://doi.org/10.1016/j.dsr2.2016.11.005

Mullison J (2017) Backscatter Estimation Using Broadband Acoustic Doppler Current Profilers - Updated. In: ASCE Hydraulic Measurements & Experimental Methods Conference

Mundy CJ, Barber DG, Michel C (2005) Variability of snow and ice thermal, physical and optical properties pertinent to sea ice algae biomass during spring. J Mar Syst 58:107–120. https://doi.org/10.1016/j.jmarsys.2005.07.003

Mundy CJ, Gosselin M, Gratton Y, et al (2014) Role of environmental factors on phytoplankton bloom initiation under landfast sea ice in Resolute Passage, Canada. Mar Ecol Prog Ser 497:39–49. https://doi.org/10.3354/meps10587

Niemi GJ, McDonald ME (2004) Application of ecological indicators. Annu Rev Ecol Evol Syst 35:89–111. https://doi.org/10.1146/annurev.ecolsys.35.112202.130132

Nilsson LAF, Thygesen UH, Lundgren B, et al (2003) Vertical migration and dispersion of sprat (Sprattus sprattus) and herring (Clupea harengus) schools at dusk in the Baltic Sea. Aquat Living Resour 16:317–324. https://doi.org/10.1016/S0990-7440(03)00039-1

Norcross BL, Holladay BA, Busby MS, Mier KL (2010) Demersal and larval fish assemblages in the Chukchi Sea. Deep Res Part II Top Stud Oceanogr 57:57–70. https://doi.org/10.1016/j.dsr2.2009.08.006

NPFMC (2009) Fishery Management Plan for Fish Resources of the Arctic Management Area

Nurser AJG, Bacon S (2014) The rossby radius in the arctic ocean. Ocean Sci 10:967–975. https://doi.org/10.5194/os-10-967-2014

Osenberg CW, Schmitt RJ, Holbrook SJ, Abu-saba KE (1994) Detection of Environmental Impacts: Natural Variability, Effect Size, and Power Analysis. Ecol Appl 4:16–30

Palmer MA, Saenz BT, Arrigo KR (2014) Impacts of sea ice retreat, thinning, and melt-pond proliferation on the summer phytoplankton bloom in the Chukchi Sea, Arctic Ocean. Deep Res Part II Top Stud Oceanogr 105:85–104. https://doi.org/10.1016/j.dsr2.2014.03.016

Parrish R, Mallicoate DL (2007) Variation in the condition factors of California pelagic fishes and associated environmental factor. Fish Oceanogr 4:171–190

Peterson WT, Miller CB, Hutchinson A (1979) Zonation and maintenance of copepod populations in the Oregon upwelling zone. Deep Sea Res Part A, Oceanogr Res Pap 26:467–494. https://doi.org/10.1016/0198-0149(79)90091-8

Piersanti A, Vitali L, Righini G, et al (2015) Spatial representativeness of air quality monitoring stations: A grid model based approach. Atmos Pollut Res 6:953–960. https://doi.org/10.1016/j.apr.2015.04.005

Pinchuk AI, Eisner LB (2017) Spatial heterogeneity in zooplankton summer distribution in the eastern Chukchi Sea in 2012–2013 as a result of large-scale interactions of water masses. Deep Res Part II Top Stud Oceanogr 135:27–39. https://doi.org/10.1016/j.dsr2.2016.11.003

Polagye B, Cleve B Van, Kirkendall K, Copping A (2011) Environmental effects of tidal energy development. NOAA Tech Memo F/SPO-116 181

Polyakov I V., Alkire MB, Bluhm BA, et al (2020) Borealization of the Arctic Ocean in Response to Anomalous Advection From Sub-Arctic Seas. Front Mar Sci 7:. https://doi.org/10.3389/fmars.2020.00491

Polyakov I V., Timokhov LA, Alexeev VA, et al (2010) Arctic ocean warming contributes to reduced polar ice cap. J Phys Oceanogr 40:2743–2756. https://doi.org/10.1175/2010JPO4339.1

Post E, Bhatt US, Bitz CM, et al (2013) Ecological Consequences of Sea-Ice Decline. Science (80-) 341:519–524. https://doi.org/10.1126/science.1235225

Questel JM, Clarke C, Hopcroft RR (2013) Seasonal and interannual variation in the planktonic communities of the northeastern Chukchi Sea during the summer and early fall. Cont Shelf Res 67:23–41. https://doi.org/10.1016/j.csr.2012.11.003

Rand KM, Whitehouse A, Logerwell EA, et al (2013) The diets of polar cod (Boreogadus saida) from August 2008 in the US Beaufort Sea. Polar Biol 36:907–912. https://doi.org/10.1007/s00300-013-1303-y

Randall JR, Busby MS, Spear AH, Mier KL (2019) Spatial and temporal variation of late summer ichthyoplankton assemblage structure in the eastern Chukchi Sea: 2010–2015. Polar Biol 42:1811–1824. https://doi.org/10.1007/s00300-019-02555-8

Ressler PH (2002) Acoustic backscatter measurements with a 153 kHz ADCP in the northeastern Gulf of Mexico: Determination of dominant zooplankton and micronekton scatterers. Deep Res Part I Oceanogr Res Pap 49:2035–2051. https://doi.org/10.1016/S0967-0637(02)00117-

6

Ressler PH, Robertis A De, Warren JD, et al (2012) Developing an acoustic survey of euphausiids to understand trophic interactions in the Bering Sea ecosystem. Deep Res Part II Top Stud Oceanogr 65–70:184–195. https://doi.org/10.1016/j.dsr2.2012.02.015

Rhodes JR, Jonzén N (2011) Monitoring temporal trends in spatially structured populations: how should sampling effort be allocated between space and time? Ecography (Cop) 34:1040–1048. https://doi.org/10.1111/j.1600-0587.2011.06370.x

Roesch A, Schimidbauer H (2018) WaveletComp: Computational Wavelet Analysis. R package

Rycroft HB (1949) Random Sampling of Rainfall. J South African For Soc 18:71–81

Schneider DC (1994) Quantitative Ecology: Spatial and Temporal Scaling. Academic Press, San Diego, CA

Schneider DC (2001) The Rise of the Concept of Scale in Ecology. Bioscience 51:545. https://doi.org/10.1641/0006-3568(2001)051[0545:trotco]2.0.co;2

Segura A, Wiff R, Jaureguizar AJ, et al (2021) A macroecological perspective on the fluctuations of exploited fish populations. Mar Ecol Prog Ser 665:177–183. https://doi.org/10.3354/meps13662

Segura AM, Calliari D, Fort H, Lan BL (2013) Fat tails in marine microbial population fluctuations. Oikos 122:1739–1745. https://doi.org/10.1111/j.1600-0706.2013.00493.x

Serreze MC, Barrett AP, Crawford AD, Woodgate RA (2019) Monthly Variability in Bering Strait Oceanic Volume and Heat Transports, Links to Atmospheric Circulation and Ocean Temperature, and Implications for Sea Ice Conditions. J Geophys Res Ocean 124:9317–9337. https://doi.org/10.1029/2019JC015422

Serreze MC, Crawford AD, Stroeve JC, et al (2016) Variability, trends, and predictability of seasonal sea ice retreat and advance in the Chukchi Sea. J Geophys Res Ocean 121:7308–7325. https://doi.org/doi:10.1002/ 2016JC011977

Sigleo AC, Mordy CW, Stabeno P, Frick WE (2005) Nitrate variability along the Oregon coast: Estuarine-coastal exchange. Estuar Coast Shelf Sci 64:211–222. https://doi.org/10.1016/j.ecss.2005.02.018

Sigler MF, Mueter FJ, Bluhm BA, et al (2017) Late summer zoogeography of the northern Bering and Chukchi seas. Deep Res Part II Top Stud Oceanogr 135:168–189. https://doi.org/10.1016/j.dsr2.2016.03.005

Sigler MF, Rooper CN, Hoff GR, et al (2015) Faunal features of submarine canyons on the eastern Bering Sea slope. Mar Ecol Prog Ser 526:21–40. https://doi.org/10.3354/meps11201

Simmonds EJ, MacLennan DN (2005) Fisheries Acoustics. Theory and Practice. Blackwell Publishing, Oxford

Sims DW, Southall EJ, Humphries NE, et al (2008) Scaling laws of marine predator search behaviour. Nature 451:1098–1102. https://doi.org/10.1038/nature06518

Soininen J, McDonald R, Hillebrand H (2007) The distance decay of similarity in ecological communities. Ecography (Cop) 30:3–12. https://doi.org/10.1111/j.2006.0906-7590.04817.x

Søreide JE, Leu EVA, Berge J, et al (2010) Timing of blooms, algal food quality and Calanus glacialis reproduction and growth in a changing Arctic. Glob Chang Biol 16:3154–3163. https://doi.org/10.1111/j.1365-2486.2010.02175.x

Spear A, Duffy-Anderson J, Kimmel D, et al (2019) Physical and biological drivers of zooplankton communities in the Chukchi Sea. Polar Biol 42:1107–1124. https://doi.org/10.1007/s00300-019-02498-0

Spear A, Napp J, Ferm N, Kimmel D (2020) Advection and in situ processes as drivers of change for the abundance of large zooplankton taxa in the Chukchi Sea. Deep Res Part II Top Stud Oceanogr 177:104814. https://doi.org/10.1016/j.dsr2.2020.104814

Spellerberg IF (1991) Monitoring ecological change. Cambridge University Press, Cambridge

Steele M, Ermold W, Zhang J (2008) Arctic Ocean surface warming trends over the past 100 years. Geophys Res Lett 35:1–6. https://doi.org/10.1029/2007GL031651

Steele M, Zhang J, Ermold W (2010) Mechanisms of summertime upper Arctic Ocean warming and the effect on sea ice melt. J Geophys Res Ocean 115:1–12. https://doi.org/10.1029/2009JC005849

Stigebrandt A (1984) The North Pacific: A Global-Scale Estuary. J. Phys. Oceanogr. 14:464–470

Stommel H (1963) Varieties of Oceanographic Experience: The ocean can be investigated as a hydrodynamical phenomenon as well as explored geographically. Science (80-) 139:572–576. https://doi.org/10.1126/science.139.3555.572

Stroeve J, Holland MM, Meier W, et al (2007) Arctic sea ice decline: Faster than forecast. Geophys Res Lett 34:1–5. https://doi.org/10.1029/2007GL029703

Sullivan LM (2006) Estimation from samples. Circulation 114:445–449. https://doi.org/10.1161/CIRCULATIONAHA.105.600189

Taylor LR (1961) Aggregation, variance and the mean. Nature 189:732–735

Taylor LR, Woiwod I. P (1982) Comparative Synoptic Dynamics. I. Relationships Between Inter- and Intra-Specific Spatial and Temporal Variance/Mean Population Parameters. Br Ecol Soc 51:879–906

Thorson JT, Arimitsu ML, Barnett LAK, et al (2021) Forecasting community reassembly using climate-linked spatio-temporal ecosystem models. Ecography (Cop) 44:612–625. https://doi.org/10.1111/ecog.05471

Torgersen CE, Gresswell RE, Bateman DS (2004) Pattern detection in stream networks: quantifying spatial variability in fish distribution. In: Nishida T, Kailola PJ, Hollingworth CE (eds) GIS/Spatial Analyses in Fishery and Aquatic Sciences. University of Sussex, Brighton, pp 405–420

Torrence C, Compo GP (1998) A Practical Guide to Wavelet Analysis. Bull Am Meteorol Soc 79:61–78. https://doi.org/10.1175/1520-0477(1998)079<0061:APGTWA>2.0.CO;2

Underwood AJ (1991) Beyond baci: Experimental designs for detecting human environmental impacts on temporal variations in natural populations. Mar Freshw Res 42:569–587. https://doi.org/10.1071/MF9910569

Urmy SS (2012) Temporal Variability and Bio-Physical Coupling in the Pelagic Fauna of Monterey Bay. Dissertation. University of Washington

Urmy SS, Horne JK, Barbee DH (2012) Measuring the vertical distributional variability of pelagic fauna in Monterey Bay. ICES J Mar Sci 69:184–196. https://doi.org/10.1093/icesjms/fst034

Venables WN, Ripley BD (2002) Modern Applied Statistics with S, 4th edn. Springer, New York

Vestfals CD, Mueter FJ, Duffy-Anderson JT, et al (2019) Spatio-temporal distribution of polar cod (Boreogadus saida) and saffron cod (Eleginus gracilis) early life stages in the Pacific Arctic. Polar Biol 42:969–990. https://doi.org/10.1007/s00300-019-02494-4

Viehman HA, Zydlewski GB (2017) Multi-scale temporal patterns in fish presence in a highvelocity tidal channel. PLoS One 12:1–20. https://doi.org/10.1371/journal.pone.0176405

Viehman HA, Zydlewski GB (2014) Fish Interactions with a Commercial-Scale Tidal Energy Device in the Natural Environment. Estuaries and Coasts 38:241–252.

https://doi.org/10.1007/s12237-014-9767-8

Viswanathan GM (2010) Fish in Lévy-flight foraging Expanding islands of speciation. Nature 465:1018–1019

Wallace MI, Cottier FR, Berge J, et al (2010) Comparison of zooplankton vertical migration in an ice-free and a seasonally ice-covered Arctic fjord: An insight into the influence of sea ice cover on zooplankton behavior. Limnol Oceanogr 55:831–845. https://doi.org/10.4319/lo.2009.55.2.0831

Weingartner T, Aagaard K, Woodgate R, Danielson S (2005) Circulation on the north central Chukchi Sea shelf. Deep Res Part II Top Stud Oceanogr 52:3150–3174. https://doi.org/10.1016/j.dsr2.2005.10.015

Weingartner T, Dobbins E, Danielson S, et al (2013) Hydrographic variability over the northeastern Chukchi Sea shelf in summer-fall 2008-2010. Cont Shelf Res 67:5–22. https://doi.org/10.1016/j.csr.2013.03.012

Welch HE, Bergmann MA, Siferd TD, et al (1992) Energy Flow through the Marine Ecosystem of the Lancaster Sound Region , Arctic Canada. Artic Inst North Am 45:343–357

Whitehouse GA, Aydin K, Essington TE, Hunt GL (2014) A trophic mass balance model of the eastern Chukchi Sea with comparisons to other high-latitude systems. Polar Biol 37:911–939. https://doi.org/10.1007/s00300-014-1490-1

Wiens JA (1989) Spatial scaling in ecology. Funct Ecol 3:385–397

Wiens JA (1976) Population Responses to Patchy Environments. Annu Rev Ecol Syst 7:81–120. https://doi.org/10.1146/annurev.es.07.110176.000501

Wiesebron LE, Horne JK, Hendrix AN (2016a) Characterizing biological impacts at marine renewable energy sites. Int J Mar Energy 14:27–40. https://doi.org/10.1016/j.ijome.2016.04.002

Wiesebron LE, Horne JK, Scott BE, Williamson BJ (2016b) Comparing nekton distributions at two tidal energy sites suggests potential for generic environmental monitoring. Int J Mar Energy 16:235–249. https://doi.org/10.1016/j.ijome.2016.07.004

Wood KR, Bond NA, Danielson SL, et al (2015) A decade of environmental change in the Pacific Arctic region. Prog Oceanogr 136:12–31. https://doi.org/10.1016/j.pocean.2015.05.005

Wood S (2004) Stable and efficient multiple smoothing parameter estimation for generalized

additive models. J Am Stat Assoc 99:673–686. https://doi.org/10.1198/016214504000000980

Wood S (2017) Gneralized additive models: An intriduction with R, Second. Chapman and Hall/CRC press

Wood S (2011) Fast stable restricted maximum likelihood and marginal likelihood estimation of semiparametric generalized linear models. J R Stat Soc Ser B Stat Methodol 73:3–36. https://doi.org/10.1111/j.1467-9868.2010.00749.x

Woodgate RA (2018) Increases in the Pacific inflow to the Arctic from 1990 to 2015, and insights into seasonal trends and driving mechanisms from year-round Bering Strait mooring data. Prog Oceanogr 160:124–154. https://doi.org/10.1016/j.pocean.2017.12.007

Woodgate RA, Peralta-Ferriz C (2021) Warming and Freshening of the Pacific Inflow to the Arctic From 1990-2019 Implying Dramatic Shoaling in Pacific Winter Water Ventilation of the Arctic Water Column. Geophys Res Lett 48:1–11. https://doi.org/10.1029/2021GL092528

Wright G (2014) Strengthening the role of science in marine governance through environmental impact assessment: A case study of the marine renewable energy industry. Ocean Coast Manag 99:23–30. https://doi.org/10.1016/j.ocecoaman.2014.07.004

Wuertz D, Setz T, Chalabi Y, et al (2020) fGarch: Rmetrics - Autoregressive Conditional Heteroskedastic Modelling

Yang Y, Bai X (2020) Summer changes in water mass characteristics and vertical thermohaline structure in the eastern Chukchi Sea, 1974-2017. Water (Switzerland) 12:. https://doi.org/10.3390/w12051434

Yatkin S, Gerboles M, Belis CA, et al (2020) Representativeness of an air quality monitoring station for PM2.5 and source apportionment over a small urban domain. Atmos Pollut Res 11:225–233. https://doi.org/10.1016/j.apr.2019.10.004

Zar JH (2010) Biostatistical Analysis, 5th edn. Pearson: Upper Saddle River, New Jersey

Zedel L, Knutsen T, Patro R (2003) Acoustic Doppler curren profiler observations of herring movement. ICES J Mar Sci J du … 60:846–859. https://doi.org/10.1016/S1054

Zhang J, Ashjian C, Campbell R, et al (2015) The influence of sea ice and snow cover and nutrient availability on the formation of massive under-ice phytoplankton blooms in the Chukchi Sea. Deep Res Part II Top Stud Oceanogr 118:122–135.

https://doi.org/10.1016/j.dsr2.2015.02.008

Zhang W, Wang Q, Wang X, Danilov S (2020) Mechanisms Driving the Interannual Variability of the Bering Strait Throughflow. J Geophys Res Ocean 125:. https://doi.org/10.1029/2019JC015308

Zhao H, Shao J, Han G, et al (2015) Influence of Typhoon Matsa on phytoplankton chlorophyll-a off East China. PLoS One 10:1–13. https://doi.org/10.1371/journal.pone.0137863

Zuur AF, Ieno EN, Walker NJ, et al (2009) Mixed Effects Models and Extensions in Ecology with R. Springer, New York

APPENDIX A

Wavelet coherence between hourly values of fish and zooplankton metrics of density and vertical distributions derived from acoustic backscatter (mean Sv: mean volume backscattering strength, CM: center of mass, inertia, and aggregation index) and sun altitude from Chapter 2. Data was collected at the Chukchi Ecosystem observatory from September 1st, 2015 to August 18th, 2019. In the plots, the color bar represents wavelet coherence. The shaded area represents the cone of influence (edge effects) and the areas of significance are traced with a black line (95% confidence against white noise). Arrows indicate the phase difference between the two variables of the wavelet spectra (right arrows indicate series are in phase, left arrows indicate series are completely out of phase (180°), and an arrow pointing vertically upward means the second series lags the first by 90°.

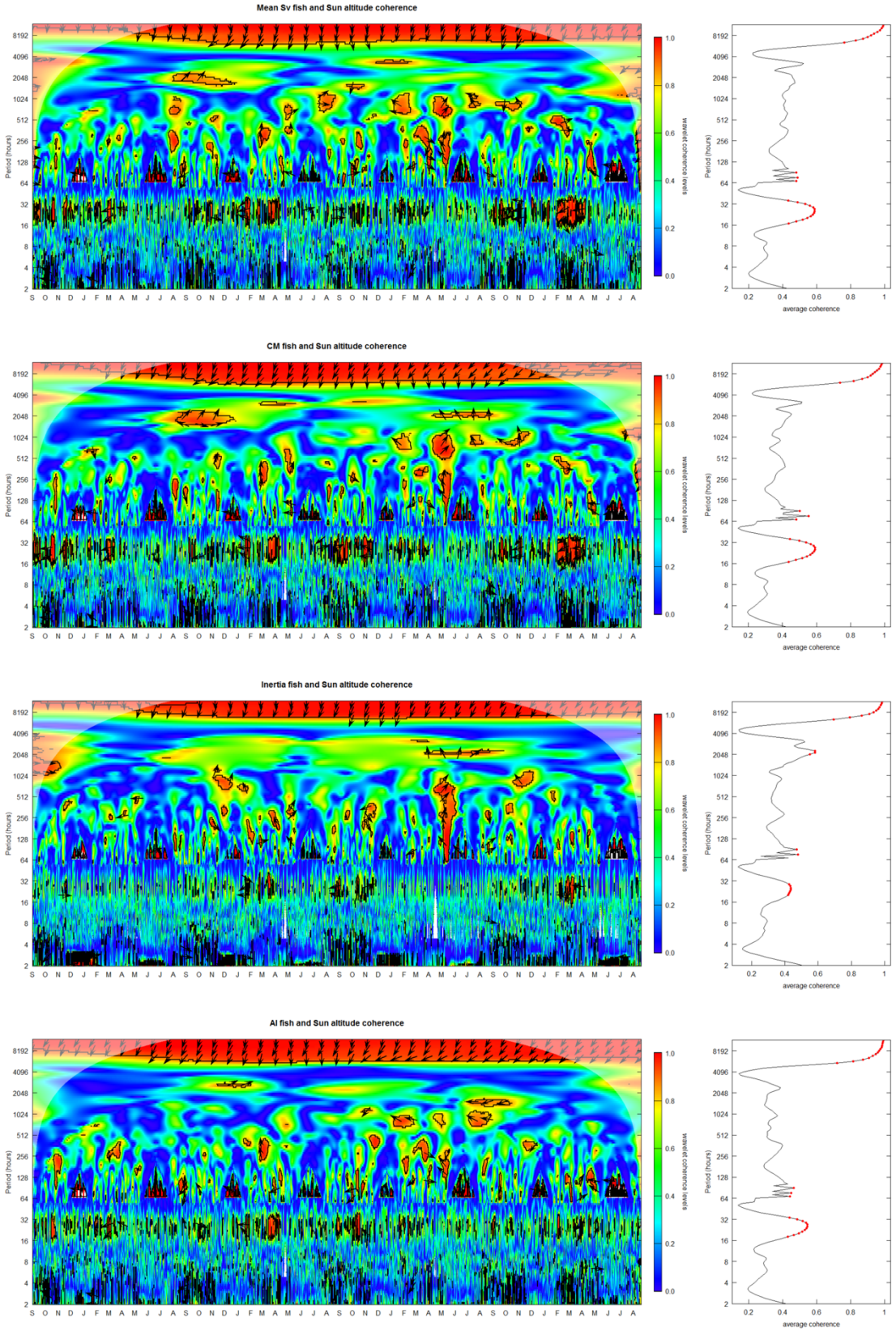

Figure A1. Wavelet coherence between hourly values of fish metrics and sun altitude.

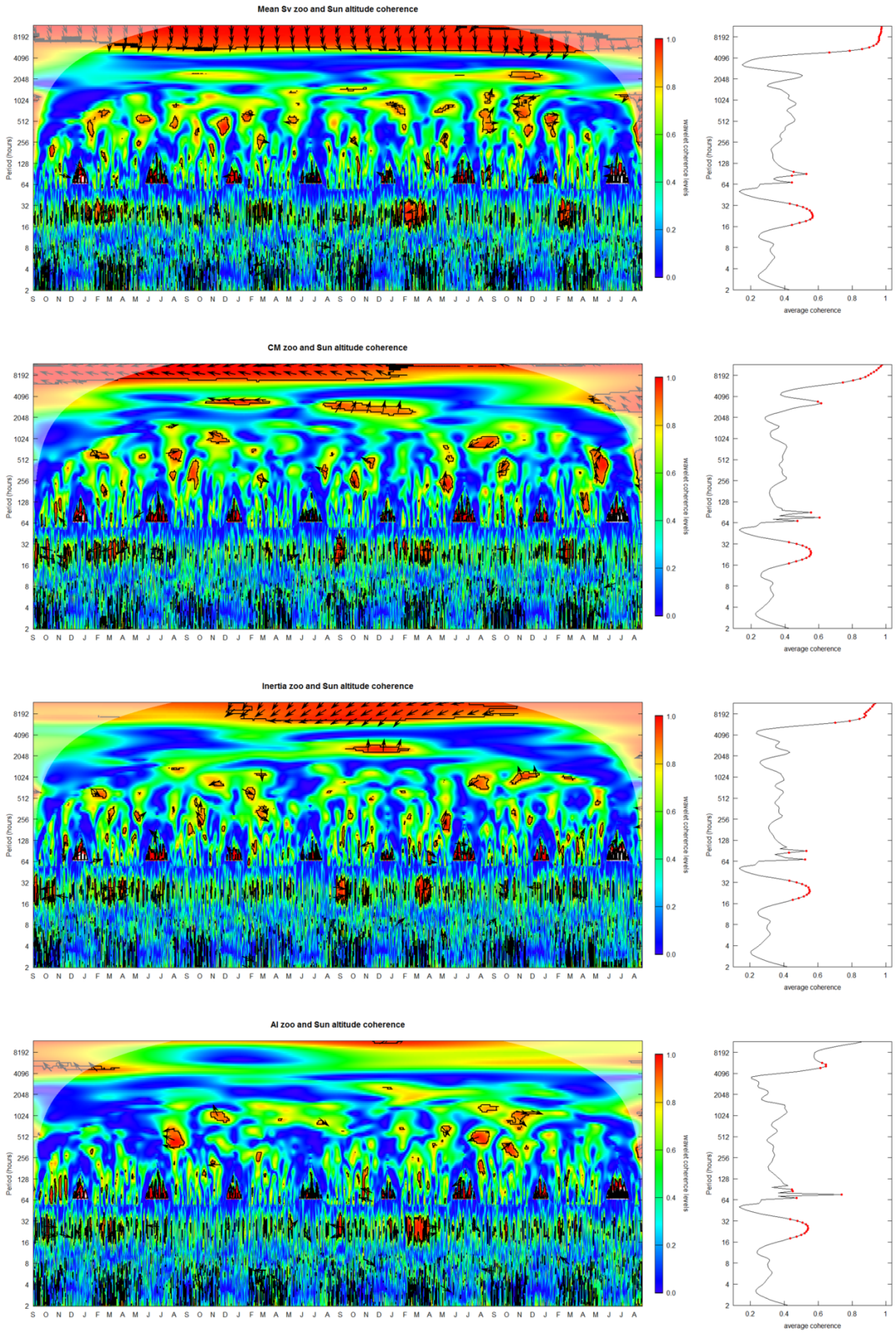

Figure A2. Wavelet coherence between hourly values of zooplankton metrics and sun altitude.

APPENDIX B

Wavelet coherence between daily values of fish and zooplankton metrics of density and vertical distributions derived from acoustic backscatter (mean Sv: mean volume backscattering strength, CM: center of mass, inertia, and aggregation index) and environmental variables from Chapter 2. Data was collected at the Chukchi Ecosystem Observatory from September 1st, 2015 to August 18th, 2019. In the plots, the color bar represents wavelet coherence. The shaded area represents the cone of influence (edge effects) and the areas of significance are traced with a black line (95% confidence against white noise). Arrows indicate the phase difference between the two variables of the wavelet spectra (right arrows indicate series are in phase, left arrows indicate series are completely out of phase (180°), and an arrow pointing vertically upward means the second series lags the first by 90°.

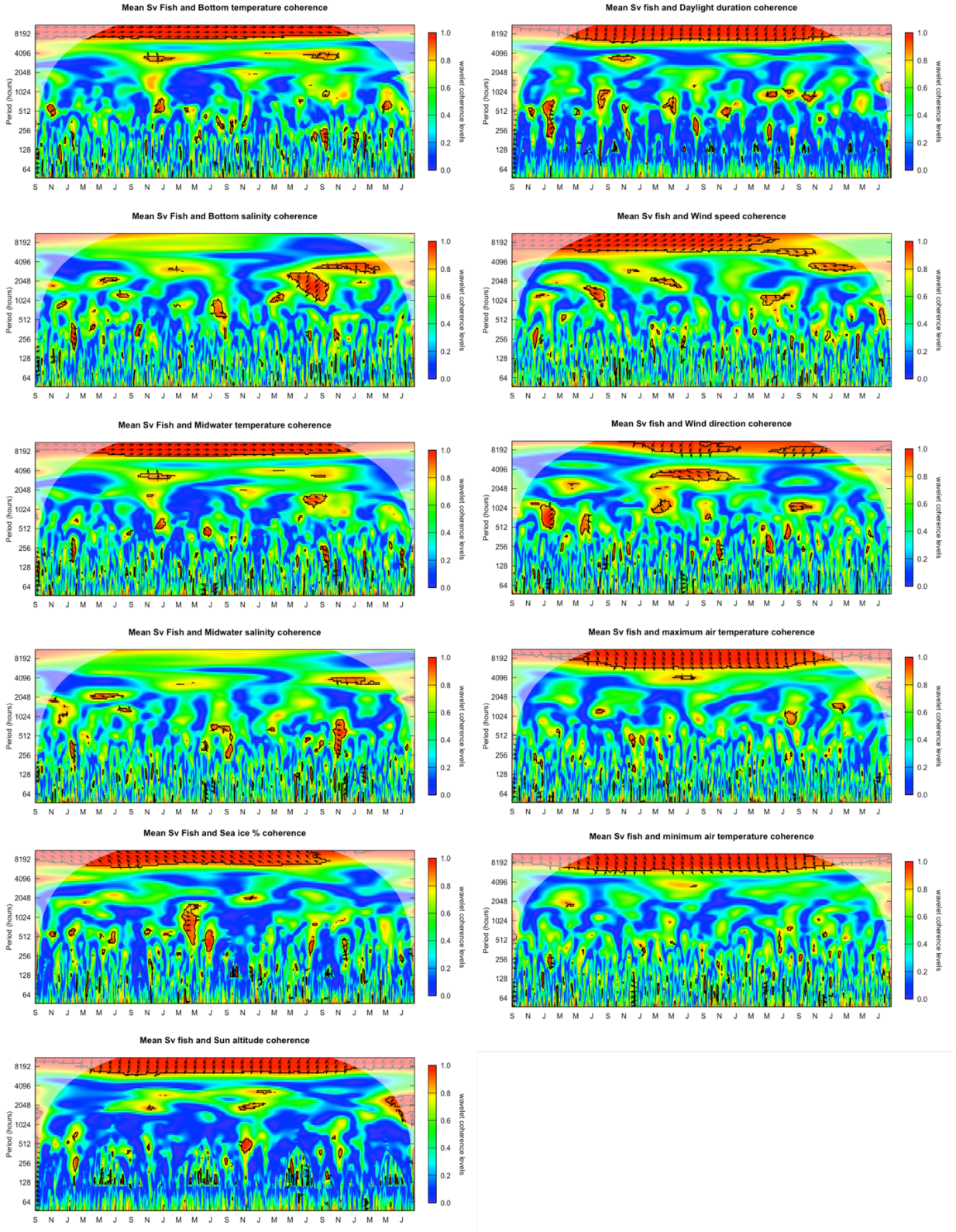

Figure B1. Wavelet coherence between fish mean volume backscattering strength and environmental variables.

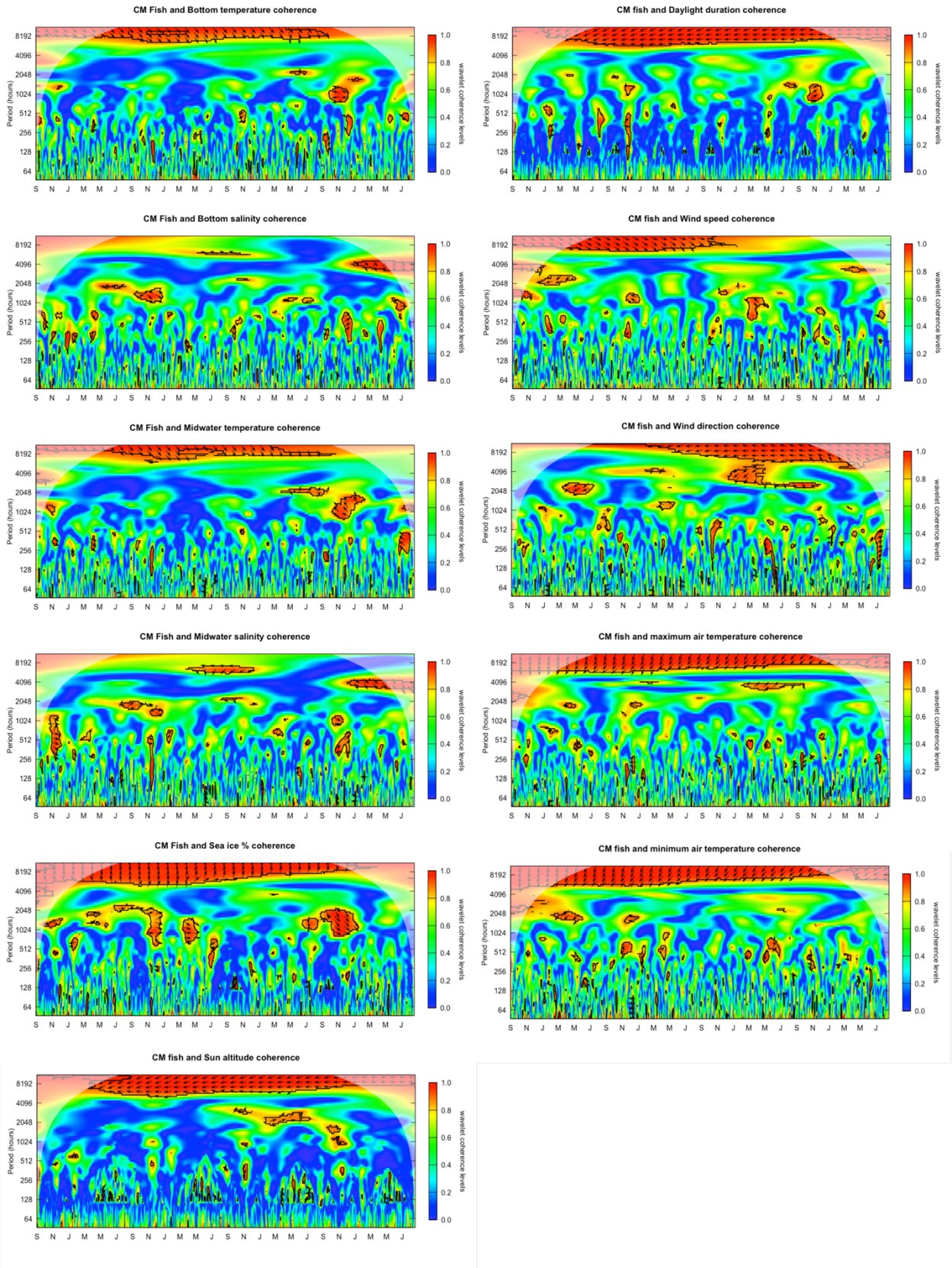

Figure B2. Wavelet coherence between fish center of mass and environmental variables.

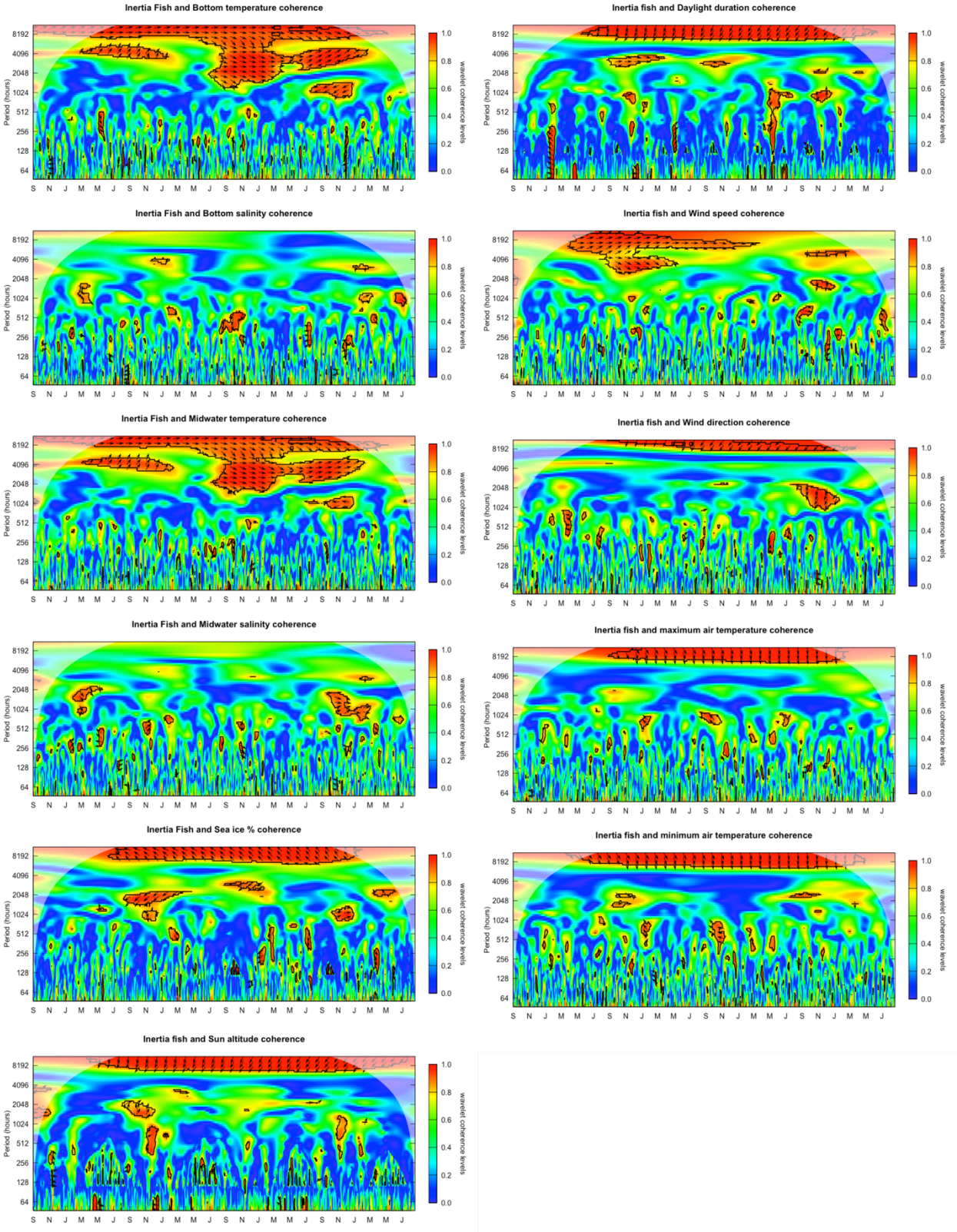

Figure B3. Wavelet coherence between fish inertia and environmental variables.

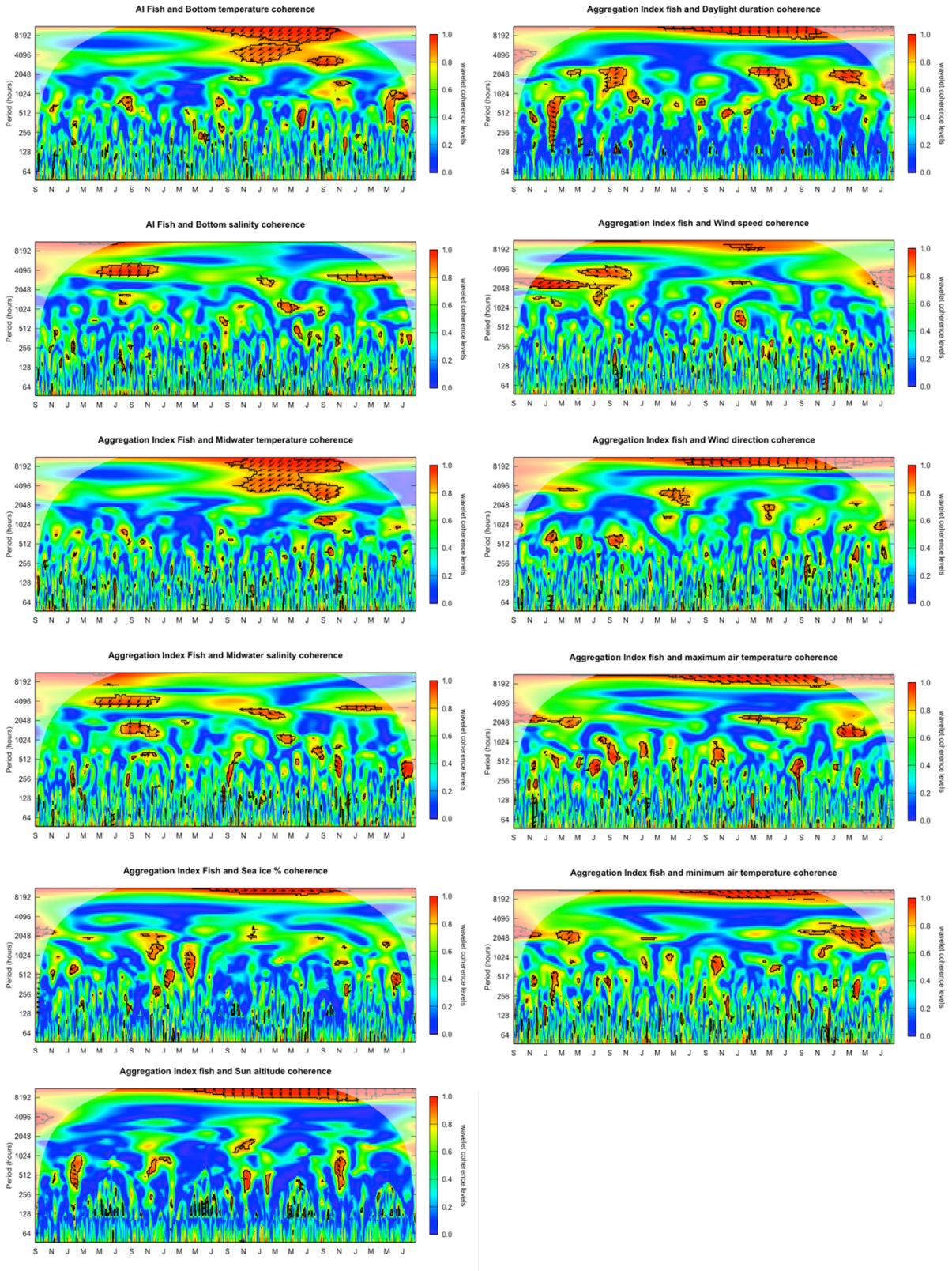

Figure B4. Wavelet coherence between fish aggregation index and environmental variables.

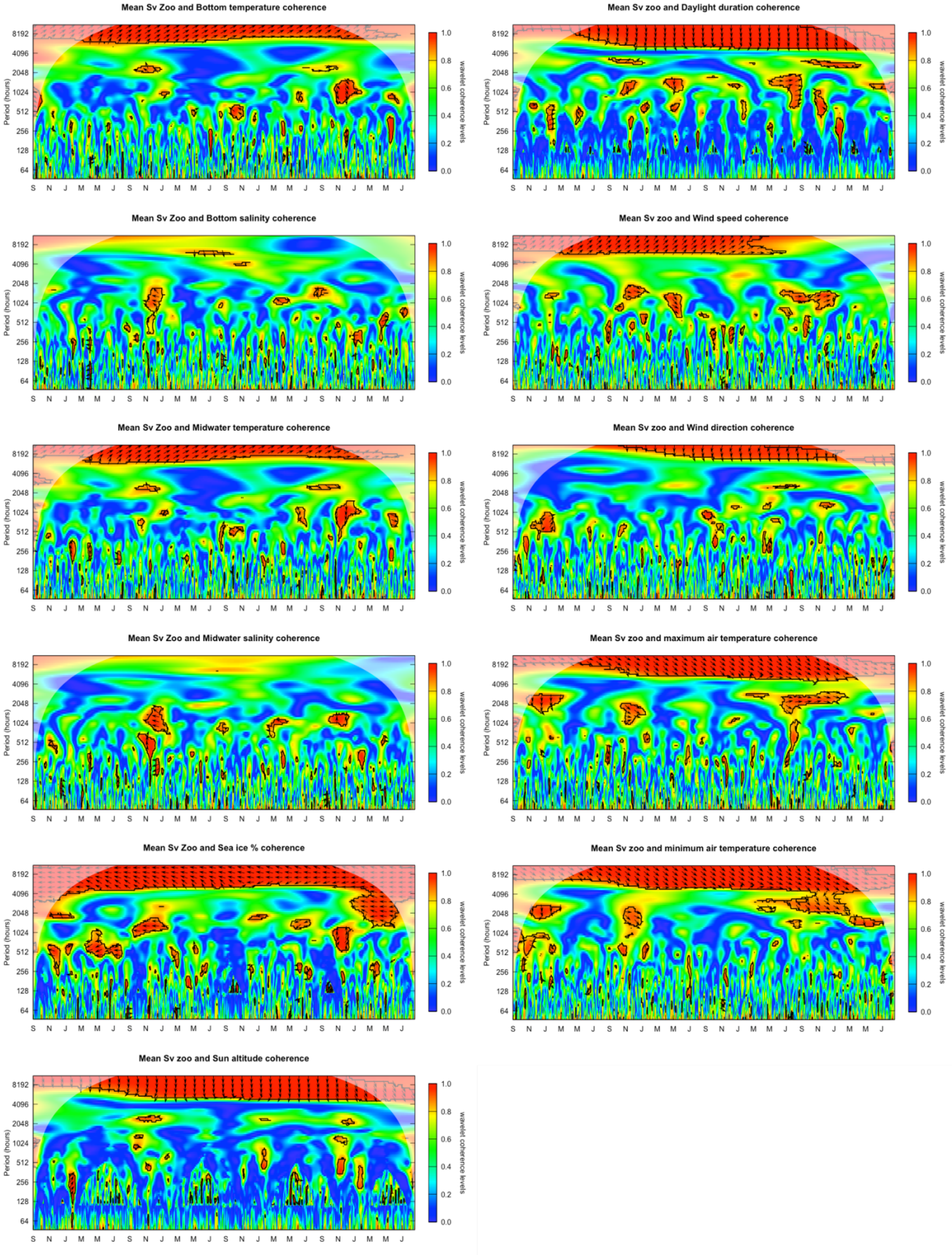

Figure B5. Wavelet coherence between zooplankton mean Sv and environmental variables.

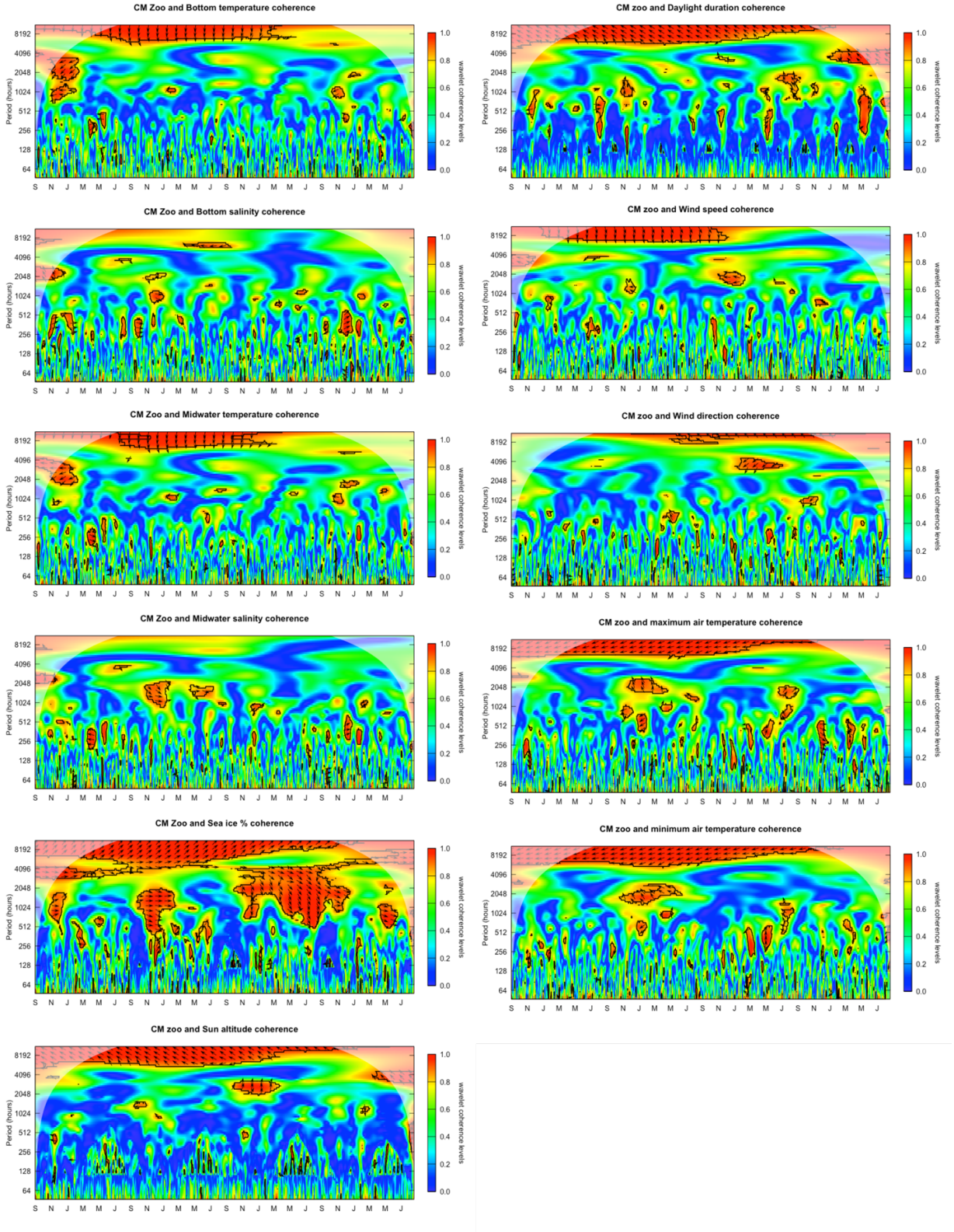

Figure B6. Wavelet coherence between zooplankton center of mass and environmental variables.

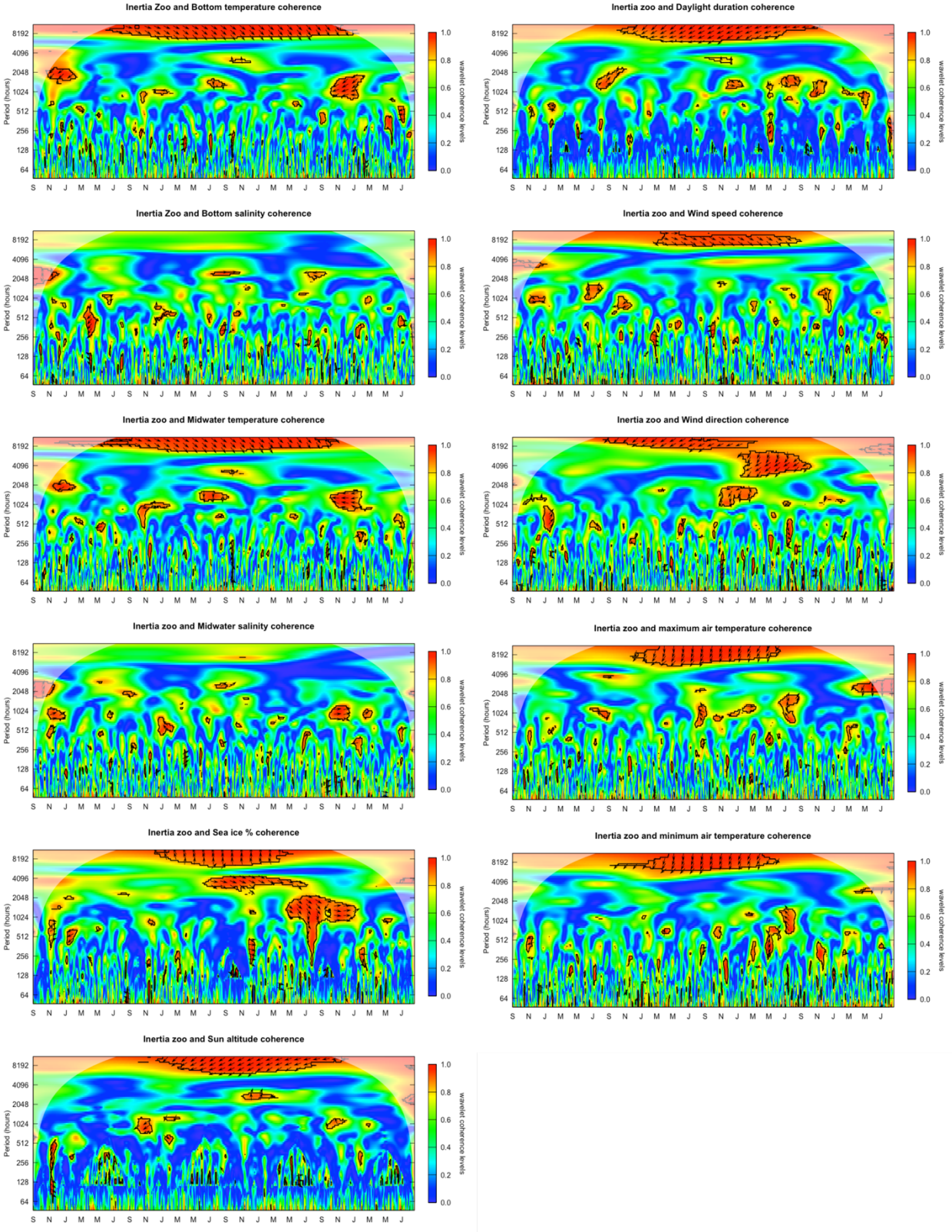

Figure B7. Wavelet coherence between zooplankton inertia and environmental variables.

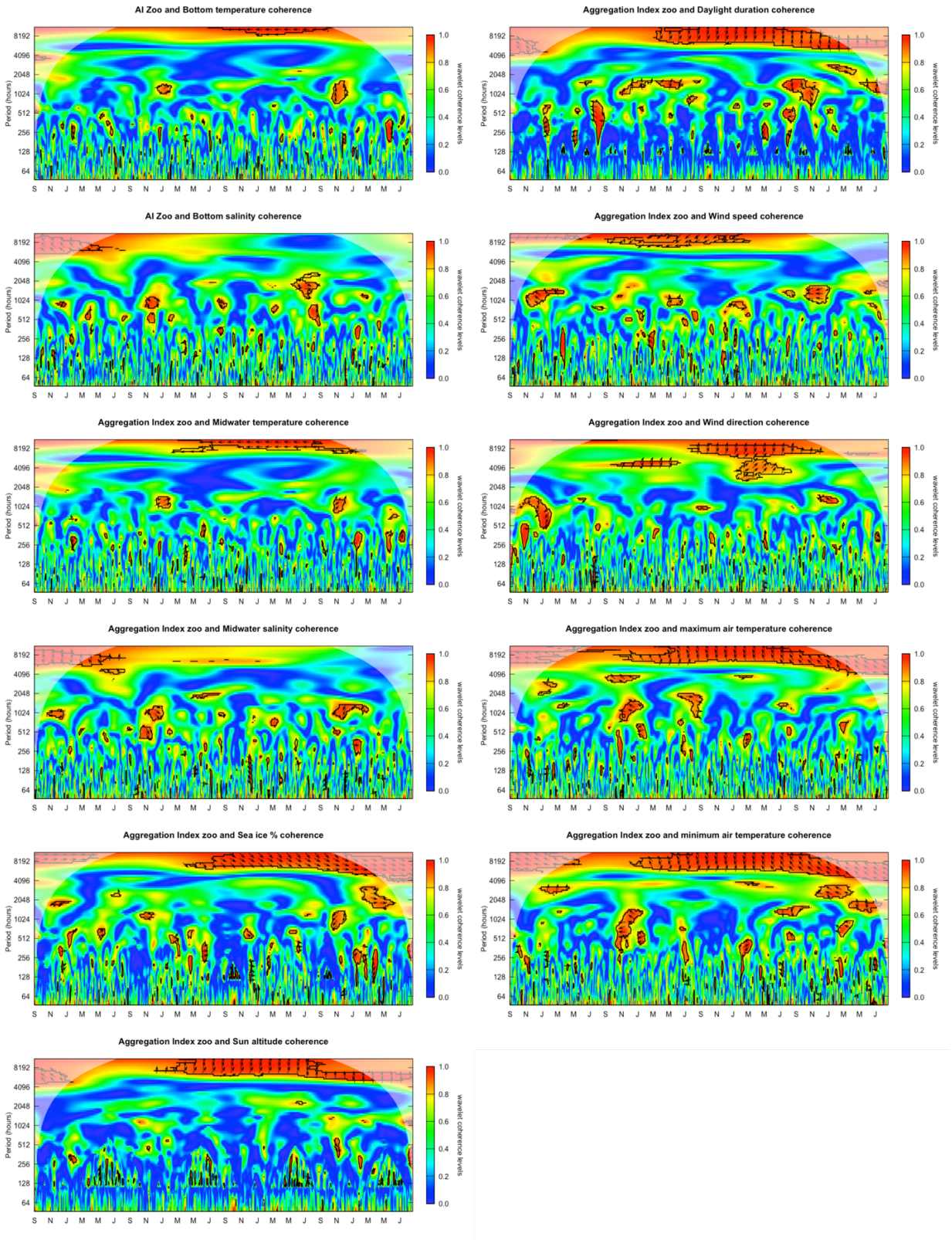

Figure B8. Wavelet coherence between zooplankton aggregation index and environmental variables.

APPENDIX C

Wavelet decomposition of environmental variables from Chapter 2.

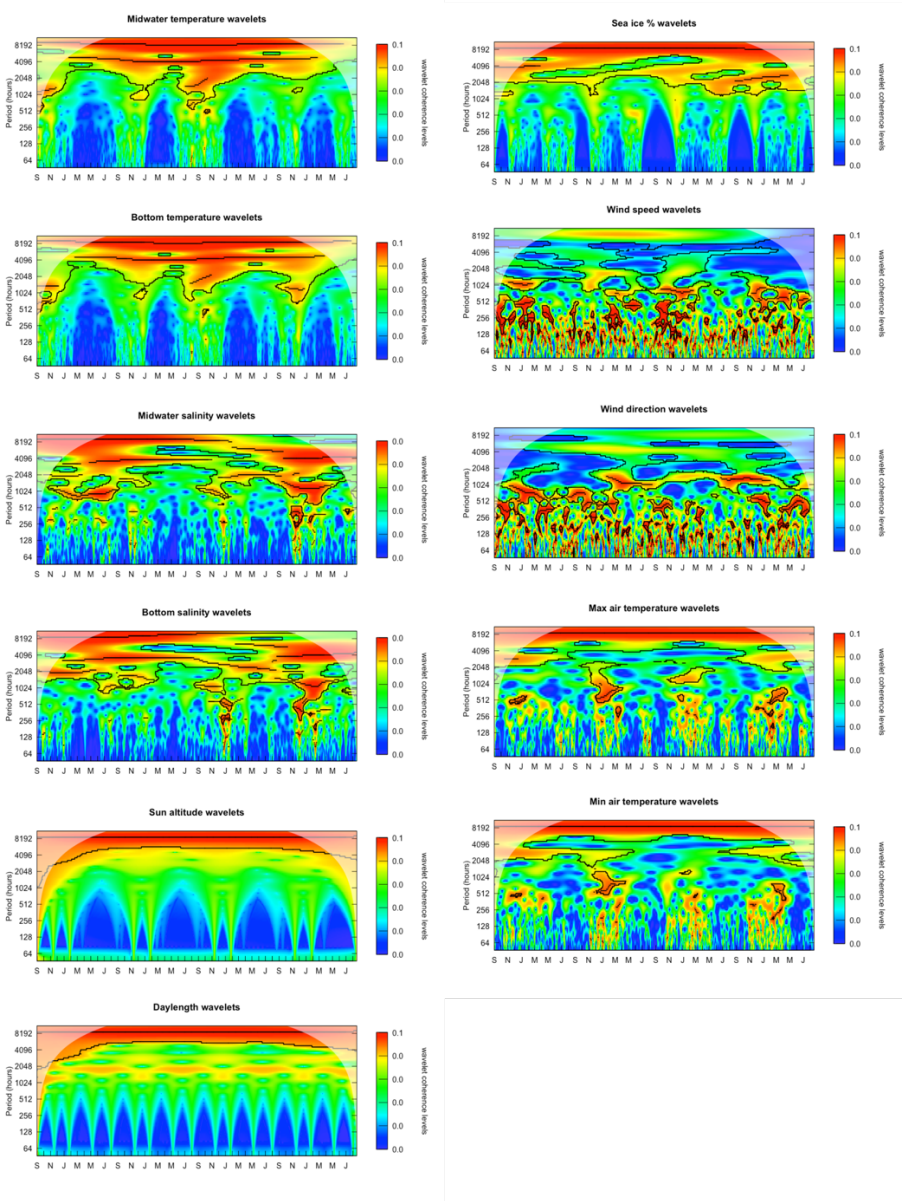

Figure C1. Time-scale decomposition of environmental variables. Data was collected at the Chukchi Ecosystem observatory from September 1st, 2015 to August 18th, 2019. The color bar represents the wavelet power (σ2). The shaded area represents the cone of influence (edge effects) and the black contour lines indicate areas of significance (95% confidence against white noise).

APPENDIX D

Additional results and figures for Chapter 3.

Water masses

Fish backscatter in association with midwater water masses (33 m depth) recorded at the CEO during 2016–2019 are shown in Figure D1. Fish backscatter was observed in both, Bering Chukchi Winter Water (BCWW) and Bering Chukchi Summer Water (BCSW) but highest backscatter values were recorded in Modified Winter Water (MWW), cool Shelf Water (cSW), and warm Shelf Water (wSW) with temperatures above -1 °C and salinities of 31.5–32.5 (Figure D1). Warm Shelf Water was only present in 2017 and 2019 when overall temperatures were higher in the study area (Figure D1). Days with an empty water column only occurred in presence of WW.

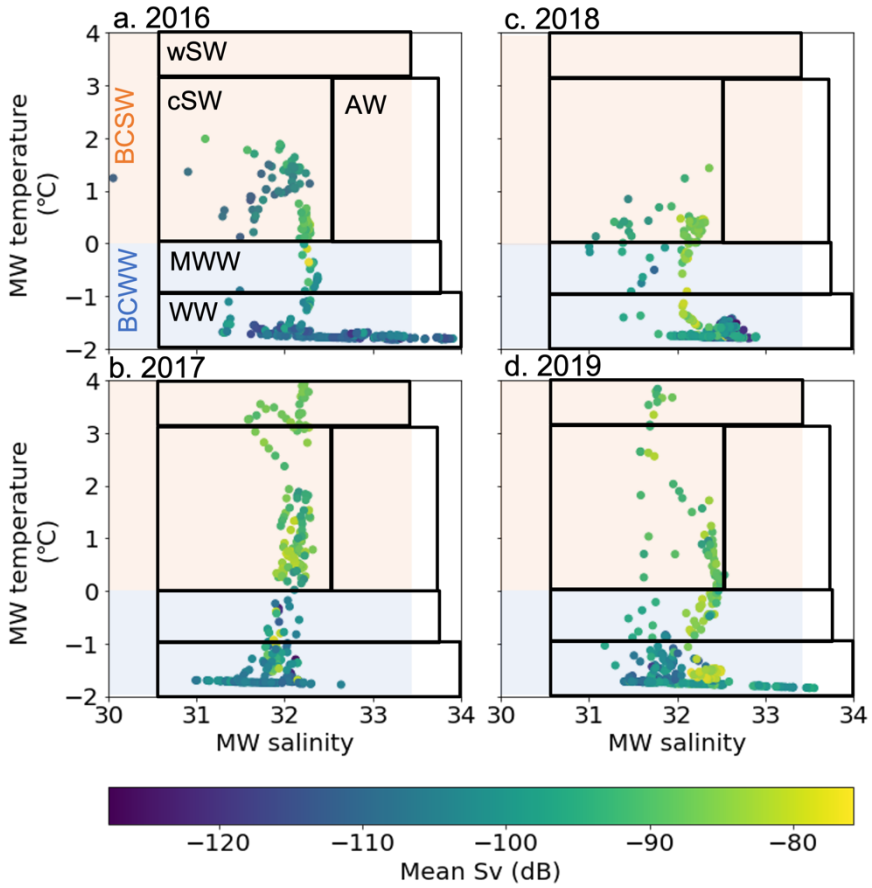

Figure D1. Daily averages of midwater temperature and salinity measured at 33 m depth at the Chukchi Ecosystem Observatory during 2016–2019. Color bar represents mean volume backscattering strength (mean Sv, dB) corresponding to fish. Classification of water masses was based on Danielson et al. (2017, 2020). Abbreviations include: MWW = Modified Winter Water; WW = Winter Water; wSW = warm Shelf Water; cSW = cool Shelf Water; AW = Anadyr Water. The orange and blue areas represent Bering-Chukchi Summer Water (BCSW) and Bering-Chukchi Winter Water (BCWW), respectively.

Primary production

Average chlorophyll a concentration from *in situ* fluorescence measurements were higher in 2017 (1.04 mg m^{-3}) and 2019 (1.16 mg m^{-3}) than in 2016 (0.64 mg m^{-3}) and 2018 (0.82 mg m^{-3}) (Figure D2a). Peaks in chlorophyll a occurred earlier and persisted over longer periods in “warm” years

than in “cold” years (Figure D2a). Multiple chlorophyll peaks were observed from mid-May to August/September in 2017/2019 with the first peak in early June (8^{th}–10^{th}), 5–29 days after sea retreat (Figure D2a). This indicates that earlier sea ice retreat triggers earlier phytoplankton blooms but not before June. In “cold” years highest chlorophyll concentrations were observed from mid-July/June to mid-August in 2016/2018 with peak concentrations occurring once there was no sea ice in the area (Figure D2a). Nitrate concentrations are relatively high throughout the year in both “cold” and “warm” years (Figure D2b). Pre-bloom nitrate concentrations (April and May averages) were 9.44–10.97 μmol L^{-1} in “warm” years and 12.10–18.20 μmol L^{-1} in “cold” years. In “warm” years, declines in chlorophyll a by the end of the summer/early fall coincide with a decline in nitrate concentrations to values approaching zero suggesting a depletion of nutrients and cease of primary production by the time irradiance is minimal (Figure D2b and Figure D2c). In “cold” years nutrients remain at relatively high concentrations for ~ 2–3 months after the decline of chlorophyll concentrations (Figure D2b). Peaks in photosynthetically active radiation were higher in “warm” years (3.13–7.15 μmol photons m^{-2} s^{-1}) than in “cold” years (0.70–2.02 μmol photons m^{-2} s^{-1}) (Figure D2c).

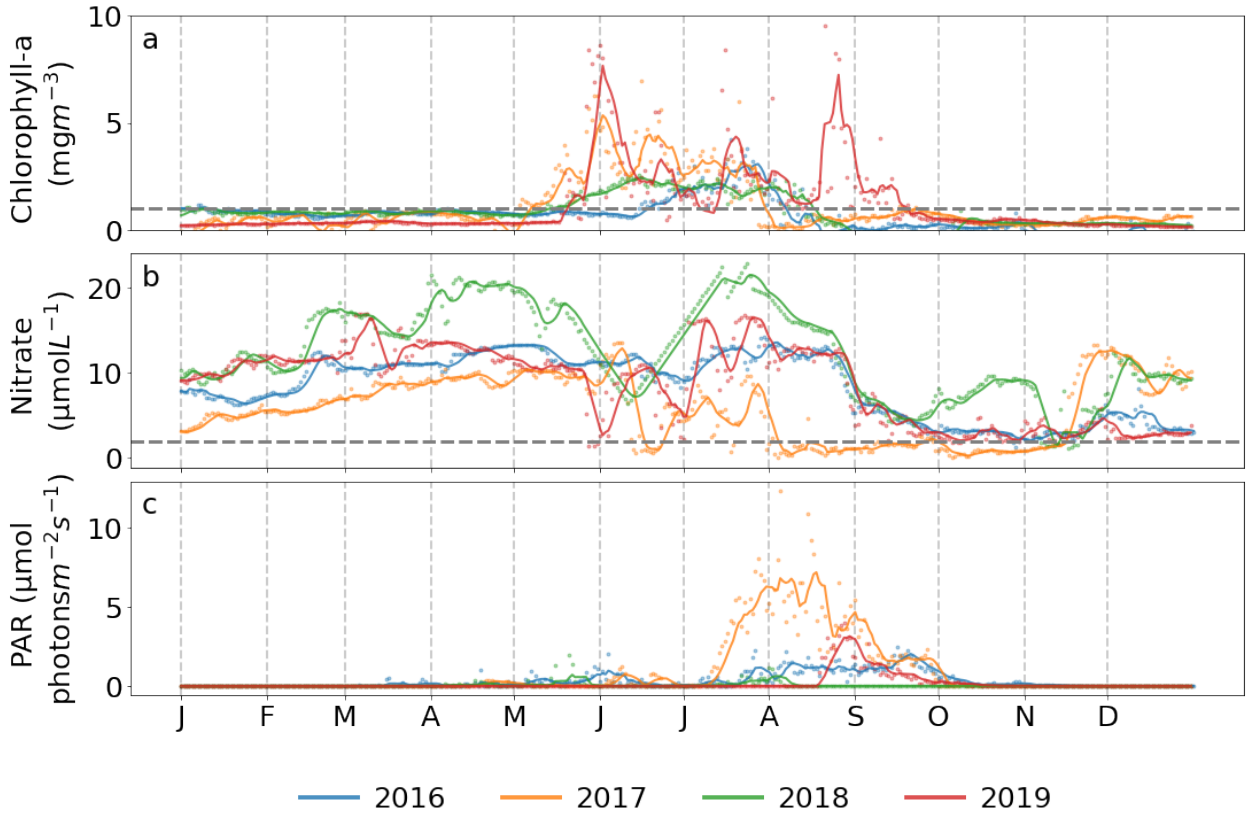

Figure D2. Daily averages of in situ midwater (33 m depth) measurements of (a) chlorophyll a fluorescence, (b) nitrate concentration, and (c) photosynthetically active radiation (PAR) at the Chukchi Ecosystem Observatory during 2016–2019. Lines represent weekly moving averages.

Zooplankton

Zooplankton backscatter was higher in spring and summer in "warm" than in "cold" years (Figure D3). In 2019 when sea ice retreat occurred in May, zooplankton densities were lower than in 2017, when sea ice retreat was in June (Figure D3). The medians of zooplankton backscatter distributions were -89.64 dB (2016) and -83.74 dB (2018) in "cold" years, and -77.13 dB (2017) and -82.42 dB (2019) in "warm" years, with 2019 being higher but more similar to the median in "cold" years.

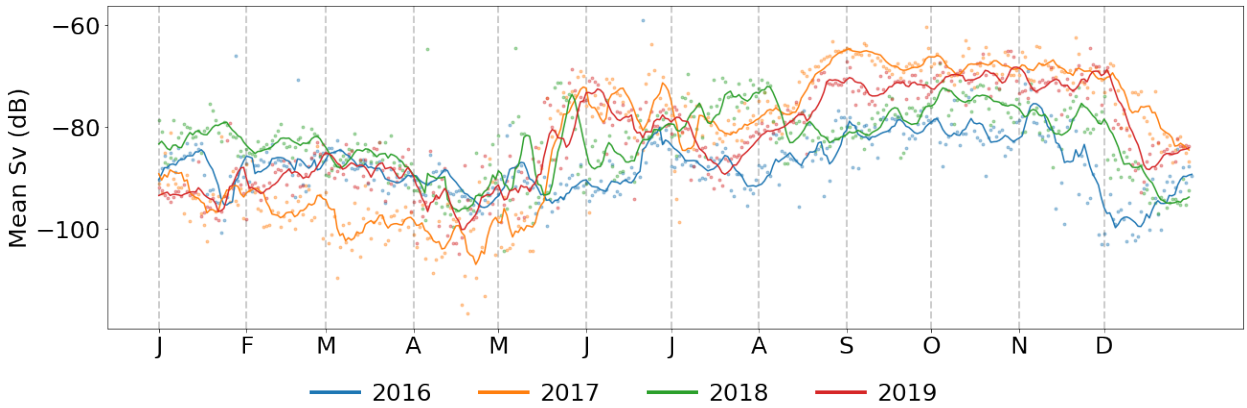

Figure D3. Daily averages of mean volume backscattering strength (Mean Sv) corresponding to zooplankton at the Chukchi Ecosystem Observatory during 2016–2019. Lines correspond to a seven-day moving average.

Environmental variables included in Generalized Additive models are shown in Figure D4 and Figure D5. Only covariates that were not colinear were included at the same time in candidate models. Correlation matrix for all variables is shown in Table D1 and Variance Inflation Factor for variables included in the selected GAM are shown in Table D2. Residuals diagnostic plots are shown in Figure D6 and Figure D7.

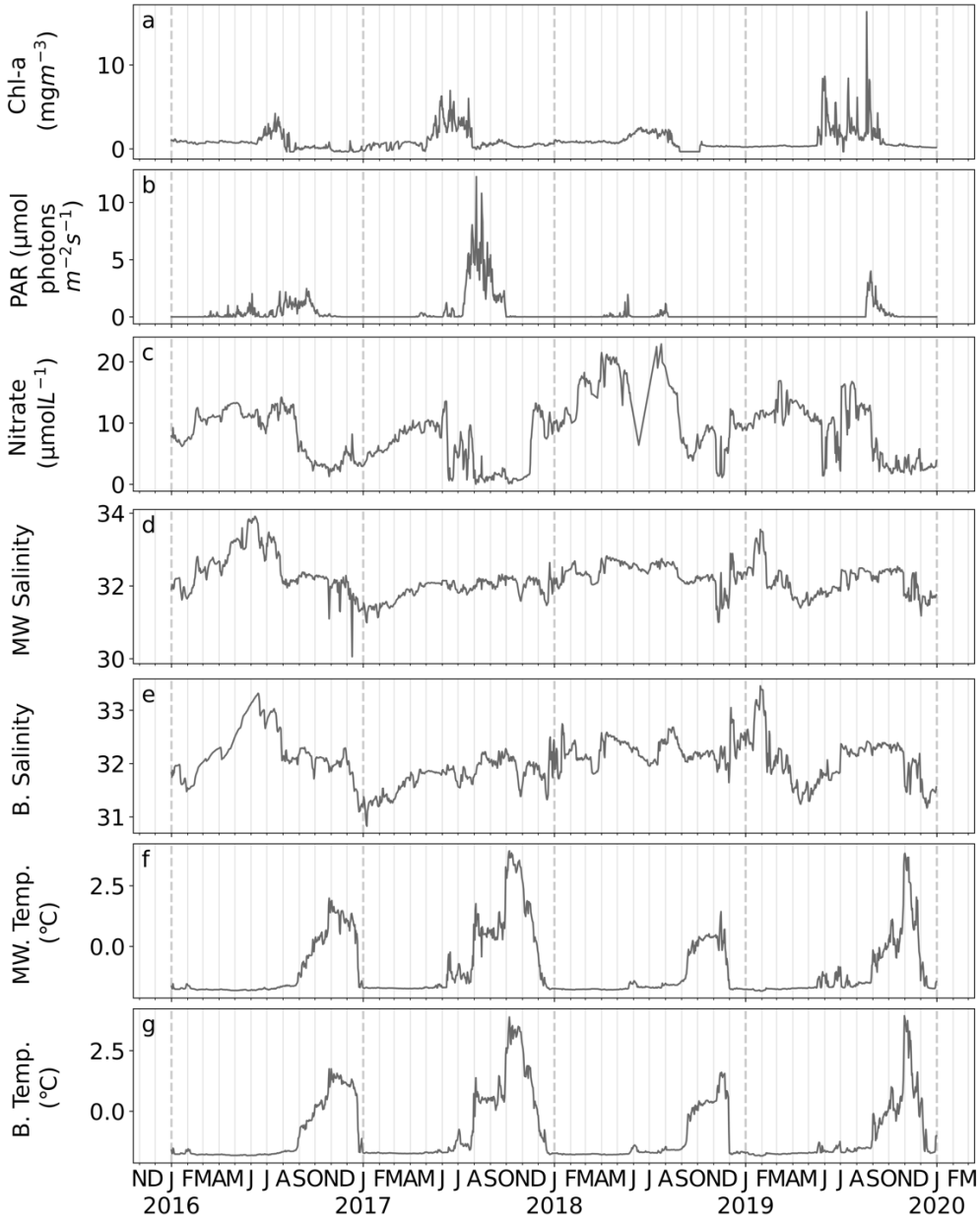

Figure D4. Daily averages of environmental covariates measured in situ at the Chukchi Ecosystem Observatory during 20162019 and included in candidate Generalized Additive Models. Equipment and measurement descriptions are detailed in the main text. (a) Chlorophyll-a fluorescence, (b) photosynthetically active radiation (PAR), (c) nitrate concentration, (d) midwater salinity, (e) near-bottom salinity, (f) midwater temperature, (g) near-bottom temperature.

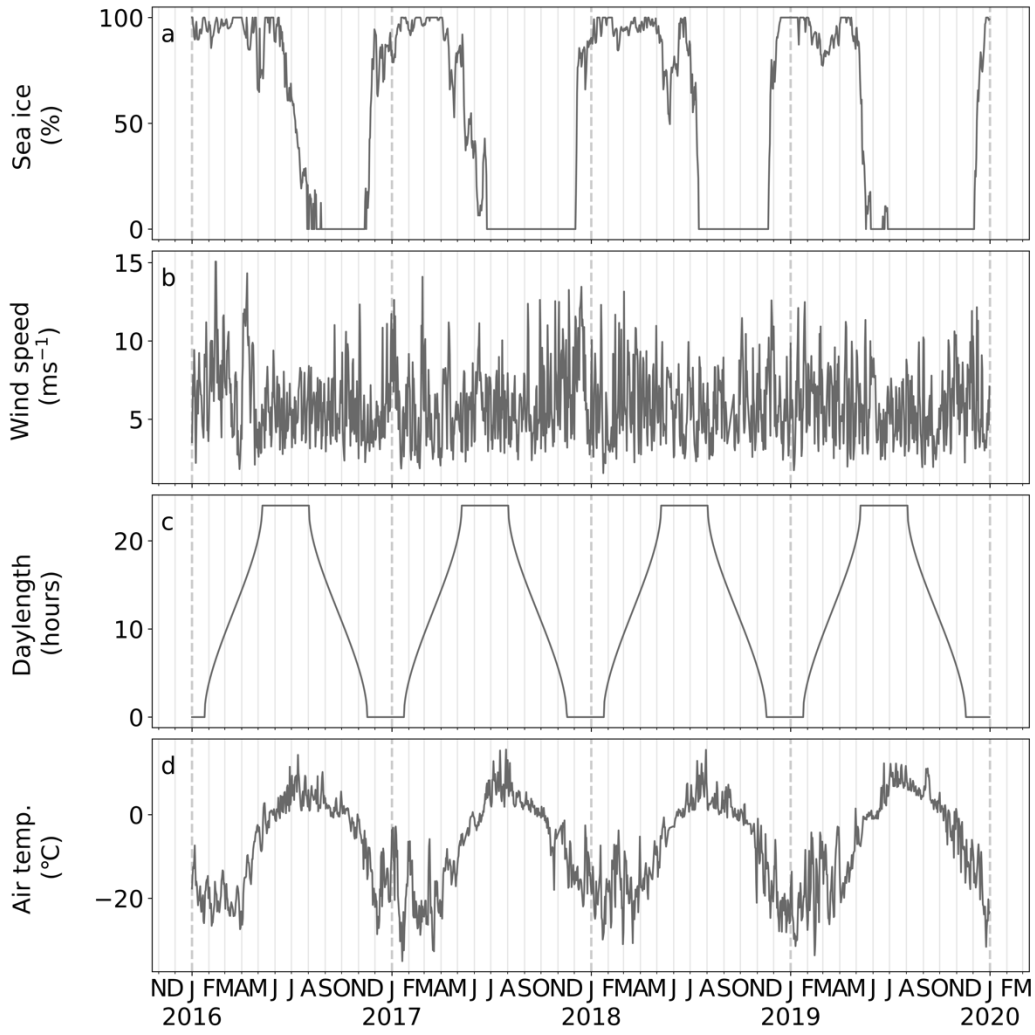

Figure D5. Daily averages of environmental covariates included in candidate Generalized Additive Models. Source of each covariate is described in the main text. (a) Sea ice concentration, (b) wind speed, (c) daylength, (d) air temperature.

Table D1. Correlation matrix for all environmental variables included in Generalized Additive Models.

	B. Temp.	B. Sal.	MW Temp.	MW Sal.	PAR	Sea ice	Wind speed	Air temp.	Wind speed^3	Nitrate	Daylength	Days after retreat	Julian day
B. Temperature													
B. Salinity	-0.09652												
MW Temperature	0.983559	-0.089181											
MW Salinity	-0.224484	0.889225	-0.197093										
PAR	0.139831	0.022824	0.161192	-0.003083									
Sea ice	-0.571836	-0.051549	-0.58799	0.091302	-0.310773								
Wind speed	0.025251	-0.085074	0.014807	-0.070506	-0.070898	0.049848							
Air Temperature	0.166432	0.267191	0.204711	0.234488	0.33833	-0.708982	-0.071431						
Wind speed^3	0.024895	-0.11032	0.01119	-0.088681	-0.081083	0.08058	0.913746	-0.116176					
Nitrate	-0.64132	0.346964	-0.644619	0.44869	-0.228205	0.391167	-0.002146	-0.063683	-0.011379				
Daylength	-0.326908	0.255321	-0.276575	0.361458	0.235286	-0.225634	-0.116408	0.656354	-0.153637	0.364764			
Days after retreat	-0.320009	0.085467	-0.335881	0.262847	-0.278622	0.747287	0.033071	-0.417652	0.051081	0.35268	-0.008713		
Julian day	0.627572	0.030439	0.600273	-0.118621	0.123351	-0.61927	-0.033325	0.346928	-0.037431	-0.431195	-0.14801	-0.418928	
Chl-a	-0.262486	0.078561	-0.220675	0.107582	0.058434	-0.167426	-0.024359	0.347486	-0.049604	0.149189	0.503367	-0.104232	-0.114208

Table D2. Variable inflation factor (VIF) for covariates included in selected Generalized Additive Model.

Feature	VIF factor
Bottom temperature	2.074741
Days after ice retreat	4.763959
Midwater salinity	7.443915
Wind speed^3	1.679815
PAR	1.306611
Daylength	3.8671

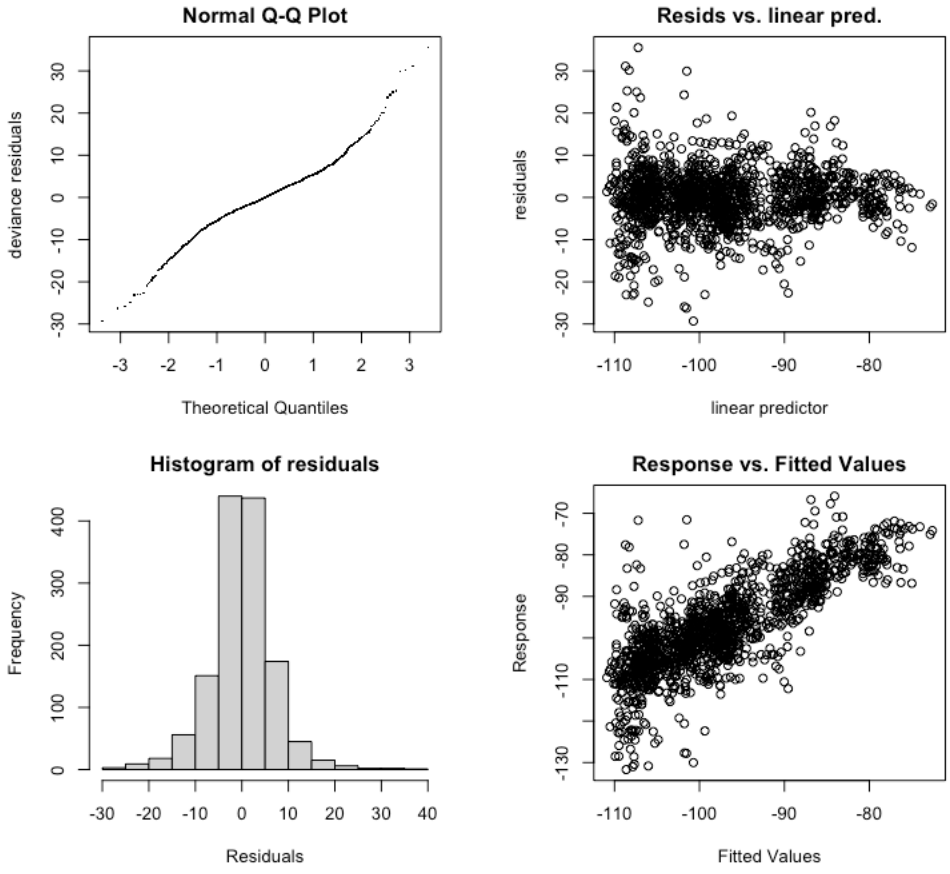

Figure D6. Residual diagnostics for the selected Generalized Additive Model.

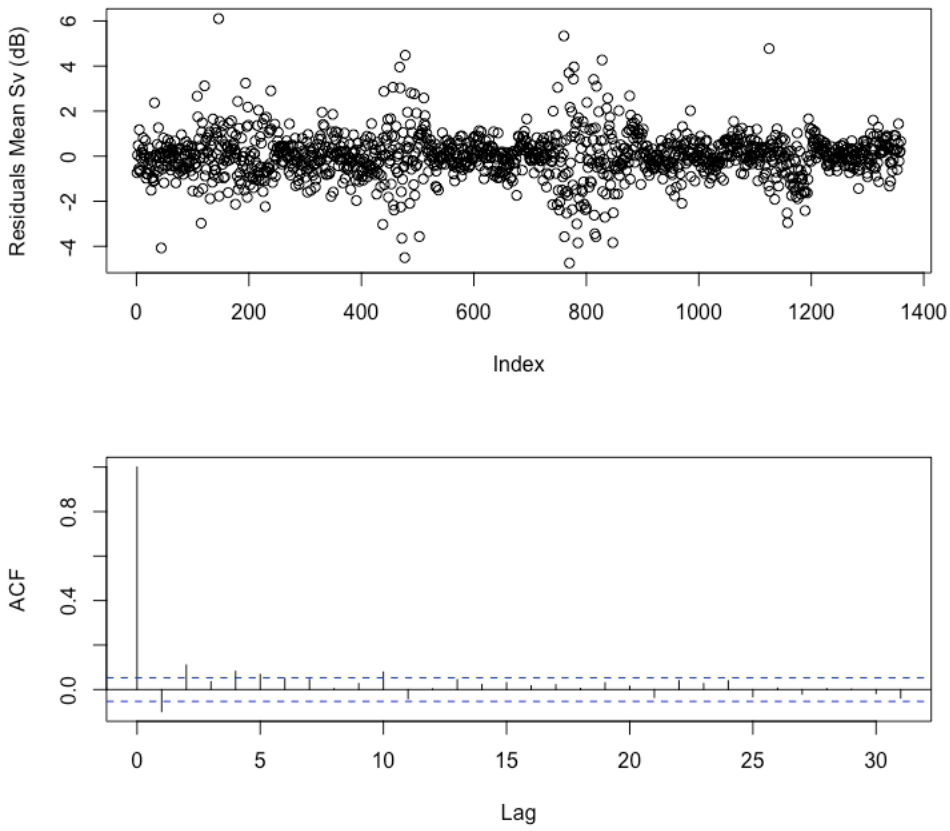

Figure D7. Residuals (top) and Autocorrelation Function (ACF) of the residuals (bottom) from the selected Generalized Additive Model.

VITA

Silvana González was born in San José, Uruguay to Mariela and Nelson González on September 2, 1985. She grew up in San José, graduating from Liceo N°1 in 2002. Silvana went to undergraduate school at Facultad de Ciencias, of Universidad de la República in Montevideo, Uruguay, achieving a Bachelor in Biological Sciences with a specialization in Oceanography in 2010. Silvana earned a Masters in Oceanography at the Facultad de Ciencias del Mar of the University of Cadiz in Spain in 2011. In 2021 she earned a Doctor of Philosophy at the University of Washington in fisheries. Silvana currently lives in Seattle in a tiny house surrounded by her growing collection of fiction books.